Needles and liver phantoms in interventional radiology

Design considerations

de Jong, Tonke L.

DOI
10.4233/uuid:315bdd4b-84bb-4a9b-8f2d-831a6a13459e

Publication date
2019

Document Version
Final published version

Citation (APA)
de Jong, T. L. (2019). *Needles and liver phantoms in interventional radiology: Design considerations*. [Dissertation (TU Delft), Delft University of Technology]. https://doi.org/10.4233/uuid:315bdd4b-84bb-4a9b-8f2d-831a6a13459e

Important note
To cite this publication, please use the final published version (if applicable).
Please check the document version above.

NEEDLES AND LIVER PHANTOMS IN INTERVENTIONAL RADIOLOGY

DESIGN CONSIDERATIONS

Tonke L. de Jong

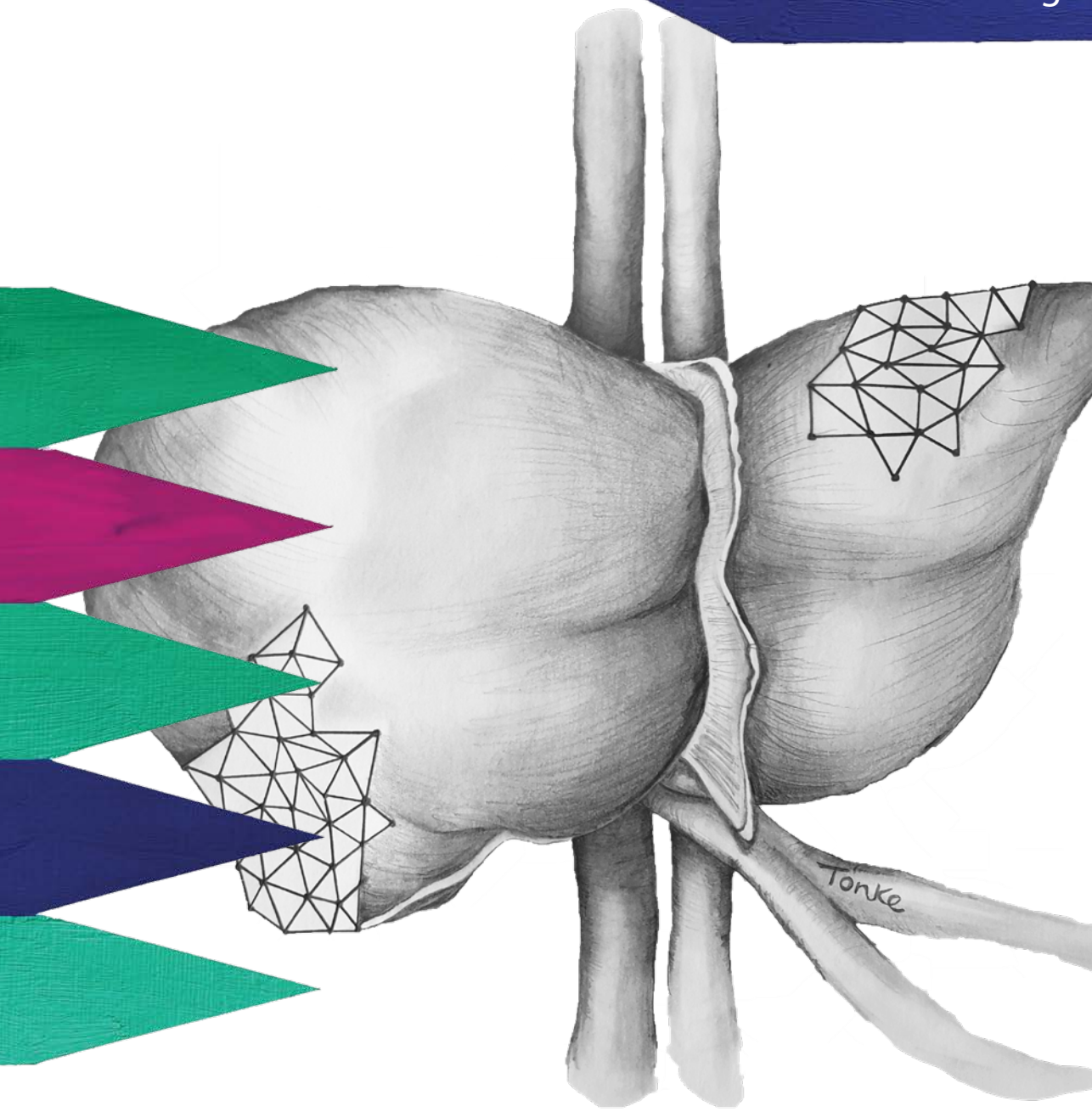

NEEDLES AND LIVER PHANTOMS IN INTERVENTIONAL RADIOLOGY
-
DESIGN CONSIDERATIONS

Tonke L. de Jong

Title Needles and liver phantoms in interventional radiology – design considerations
Author Tonke Leonie de Jong

Printed by Ridderprint BV, Ridderkerk, the Netherlands
Thesis cover and lay-out by Riet ter Ellen & Tonke de Jong
ISBN: 978-94-6375-600-6

This research was financially supported by The Netherlands Organization for Scientific Research (NWO) [nr. 12709].

NEEDLES AND LIVER PHANTOMS IN INTERVENTIONAL RADIOLOGY
-
DESIGN CONSIDERATIONS

PROEFSCHRIFT

ter verkrijging van de graad van doctor aan de Technische Universiteit Delft,
op gezag van de Rector Magnificus Prof.dr.ir. T.H.J.J. van der Hagen
voorzitter van het College voor Promoties,
in het openbaar te verdedigen op

woensdag 20 november 2019 om 15.00 uur

door
Tonke Leonie DE JONG

medisch ingenieur, Technische Universiteit Delft, Nederland
geboren te Oldenzaal, Nederland

Dit proefschrift is goedgekeurd door de promotoren:

Prof. dr. J. Dankelman
Dr. J.J. van den Dobbelsteen

Samenstelling promotiecommissie:

Rector Magnificus	voorzitter
Prof. dr. J. Dankelman	Technische Universiteit Delft, promotor
Dr. J.J. van den Dobbelsteen	Technische Universiteit Delft, promotor

Onafhankelijke commissieleden:

Prof. dr. ir. N. de Jong	Technische Universiteit Delft
Prof. dr. D. Iannuzzi	Vrije Universiteit Amsterdam
Prof. dr. M.A. van Buchem	Leids Universitair Medisch Centrum
Prof. dr. S. Misra	Universiteit Twente
Prof. dr. J. Klein	Technische Universiteit Delft, reservelid

Overig commissielid:

Dr. A. Moelker	Erasmus MC Rotterdam

CONTENTS

SUMMARY

Liver carcinoma is in the top five leading causes of cancer death worldwide. Patients often require radiologic interventions in which needles are inserted, for example when taking biopsies, accessing blood vessels or bile ducts, and ablating tumors. Accurate and precise needle placement in interventional radiology is important, but also challenging. Challenges include several factors, such as anatomical obstructions along the insertion path, patient motion, and unwanted needle bending upon insertion. Incorrect needle placement may prolong procedure time, increase radiation dose for the patient and may cause complications. Proposed approaches to improve needle placement in interventional radiology include, but are not limited to, steerable needles and liver phantoms.

Although steerable needles are technically feasible to produce, these prototypes are often general-purpose. Currently, there is a lack of (analyzed) clinical and experimental data that provide insight into needle placement, and that would clarify the right design requirements for novel needles in interventional radiology.

Another gap exists in the development of liver phantoms, which can be used in a validation set-up for novel needles and/or a training model for medical doctors. Current phantom development focusses mostly on medical imaging properties. However, matching needle-tissue interaction forces and simulating breathing motion are also crucial for a phantom to be of use in a realistic validation set-up.

Therefore, the **objectives** of this thesis are to define relevant design considerations for novel needles, and to develop a high fidelity liver phantom that features respiratory motion and that mimics needle-tissue interaction forces upon insertion. Accomplishing this will improve and advance needle placement in interventional radiology.

The first part of this thesis provides a basis for defining design considerations for novel needles and consists of three studies. The first study is a questionnaire on needle placement errors and on the clinical need for steerable needles that was distributed among 125 radiologists. Then, needle deflection was quantified in thermal ablation procedures performed on liver tumors by a CT image analysis of more than 350 insertions. In the third study, we carried out a numerical analysis to quantify the reachability of needle targets in the liver.

An important finding from the studies in the first part of this thesis is that the majority of the respondents felt that current needles need improvement and that they see added value for steerable needles in interventions. Needle deflection (>1mm) occurred in over half the needle insertions in thermal ablations, and should therefore be taken into account when developing novel needles. Our numerical analysis revealed that targets directly behind the rib cage, and cranial-posterior targets can have low reachability. On average, reachability increases from the state of expiration to inspiration. Besides

fundamental insights into the relation between topology and reachability of the liver, the proposed methods can be used in the future for decision-making in patient-specific treatment plans, for example in choosing the right instrument, and in optimizing the needle trajectory and breathing phase.

The second part of this thesis presents the development of an anthropomorphic liver phantom for needle-based interventions with respiratory motion, that was based on CT images of patients during inspiration and expiration. We searched for a liver mimicking material, in terms of needle-tissue interaction forces, by comparing force characteristics with needle insertions into ex-vivo human livers. In addition, we gathered force data upon puncturing hepatic vessel walls and compared these data with silicone vessel wall phantoms.

Polyvinyl alcohol (PVA) phantoms were developed for mimicking several needle-tissue force characteristics of human liver, such as the magnitude of peak forces, number of peak forces and friction forces along the needle shaft. We used PVA to make a liver phantom in an anthropomorphic shape and mimicked respiratory motion. Experiments with this liver phantom showed needle deflection in the same order of magnitude as observed in real procedures, and quantitatively suggests that breathing contributes to needle deflection. In addition, puncturing the hepatic vein and portal vein with a needle resulted in higher peak forces than surrounding liver tissue, indicating the need for including vessel walls in phantoms.

Summarizing, the research described in this thesis has shed new light on the clinical need for steerable needles, has defined design considerations for novel needles in interventional radiology, and has resulted in a high fidelity liver phantom. With these results, needle placement in interventional radiology can be improved in the future.

SAMENVATTING

Leverkanker staat in de top vijf van doodsoorzaken door kanker wereldwijd. Patiënten hebben vaak radiologische interventies nodig, waarbij naalden worden ingebracht, bijvoorbeeld bij het nemen van biopten, bij het aanprikken van bloedvaten of galwegen, en bij het ableren van tumoren. Het accuraat en precies plaatsen van een naald in interventieradiologie is belangrijk, maar ook uitdagend. Uitdagingen bestaan uit een verscheidenheid aan factoren, zoals anatomische obstructies op het naaldpad, bewegingen van de patiënt, en ongewenste naaldafbuiging tijdens het prikken. Incorrect geplaatste naalden kunnen de interventieduur verlengen, de straling voor de patiënt verhogen, en complicaties veroorzaken. Voorgestelde aanpakken om naaldplaatsing in interventieradiologie te verbeteren omvatten, maar zijn niet gelimiteerd tot, de ontwikkeling van stuurbare naalden en leverfantomen.

Alhoewel stuurbare naalden vanuit technisch perspectief te produceren zijn, zijn deze prototypes vaak generiek. Op dit moment is er een gebrek aan (geanalyseerde) klinische en experimentele data die inzicht geven in naaldplaatsing, en die voor duidelijke ontwerpeisen voor nieuwe naalden in interventieradiologie zouden kunnen zorgen.

Een ander hiaat bestaat in de ontwikkeling van leverfantomen, die gebruikt kunnen worden in een validatieopstelling voor nieuwe naalden en/of in een trainingsmodel voor artsen. De huidige fantoomontwikkeling richt zich met name op eigenschappen van de medische beeldvorming. Echter, overeenkomsten tussen naald-weefsel interactiekrachten en het simuleren van ademhaling zijn ook zeer belangrijke eisen voor een fantoom als deze gebruikt wordt in een realistische validatieopstelling.

Het **doel** van dit proefschrift is daarom tweeledig: het definiëren van relevante ontwerpoverwegingen voor nieuwe naalden, en het ontwikkelen van een natuurgetrouw leverfantoom, dat wordt gekenmerkt door ademhaling en nagebootste naald-weefsel interactiekrachten tijdens het prikken. Het behalen van dit doel zal naaldplaatsing in interventieradiologie kunnen verbeteren.

Het eerste deel van dit proefschrift dient als basis voor het opstellen van ontwerpoverwegingen voor nieuwe naalden en bestaat uit drie studies. In de eerste studie werd een vragenlijst uitgezet onder 125 radiologen, over fouten in naaldplaatsing en over de behoefte aan stuurbare naalden. De tweede studie kwantificeerde naaldafbuiging in thermische ablaties van levertumoren door middel van een CT beeldanalyse van meer dan 350 naaldprikken. In de derde studie voerden we een numerieke analyse uit om de bereikbaarheid van naaldtargets in de lever te kwantificeren.

Een belangrijke resultaat van de studies in het eerste deel van dit proefschrift is dat de meerderheid van de respondenten vond dat de huidige naalden verbeterd moeten worden en een meerwaarde zag voor stuurbare naalden in interventies. Naaldafbuiging (>1mm) vond plaats in meer dan de helft van de naaldplaatsingen tijdens thermische

ablaties, en moet daarom meegenomen in ontwerpoverwegingen voor nieuwe naalden. De numerieke analyse liet zien dat targets direct achter de ribben, en craniaal-posterior gelegen targets moeilijk bereikbaar kunnen zijn. Gemiddeld gezien wordt de bereikbaarheid verhoogd van uit- naar inademing. Naast fundamenteel inzicht in de relatie tussen topologie en de bereikbaarheid van de lever, kan de voorgestelde methode in de toekomst gebruikt worden voor besluitvorming in patiënt-specifieke behandelplannen, bijvoorbeeld in het kiezen van het juiste instrument, en in het optimaliseren van naaldtraject en ademhalingsfase.

Het tweede deel van dit proefschrift toont de ontwikkeling van een antropomorfisch leverfantoom voor naaldinterventies met ademhaling, dat is gebaseerd op medische CT beelden van patiënten tijdens in- en uitademing. We zochten naar een materiaal dat leverweefsel nabootst, in termen van naald-weefselinteractiekrachten, door karakteristieken van deze krachten te vergelijken met naaldplaatsingen in ex-vivo levers. Daarnaast verzamelden we krachtdata van naaldplaatsingen in leveraderwanden en vergeleken we deze data met fantoomwanden van siliconen.

Polyvinyl alcohol (PVA) bleek geschikt om verschillende karakteristieken van naald-weefselkrachten in humane lever na te bootsen, zoals de hoogte van de piekkrachten, aantal piekkrachten, en frictie langs de naaldschacht. We gebruikten PVA om een leverfantoom te ontwikkelen in een antropomorfische vorm en bootsten ademhaling na. Experimenten met dit leverfantoom toonden naaldafbuiging aan in dezelfde orde van grootte als geobserveerd in echte procedures, hetgeen kwantitatief gezien suggereert dat ademhaling bijdraagt aan naaldafbuiging. Daarnaast resulteerde het prikken van de poortader en leverader met een naald in hogere piekkrachten dan het omliggende leverweefsel, hetgeen de behoefte aantoont om bloedvaten toe te voegen aan fantomen.

Samenvattend, het onderzoek beschreven in dit proefschrift heeft nieuw licht geworpen op de klinische behoefte voor stuurbare naalden, heeft ontwerpoverwegingen voor nieuwe naalden in interventieradiologie gedefinieerd, en heeft een natuurgetrouw leverfantoom gepresenteerd. Met deze resultaten kan naaldplaatsing in interventieradiologie in de toekomst worden verbeterd.

INTRODUCTION

NEEDLES IN INTERVENTIONAL RADIOLOGY

This thesis focuses on needles that are used in interventional radiology, which is a medical discipline that diagnoses and treats organ diseases, such as *liver cancer*, by using *needles* under *image guidance*. Correct needle placement is critical in these interventions, as errors can result in decreased treatment efficiency and/or multiple needle insertion attempts. This may prolong procedure time, increase radiation dose for the patient, and cause complications.

The liver is one of the biggest organs in the human body, situated in the upper part of the abdomen (*Figure I*), partly covered by the rib cage. It can be divided in a total of eight segments, according to Couinaud's classification [1], based on the location of the liver vasculature. Filtering the portal blood is one of its most important tasks. Additionally, the liver serves as an excretory system, as an exocrine and endocrine gland, and as a chemical factory [2].

However, liver diseases, such as cirrhosis and hepatocellular carcinoma (HCC), can hamper these important functions. Cirrhosis is the last stage of progressive chronic inflammation of the liver, caused by hepatitis or alcohol abuse. This inflammation converts healthy tissue into fibrous scar tissue, causing the filtering abilities of the liver to decrease. It occurs in 0.27% of the population [3]. Ultimately, cirrhosis can lead to hepatocellular carcinoma, identified by the World Health Organisation as in the top five leading causes of cancer death worldwide [4].

These diseases can be treated by resection, which is partial removal of the liver, and/or by a total transplantation. Often, a less invasive needle-based intervention can be used as an alternative, or interim method. The needles used in interventional radiology are

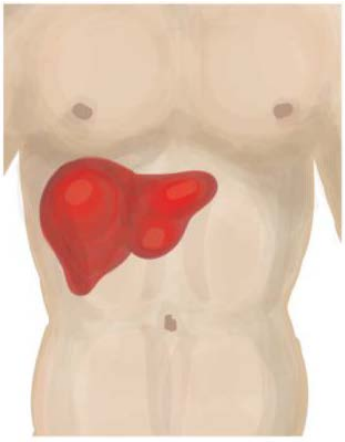

Figure I. *Position of the liver within the body.*

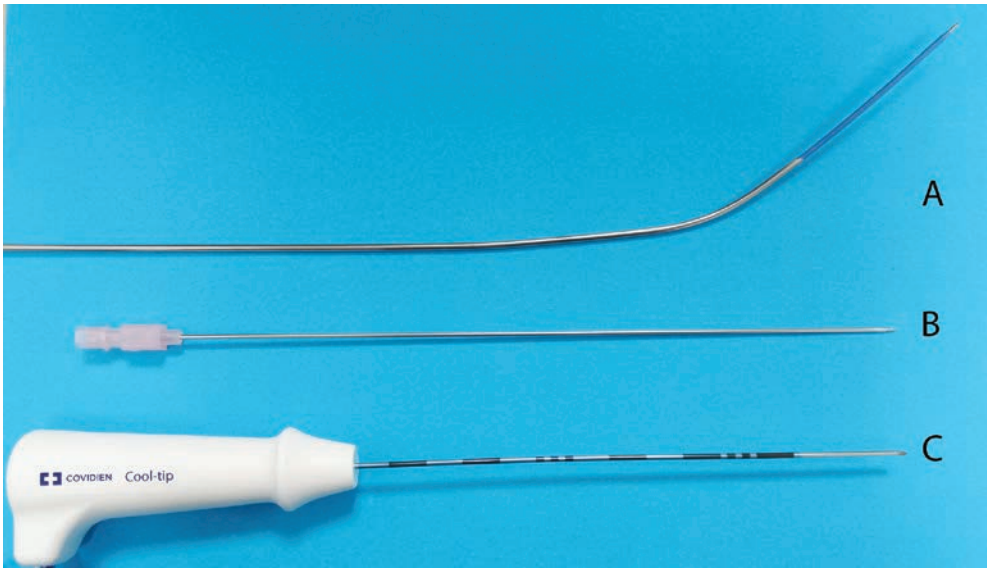

Figure II. *Example of three common needles in interventional radiology: A) Transjugular Intrahepatic Portosystemic Shunt (TIPS) access instrument set, B) 18Gauge trocar needle C) 17Gauge Cool-tip radiofrequency ablation needle.*

typically around 1mm in diameter, 15 to 25cm long, and quite flexible. *Figure II* shows three examples of such needles. Most often, the needles are inserted percutaneously, i.e. via the skin, through several tissue layers, into the desired liver location. In addition, longer needles can be used for interventions in which the liver is accessed via the jugular vein in the patient's neck.

Common procedures with these needles include liver ablations of HCC tumors and biopsies. During ablations, the tip of the needle kills the tumor by destroying the cancer cells with thermal energy. Needle biopsies are needed when part of the tissue must be removed for further examination. Another example of a, less common, procedure is the transjugular intrahepatic portosystemic shunt (TIPS). TIPS creates a tract between the hepatic vein and the portal vein via a transjugular approach to restore the blood flow through the diseased liver.

During these needle interventions, the interventional radiologist relies on image guidance, which visualizes the needle position within the patient's body on a screen. Three imaging techniques that are often used are Ultrasound, Computed Tomography (CT), and Magnetic Resonance Imaging (MRI).

PROBLEMS WITH NEEDLE PLACEMENT

Although needle procedures under image guidance improve the lives of many patients, accurate and precise needle placement within organs is difficult. Several factors exist that complicate the correct placement of the needle tip.

Imagine an interventional radiologist who has to place the needle into a tumor in a patient's liver. The patient is breathing, and the ribs are right in front of the tumor. Moreover, a vital blood vessel is situated on the planned needle path. These patient-specific factors make it challenging to position the needle correctly and to reach the desired target location.

Technical factors add further challenges. For example, the interventional radiologist cannot look through the patient's body directly, but instead he/she has to look at a 2D screen that visualizes the needle via the aforementioned imaging guidance techniques. The needle tip and tissue structures are not always easily identifiable on these images. Also, the needle can bend away from the intended straight path, due to, for example, an unequal force distribution upon insertion, as diseased liver tissue is known for being stiffer and more heterogeneous than healthy tissue [5, 6].

In short, needle interventions under image guidance, such as liver ablations and biopsies, can be used to treat and diagnose patients. Needle placement accuracy and precision remains, however, a challenge to be overcome.

CURRENT SOLUTIONS: STEERABLE NEEDLES AND LIVER PHANTOMS

Several research groups are attempting to improve needle placement using approaches, such as improving the imaging modalities, perfecting needle trajectory planners, designing *steerable needles*, and developing *liver phantoms*. This thesis focuses on the latter two solutions.

Steerable needles can enhance needle placement in interventional radiology. In theory, they can mitigate most of the aforementioned factors that complicate needle placement by steering actively around an anatomical object [7], correcting for unwanted needle deflection and target motion upon insertion [7, 8], or reaching anatomical targets that are not accessible using conventional needles [9, 10]. This way, theoretically lowering the number of punctures, procedure time, and radiation dose.

There are numerous steerable needle designs described in literature. An extensive review of design choices in needle steering is given by van de Berg et al. [11]. In addition, an overview of needle-like instruments for steering through solid organs is given by Scali et al. [12]. These novel needles can typically be manipulated at their base to change the direction of their tip, whereafter their shaft follows upon insertion. Their diameters range from 0.8mm to about 3mm; and therefore, they have roughly the same diameter as needles that are currently clinically used in interventional radiology.

In addition to steerable needles, *liver phantoms* can improve needle placement in a more indirect manner: either by training medical residents, or by validating novel needles. These phantoms are used as a substitute for real tissue in studies and training sessions where in-vivo and ex-vivo biological models are not a feasible option, due to practical and ethical issues. They consist of a tissue mimicking material (TMM) to

simulate human tissue, covering different aspects of reality.

A comprehensive overview of existing techniques, limitations and recommendations for TMMs in image-guided needle-based interventions is given by Li et al. [13]. The center of attention of most of the ongoing organ phantom research goes to the imaging properties of the TMMs. For example, Surry et al., and Zell et all., found good ultrasound mimicking properties in polyvinyl alcohol (PVA) [14, 15]. Furthermore, since the rapid development of 3D printers, more and more organ phantoms have now an anthropomorphic shape based on patient imaging data, such as, for example, described in [16-18].

To sum up, several approaches exist to improve needle placement. Among these are steerable needles and liver phantoms, on which this thesis focusses. Yet there are several factors that hinder the implementation of these solutions in clinical practice.

ISSUES WITH NOVEL NEEDLE DESIGNS AND LIVER PHANTOMS

Despite all technological developments in steerable needles and liver phantom designs, we are faced with several issues. Concerning needles the exact clinical need remains unknown, whereas the current liver phantoms lack in high fidelity regarding mechanical properties combined with breathing motion.

Novel steerable needles are now technically feasible to make and produce, as discussed. However, the current general-purpose steerable needles may not be the optimal solution for the wide variety of clinical tasks in which needles are used in interventional radiology, especially given the case-specific level of task difficulty. For example, a steerable needle used to avoid anatomical objects would need different design requirements than one used to correct for unwanted needle deflection. Currently, there is a lack of (analyzed) clinical data that give insight into these aspects and that would clarify the right design considerations for these needles.

According to the recent literature, studies of liver phantoms are mostly focused on their imaging properties. However, to make a liver phantom that mimics the heterogenic nature of tissue, more insight into needle-tissue interaction forces is needed. Currently, it is not clear whether artificial phantom materials provide a good alternative for human liver tissue when studying for example the effect of needle insertion velocity on axial force [19]. Moreover, the addition of liver motion during breathing has only been considered in separate studies. Hence, there is no high fidelity liver phantom that accounts for a combination of these features.

In short, there are a not enough data on needle-tissue interaction. From a clinical and engineering point of view, this makes it hard to further develop novel needles and liver phantoms for needle-based interventions.

AIM

The goal of this thesis is to improve needle placement in interventional radiology.

This dissertation is focusing on novel needles and liver phantom development; therefore, more specifically, its aims are as follows:

- *Providing design considerations for novel needles.* We use various methodologies to gather more insight into needle insertions, including a questionnaire, a CT image analysis, and a simulation. Based on these studies, relevant design considerations for novel needles can be given, for example to develop needles that are more case-specific than the current ones.

- *Developing and validating a high fidelity liver phantom that features respiratory motion and that mimics forces upon needle insertion*. The phantoms that are currently available do not have a combination of these advanced properties. This new model can be used to train medical residents, and to experimentally validate novel instruments in interventional radiology.

Both medical engineers and medical doctors might benefit from the insights gained through this dissertation.

APPROACH AND OUTLINE

The visual outline of this thesis is presented in *Figure III.* Overall, we explore two possible solutions to improve needle placement. *Part A* concentrates on providing clinically relevant design consideration for novel needles by first gaining insight into needle placement. The last three chapters fulfill the main aim of *Part B*: developing and validating a liver phantom. Please note that the chapters of this thesis are independent articles; therefore, some content may be repeated.

Part A: DESIGN CONSIDERATIONS FOR NOVEL NEEDLES

Part A consists of three chapters that aim to define relevant design considerations for the development of novel needles in interventional radiology. The chapters answer three separate questions using a multi-method approach.

Firstly, it is crucial to know more about what is clinically needed. Therefore, *Chapter 1* addresses the current view of 125 interventional radiologists on needle placement errors and novel needle designs, by means of a questionnaire. Remarkably, 85% of the radiologists experience unwanted needle deflection, and 95% share the opinion that needles should be improved.

Secondly, *Chapter 2* analyzes one of the factors that contribute to needle placement errors: needle deflection. Up to now, the magnitude of unwanted needle deflection

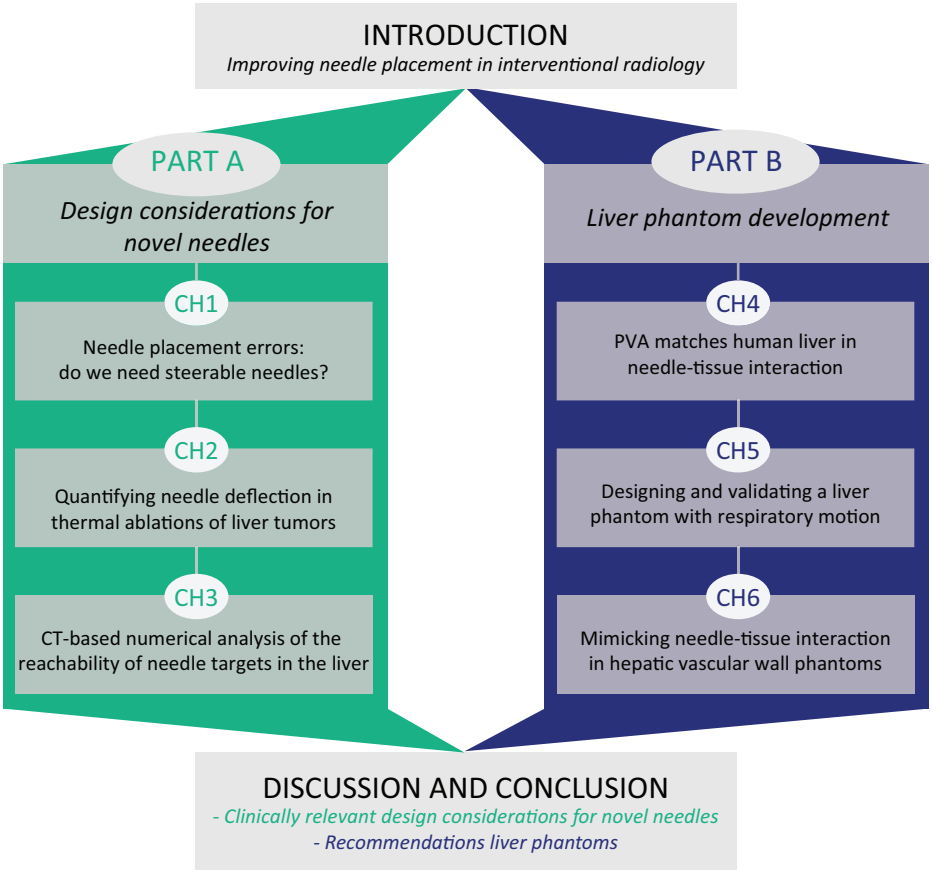

Figure III. *Visual outline of the thesis.*

has been unknown. Using a CT analysis of over 350 reconstructed needle shapes, we quantify how much needle deflection occurs in clinical thermal ablations of liver tumors.

Finally, *Chapter 3* numerically analyzes and quantifies the reachability of needle targets in the liver during inspiration and expiration of four patients. We use ray casting from target-to-skin as a collision detector of anatomical objects.

Part B: LIVER PHANTOM DEVELOPMENT

Chapter 4 studies a material, polyvinyl alcohol (PVA), that mimics human liver tissue in needle-tissue interaction forces. In doing so, the study compares force characteristics of needle punctures in human livers with punctures into PVA specimens with different concentrations and fabrication methods.

The material found in *Chapter 4* is used in *Chapter 5* to develop and validate a high

fidelity liver phantom that features respiratory motion. This liver phantom is created based on segmentation of CT scans of real patients. Subsequently, we calculate the motion patterns of the liver based on CT scans of patients during inspiration and expiration. A motion stage with a sinusoidal movement actuates the liver phantom to mimic these patterns.

The final chapter of this part (*Chapter 6*) studies the needle-vascular wall interaction forces in the liver and presents a tissue mimicking material that resembles these forces. This material can be incorporated in the polyvinyl alcohol phantoms described in the first two chapters of this part, by means of a connecting mesh.

At the end of this thesis, we discuss the accomplishments of the presented studies, we give recommendations for future work in the field of phantom development, and we define design considerations for novel needles in interventional radiology.

REFERENCES

[1] Bismuth H(1982) Surgical anatomy and anatomical surgery of the liver. World Journal of Surgery 6(1):3-9.

[2] Boron WF, and Boulpaep EL (2012) Medical physiology: a cellular and molecular approach. Elsevier Health Sciences.

[3] Scaglione S, Kliethermes S, Cao G, Shoham D, Durazo R, Luke A, and Volk ML (2015) The epidemiology of cirrhosis in the United States: a population-based study. Journal of Clinical Gastroenterology 49(8):690-696.

[4] World Health Organisation (2012) Liver cancer: estimated incidence, mortality and prevalence worldwide [2019-09-05] *http://globocan.iarc.fr/old/FactSheets/cancers/liver-new.*

[5] Yu H, Mouw JK, and Weaver VM (2011) Forcing form and function: biomechanical regulation of tumor evolution. Trends in Cell Biology 21(1):47-56.

[6] Paszek MJ, Zahir N, Johnson KR, Lakins JN, Rozenberg GI, Gefen A, Reinhart-King CA, Margulies SS, Dembo M, Boettiger D, Hammer DA, and Weaver VM (2005) Tensional homeostasis and the malignant phenotype. Cancer Cell 8(3):241-254.

[7] Webster RJ, Memisevic J, and Okamura AM (2005) Design Considerations for Robotic Needle Steering. Proceedings of the 2005 IEEE International Conference on Robotics and Automation:3588-3594.

[8] Kratchman LB, Rahman MM, Saunders JR, Swaney PJ, and Webster III RJ, "Toward robotic needle steering in lung biopsy: a tendon-actuated approach." pp. 79641I-79641I-8.

[9] Cowan NJ, Goldberg K, Chirikjian GS, Fichtinger G, Alterovitz R, Reed KB, Kallem V, Park W, Misra S, and Okamura AM (2011) Robotic needle steering: Design, modeling, planning, and image guidance. Surgical Robotics:557-582.

[10] Reed KB, Majewicz A, Kallem V, Alterovitz R, Goldberg K, Cowan NJ, and Okamura AM (2011) Robot-Assisted Needle Steering. IEEE Robotics & Automation Magazine 18(4):35-46.

[11] van de Berg NJ, van Gerwen DJ, Dankelman J, and van den Dobbelsteen JJ (2015) Design Choices in Needle Steering - A Review (2015) IEEE/ASME Transactions on Mechatronics 20(5):2172-2183.

[12] Scali M, Pusch TP, Breedveld P, and Dodou D (2017) Needle-like instruments for steering through solid organs: A review of the scientific and patent literature. Proceedings of the Institution of Mechanical Engineers, Part H: Journal of Engineering in Medicine 231(3):250-265.

[13] Li P, Yang Z, and Jiang S (2018) Tissue mimicking materials in image-guided needle-based interventions: A review. Materials Science and Engineering: C 93:1116-1131.

[14] Zell K, Sperl J, Vogel M, Niessner R, and Haisch C (2007) Acoustical properties of selected tissue phantom materials for ultrasound imaging. Physics in Medicine and Biology 52(20):N475.

[15] Surry K, Austin H, Fenster A, and Peters T (2004) Poly (vinyl alcohol) cryogel phantoms for use in ultrasound and MR imaging. Physics in Medicine and Biology 49(24):5529.

[16] Adams F, Qiu T, Mark A, Fritz B, Kramer L, Schlager D, Wetterauer U, Miernik A, and Fischer P (2017) Soft 3D-printed phantom of the human kidney with collecting system. Annals of Biomedical Engineering 45(4)963-972.

[17] Lurie KL, Smith GT, Khan SA, Liao JC, and Ellerbee AK (2014) Three-dimensional, distendable bladder phantom for optical coherence tomography and white light cystoscopy. Journal of Biomedical Optics 19(3):036009.

[18] Öpik R, Hunt A, Ristolainen A, Aubin PM, and Kruusmaa M (2012) Development of high fidelity liver and kidney phantom organs for use with robotic surgical systems. IEEE RAS & EMBS International Conference on Biomedical Robotics and Biomechatronics:425-430.

[19] van Gerwen DJ, Dankelman J, and van den Dobbelsteen JJ (2012) Needle–tissue interaction forces – A survey of experimental data. Medical Engineering & Physics 34(6):665-680.

PART A

DESIGN CONSIDERATIONS FOR NOVEL NEEDLES

1

1

Needle placement errors: do we need steerable needles in interventional radiology?

Tonke L. de Jong, Nick J. van de Berg, Lisette Tas, Adriaan Moelker, Jenny Dankelman, John J. van den Dobbelsteen

Published in Medical Devices: Evidence and Research (2018)

"This dissertation aims to improve needle placement in interventional radiology. Part A presents the research that is needed to define relevant design considerations for novel needles. First, this chapter points out the challenges in needle placement in interventional radiology and explores the clinical need for steerable needles, thereby asking medical experts' view by using a questionnaire. It also paves the way for the research presented in the next chapters."

ABSTRACT – Accurate and precise needle placement is of utmost importance in interventional radiology. However, targeting can be challenging due to e.g. tissue motion and deformation. Steerable needles are a possible solution to overcome these challenges. The present work studied the clinical need for steerable needles. Three sub-questions were aimed to be answered: 1) What are the current challenges in needle placement? 2) What are allowable needle placement errors? and 3) Do current needles need improvement and would steerable needles add clinical value?

A questionnaire was conducted at the Annual Meeting of Cardiovascular and Interventional Radiology Society of Europe (CIRSE) in 2016. In total, 153 respondents volunteered to fill out the survey, among them 125 (interventional) radiologists with experience in needle placement.

Results are as follows: 1) Current challenges in needle placement include patient-specific and technical factors. Movement of the target due to breathing makes it most difficult to place a needle (90%). 2) The mean maximal allowable needle placement error in targeted lesions is 2.7mm. A majority of the respondents (85%) encounter unwanted needle bending upon insertion. The mean maximal encountered unwanted needle bending is 5.3mm. 3) Needles in interventional radiology need improvement, e.g. improved needle visibility and manipulability, according to 95% of the respondents. Added value for steerable needles in current interventions is seen by 93% of the respondents.

In conclusion, steerable needles have the potential to add clinical value to radiologic interventions. The current data can be used as input for defining clinical design requirements for technical tools, such as steerable needles and navigation models, with the aim to improve needle placement in interventional radiology.

Abbreviations radiologic interventions

PTC Percutaneous Transhepatic Cholangiography
TIPS Transjugular Intrahepatic Portosystemic Shunt

1.1. INTRODUCTION

In interventional radiology, needles are placed under image guidance into organs to treat or diagnose patients, e.g. in thermal ablation and biopsy procedures, respectively. However, accurate and precise needle placement is challenging, due to several patient-specific and technical factors, such as tissue motion and deformation. Solutions to challenges in needle placement can e.g. be found in developments in imaging, improved instruments and guiding tools, and better training. One proposed technical innovation to overcome some of the challenges in needle placement, and thus decreasing the needle placement error in interventional radiology, is a *steerable needle*. Such a needle would not only help in decreasing the placement error, but also in reducing the number of punctures and lowering the overall procedure time.

1.1.1 Background steerable needles and mechanisms

Several medical engineering research groups are working on the development of steerable needles. According to research, these needles can be used to correct for unwanted needle bending and lesion motion [2][3], actively steer around anatomical obstacles, or even reach anatomical targets that are not accessible using conventional needles [4][5].

An extensive review on design choices in needle steering is given by van de Berg et al. [1]. *Figure 1.1* shows various passive and active needle steering mechanisms. Examples of passive steering mechanisms are manipulation at the base of the needle and asymmetric bevel tip needles. Examples of active mechanisms include pre-curved needle stylets, active cannulas, programmable bevel tips and tendon actuated active needle tips In addition, an overview of needle-like instruments for steering through solid organs is given by Scali et al. [6].

Examples of three steerable needle prototypes with tendon actuated active needle tips are given in *Figure 1.2*. Typically, these needles can be manipulated at the base of the needle to change the direction of the needle tip, where after the shaft of the needle follows upon insertion. They range from 0.8mm to about 3mm in diameter
and have roughly the same diameter as needles that are currently clinically used in interventional radiology (~0.5-2.5mm). Steerable needle prototypes can either be manually inserted (e.g. [7-9]), robotically controlled (e.g. [10][11]), or inserted with a hybrid approach (e.g.[12][13]).

Steerable needles have mostly been tested in experimental settings with the use of a phantom material or animal tissue. For example, Majewicz et al. [14] studied the

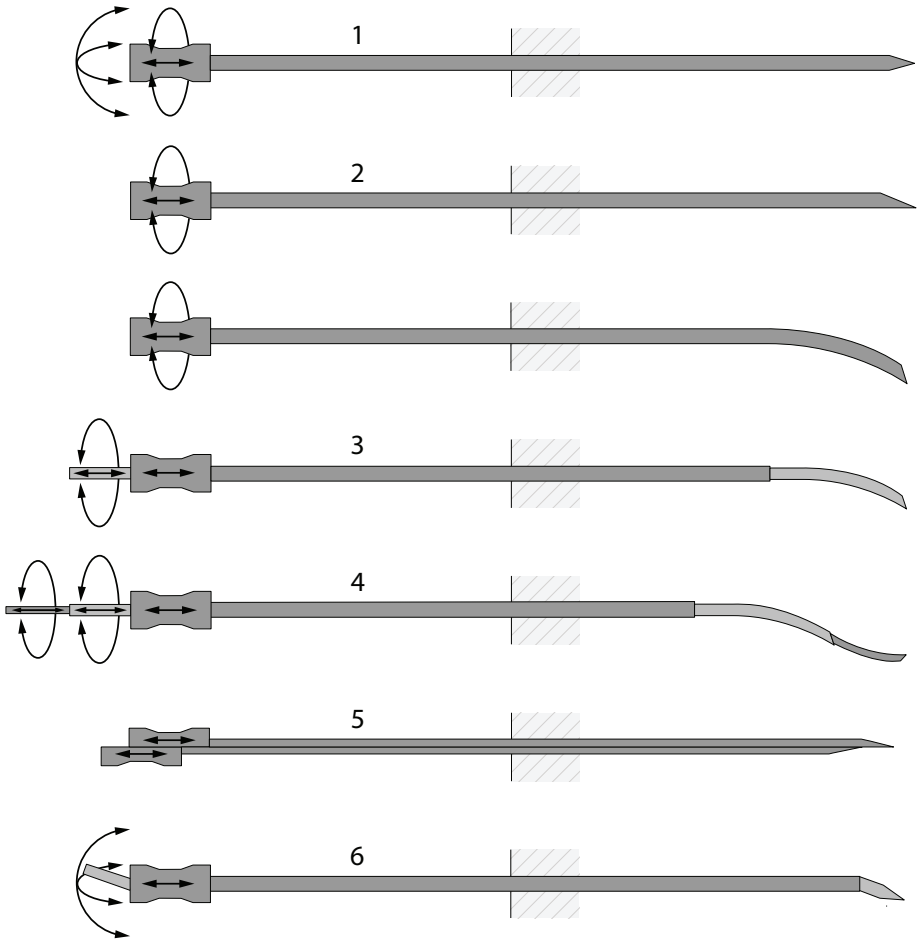

Figure 1.1. *Examples of steerable needles and their degrees of freedom in actuation. The depicted techniques are: 1) base manipulation, 2) bevel tip with and without precurve, 3) precurved stylet, 4) active cannula, 5) programmable bevel, and 6) tendon actuated tip steering. Picture retrieved from review article on design choices in needle steering [1].*

Figure 1.2. *Examples of steerable needle prototypes – a) a steerable needle with stainless steel segments, b) an MRI compatible steerable needle, and c) a needle with a steerable tip positioned on top of a miniature ball joint. [all prototypes designed and fabricated in the MISIT lab of the Delft University of Technology, The Netherlands].*

repeatability of tip-steerable needle insertions in ex-vivo and in-vivo canine prostate, kidney and liver tissue. On top of that, some experiments have been performed in a clinical environment. Podder et al. [15] studied the dosimetric benefit of a curvilinear distribution of seeds for low-dose-rate prostate brachytherapy, by inserting the seeds using a smart bevel tip needle into patients. Furthermore, Murphy et al. [16] described the novel use of a curved steerable needle to access symptomatic osseous lesions in the pelvis and sacrum of seven patients.

1.2.2 Rationale and goal

Nowadays, steerable needles are technically feasible to make and produce. However, the current general purpose steerable needle may not be the optimal solution, as a result of 1) the wide variety of clinical tasks in which needles are used in interventional radiology, 2) the case-specific level of task difficulty, and 3) the physiological and anatomical variations within and among patients. Instead, specialized instrument designs may have to be developed to aid specific clinical tasks. To develop such *clinically relevant* technical tools to improve needle placement, we need more insight into the clinical practice: the challenges in needle placement, the magnitude of needle placement errors, and the difficulties in interventions. The clinical view of experts on this matter is crucial for defining the proper indications for needle steering in clinical practice, but also for retrieving the right design criteria for these needles.

Therefore, the goal of the current study is to provide insight into the experts' view on needle placement errors in interventional radiology and their view on the clinical applicability of steerable needles, by means of a questionnaire. The main question that is aimed to be answered is as follows: Is there a clinical need for steerable needles in interventional radiology? This question was divided into three sub-questions:

1. What are the challenges in needle placement in interventional radiology?
2. What is the acceptable needle placement error in current clinical practice?
3. Do current needles in interventional radiology need improvement, and when and where would steerable needles add clinical value?

1.2. MATERIALS AND METHODS

1.2.1 Research tool and respondents

A questionnaire was constructed by medical engineers and pre-tested by interventional radiologists. A summarized version of the questionnaire can be found in *Figure 1.3*. The questionnaire was divided in accordance to the sub-questions. The section focused on the added value of steerable needles was only filled out by the respondents that shared the opinion that steerable needles would be of added value. All questions were multiple choice, with the ability to add comments, if necessary. Questions regarding the opinion of the respondents were either yes/no questions, or Likert-type (ordinal

Current challenges in needle placement

- Which technical factors make it difficult to reach a target? (LIKERT)
    - Unwanted needle bending
    - Limited imaging possibilities
    - Poor visibility of the needle
- Which patient specific factors make it difficult to reach a target? (LIKERT)
    - Movement of the target due to needle insertion
    - Movement of the target due to breathing
    - Intervening anatomy between target and needle tip

Needle placement accuracy, precision and bending

- What is the maximal allowable needle placement error in targeted lesions?
- Do you experience unwanted needle bending in interventions?
- In which procedures do you experience unwanted needle bending?
- What is the maximal unwanted needle bending you have encountered?

Current needle design and steerable needles

- Do current needles in interventional radiology need improvement?
- Needles in interventional radiology schould have (LIKERT):
    - Improved visibility
    - Improved manipulability/mobility
- Do you see added value for steerable needles in interventional radiology?
- The added value of a steerable needle is its ability to (LIKERT):
    - Steer around obstacles
    - Correct for unwanted needle bending to steer actively towards the target
- What would be your preferred method of actuation? Manual/Robotic?
- For which specific interventions a steerable needle would be of added value?
- How advantageous would a steerable needle be for targeted lesions in:
    - Breast/kidney/liver/lung/pancreas/prostate/soft tissue (LIKERT)
- Steerable needles will make new interventions possible (LIKERT)

Figure 1.3. *Summarized version of the questionnaire.*

data) questions with five items.

The questionnaire was conducted at the Annual Meeting of Cardiovascular and Interventional Radiology Society of Europe in 2016, at the technical exhibition. Visitors were asked to fill out the questionnaire and were told that the study investigated the

view of clinical experts on needle placement in general and their view on the clinical applicability of steerable needles. In addition, a demonstration of several steerable needle prototypes was given, to familiarize the participants with this concept. Potential participants were approached personally. Data were collected by self-completion of paper questionnaires with the surveyors present.

Review for this research by an institutional review board and written informed consent from the respondents was not required, as we did not record any personal details of the respondents. Furthermore, all data were anonymously processed and archived to ensure privacy of the respondents.

1.2.2 Data analysis

Response data were analyzed using Matlab 2016b. All (sub)questions were checked on missing data. The percentage of missing data was calculated per question and reported when higher than 20%.

Ordinal Likert-type data are displayed using diverging stacked bar charts. Row counts, i.e. the number of radiologists that answered the specific question, are provided for each individual sub-question. Answers were sorted based on the frequencies of positive answers.

Unequal interval data are presented using frequency density histograms with different bin width. Means were calculated by multiplying the central x-values of the bin width to the corresponding frequency, after which the summation of these products were divided by the total number of respondents. The means were compared amongst sub-questions.

The data from the remaining multiple choice questions regarding clinical interventions are illustrated using bar graphs. Frequencies of the answers to the yes/no questions were calculated and are presented in text.

1.3. RESULTS

1.3.1 Descriptive statistics

In total, 153 persons filled out the questionnaire voluntarily. A majority of them were (interventional) radiologists with experience in needle placement (n = 125, 82%), and were included for further analysis. Other respondents included, but were not limited to, surgeons, medical doctors and students. The (interventional) radiologists consisted of participants from 40 different countries, with different levels of experience: they all had at least 1 year of experience, whereas 50% of the respondent group had over 10 years of experience.

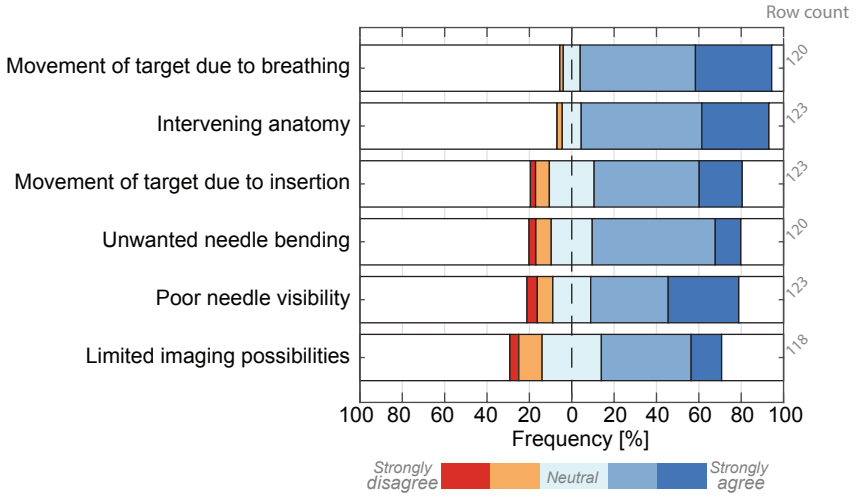

Figure 1.4. *The extent of agreement on: "Which factor makes it difficult to reach a target?"*

1.3.2 Challenges in needle placement

Respondents experience challenges in needle placement in interventional radiology. The overall agreement with each complicating factor is shown in *Figure 1.4*. These factors can be divided into patient-specific and technical factors. Examples of patient-specific characteristics that make it difficult to reach a target are: movement of the target due to breathing of the patient, intervening anatomy between needle tip and target (e.g. ribs and large blood vessels), and movement of the target upon needle insertion. Examples of technical factors are: unwanted needle bending/deflection inside tissue, poor needle visibility and limited imaging possibilities. The figure shows that 90% of the respondents (strongly) agree that the target reachability is complicated by target movements due to breathing, whereas 57% (strongly) agree that the current limits to imaging possibilities play a role. In general, patient-specific factors make it more difficult to reach a target than technical factors, according to the radiologists.

1.3.3 Needle placement errors

The aforementioned factors can contribute to needle placement errors, i.e. the difference between the needle tip position and its intended position. The respondents were asked to indicate the maximal allowed needle placement error when targeting lesions and to estimate the maximally encountered unwanted needle bending. The results are depicted in *Figure 1.5*. Three percent of the respondents indicated that zero error is accepted in needle placement. The mean maximal acceptable error was 2.7mm, as indicated by the circle in the figure. Significant unwanted needle bending in interventions is experienced by 85% of the respondents. The maximal encountered unwanted needle bending is shown in the same figure, by means of the pink bars. The

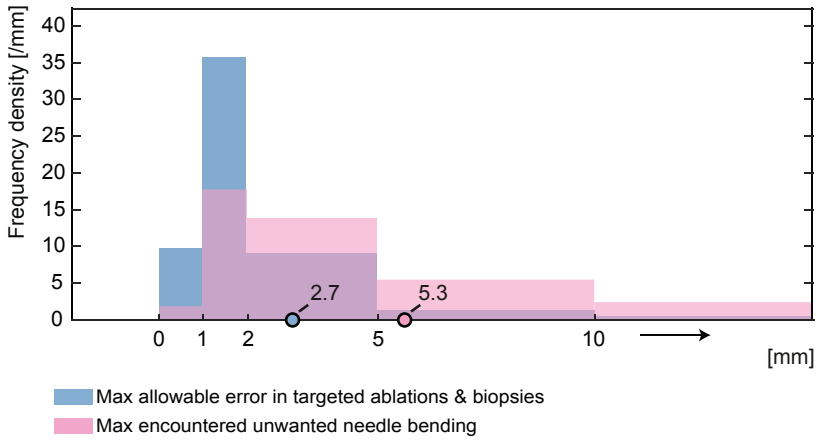

Figure 1.5. *Frequency density distribution of the maximal allowable placement error (mean 2.7mm) and the maximal encountered unwanted needle bending (mean 5.3mm).*

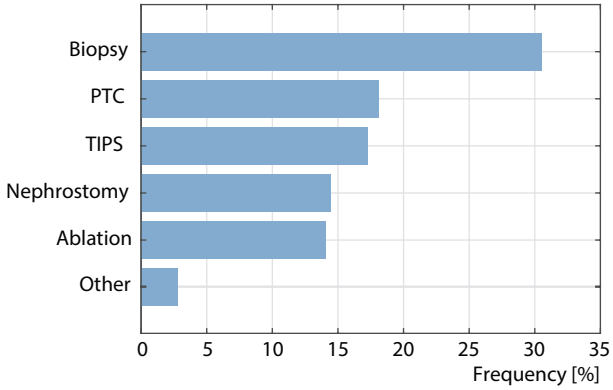

Figure 1.6. *Frequency bar chart of the interventions in which significant unwanted needle bending is encountered (n=125).*

mean maximal encountered unwanted needle bending in interventions was 5.3mm.

Figure 1.6 illustrates the procedures in which the respondents encounter significant needle bending. Biopsies were named the most (>30%), whereas the other procedures were relatively close to each other, and named less frequent.

1.3.4 Improving needles

Most radiologists (95%) share the opinion that current needles in interventional radiology need improvement. The respondents were asked to indicate the extent of their agreement on improvement aspects. In *Figure 1.7* it can be seen that within the respondent group, the desire for an improved needle manipulability/steerability was

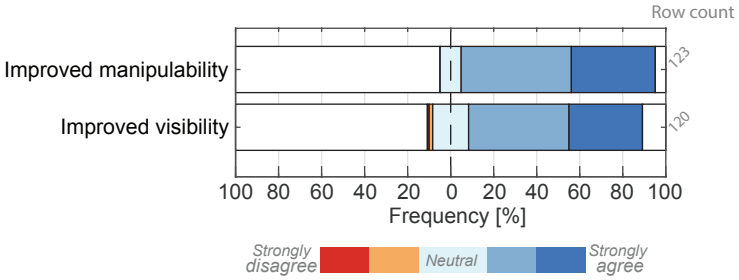

Figure 1.7. *The extent of agreement on "needles in radiology should have improved manipulability and/or improved visibility."*

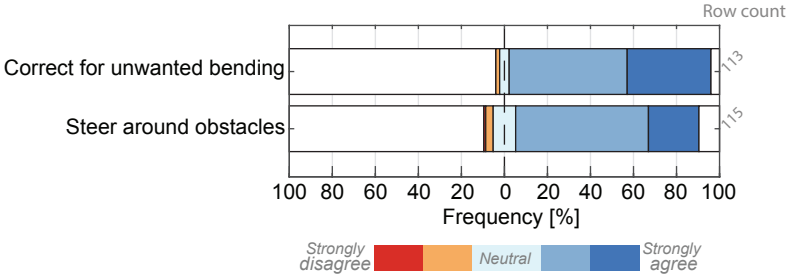

Figure 1.8. *The extent of agreement on "the added value of a steerable needle is its ability to correct for unwanted bending and/or steer around obstacles."*

even larger than the desire for an improved needle visibility. The percentages of the respondents that (strongly) agreed with these desires were 90% and 81%, respectively.

The majority of the respondent group (93%) see added value for steerable needles in interventional radiology. Their preferred actuation method for steerable needles would be manual (91%) in favor of robotic (9%). However, a preference, here, was indicated by only 42% of the respondents.

Figure 1.8 shows the added value of steerable needles, according the respondent group. The greater number of respondents (94%) agree to some extent that these needles would be helpful to correct for unwanted needle bending to steer actively towards the target, whereas 85% of the respondents agree on this for steering around anatomic obstacles.

In addition, the respondents were asked to assess the potential benefit of steerable needles for targeted lesions. Results are shown in *Figure 1.9*. According to the respondents, a steerable needle would be most advantageous for interventions in the liver (91% advantageous, 3% disadvantageous), and least advantageous for interventions in the breast (31% advantageous, 27% disadvantageous). Missing data of more than 20% were found for the prostate and breast.

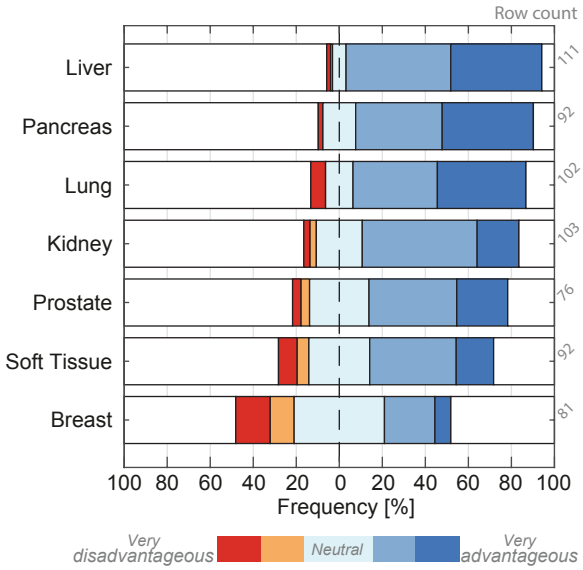

Figure 1.9. *The extent of agreement on "steerable needles would be advantageous for targeted lesions in the specified organs."*

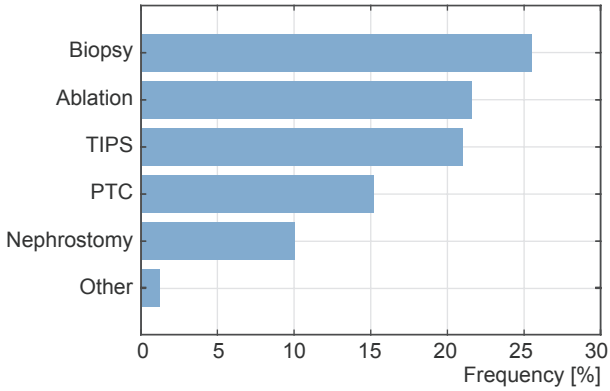

Figure 1.10. *Frequency bar chart of the interventions in which a steerable needle would be of added value (n=125).*

Figure 1.10 shows the respondents' view towards the question: "for which specific interventions would a steerable needle be of added value?". Most frequently named was the biopsy procedure, with 25.5%, whereas nephrostomy and others were named less frequent.

Finally, respondents were asked to what extent they agreed on the following statement: "Steerable needles would make new interventions possible", as shown in *Figure 1.11*. 75% of the radiologists (strongly) agreed on this, whereas 2% (strongly) disagreed.

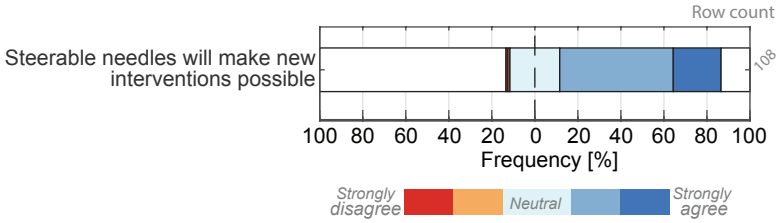

Figure 1.11. *The extent of agreement on "steerable needles would make new interventions possible."*

1.4. DISCUSSION

This is the first time, to the authors' knowledge, that a structured research has been carried out on the challenges in needle placement in interventional radiology, and the view of clinical experts on steerable needles, by means of a questionnaire. The present study revealed the most prevalent and important problems in needle placement in interventional radiology.

Limitations of the study should be taken into account when interpreting the results. First, no exact response rate could be given, due to the fact that the questionnaires were manually administered at the Annual Meeting of Cardiovascular and Interventional Radiology Society of Europe. Second, the respondents that were willing to fill out the questionnaire may be biased in favour of new technologies such as steerable needles. However, given the large number of respondents, it is assumed that the presented survey sample gives a representative image of the interventional radiologists' view.

Although most questions had high completion rates, the percentage of missing data was higher than 20% for the question regarding preferred actuation method for steerable needles. Moreover, the row counts for prostate, and breast, as shown in *Figure 8*, are below 80% (61% and 65%, respectively). Possible explanations could be the low familiarity with the associated interventions and/or definitions.

In the current large-scale questionnaire among radiologists, it has been demonstrated that the alleged minimally required accuracy for needle placement is not sufficiently reached in clinical practice. The respondents ranked possible factors that can contribute to needle placement errors. Among respondents, steerable needles were considered a viable alternative to improve current interventions.

It should be noted that the developments in image guidance systems needed for steerable needle imaging were not part of the focus of the presented work. Nonetheless, we stress the importance of reliable and robust imaging systems to be used with steerable needles, as these needles move out-of-plane in conventional two dimensional ultrasound imaging. We believe that 3D ultrasound will be a good solution to this problem, only if the resolution is improved. A recent study showed that needles with

arrays of kerfs, often found in compliant joint structures of tip-steered needles, have better contrast-to-noise ratio on ultrasound images than smooth surface needles [17]. Another solution would be automatic image guidance to keep the needle tip in plane [18].

The findings of the current study can guide medical engineers in their developments of technical tools to improve needle placement accuracy and precision in clinical practice. More specifically, this will result in improved understanding of the clinical context for engineers to work with, and could result in enhanced clinical design requirements for steerable needles and other technical tools in interventional radiology.

1.5. CONCLUSION

The answers to the questions stated in the introduction are as follows:

1. Challenges in needle placement in interventional radiology concern patient-specific and technical factors. Remarkably, the respondents found patient-specific factors more of a challenge than the technical factors. For people involved in the development of new medical tools for interventional radiology, the take-home message is therefore to focus not only on improving imaging quality and needle visibility, but also on finding solutions for patient-specific challenges. One could think of steerable needles that can be steered during insertion, but also path planners that incorporate breathing motion of the patient and tissue properties.

2. Significant unwanted needle bending is experienced by the majority of the interventional radiologists (85%). Unwanted needle bending complicates placing the needle at the right spot, induces re-puncturing, and thus increases procedure time. The mean maximal encountered unwanted needle bending in interventional procedures is 5.3mm. However, the mean acceptable needle placement error in targeted lesions is considered to be as small as 2.7mm. This implies that unwanted needle bending, which is only one complicating factor in needle placement, is higher than what is considered to be acceptable.

3. Current needles in interventional radiology need improvement, according to 95% of the (interventional) radiologists. One might think of improved manipulability/steerability, but also improved needle visibility. According to 93% of the respondents, steerable needles would be of added value in interventional radiology. More specifically, most clinical added value can be found for biopsies and ablations in livers. In addition to these conclusions, a majority of the interventional radiologists foresee that steerable needles would not only add clinical value to current procedures, but would also make new interventions possible.

All in all, we can conclude that steerable needles have the potential to add clinical value to current procedures, with the aim to improve needle placement in interventional radiology.

REFERENCES

[1] van de Berg NJ, van Gerwen DJ, Dankelman J, van den Dobbelsteen JJ (2015) Design choices in needle steering – a review. IEEE/ASME TRANSACTIONS ON MECHATRONICS 20(5):2172–2183.

[2] Webster III RJ, Memisevic J, Okamura AM (2005) Design considerations for robotic needle steering. Proceedings of the 2005 IEEE International Conference on Robotics and Automation:3588–3594.

[3] Kratchman LB, Rahman MM, Saunders JR, Swaney PJ, Webster III RJ (2011) Toward robotic needle steering in lung biopsy: a tendon-actuated approach. Proceedings of the Society of Photographic Instrumentation Engineers (SPIE), Medical Imaging: Visualization, Image-Guided Procedures, and Modeling 7964:79641I.

[4] Cowan NJ, Goldberg K, Chirikjian GS, et al. (2011) Robotic needle steering: design, modeling, planning, and image guidance. Surgical Robotics:557–582.

[5] Reed KB, Majewicz A, Kallem V, et al. (2011) Robot-assisted needle steering. IEEE Robotics and Automation Magazine 18(4):35–46.

[6] Scali M, Pusch TP, Breedveld P, Dodou D. (2017) Needle-like instruments for steering through solid organs: A review of the scientific and patent literature. Proceedings of the Institution of Mechanical Engineers Part H 231(3):250–265.

[7] Okazawa S, Ebrahimi R, Chuang J, Salcudean SE, Rohling R. Hand-heldsteerable needle device. IEEE/ASME Trans Mech. 2005;10(3):285–296.

[8] van de Berg NJ, Dankelman J, van den Dobbelsteen JJ (2017) Endpoint accuracy in manual control of a steerable needle. Journal of Vascular and Interventional Radiology 28(2):276–283

[9] Sears P, Dupont P. (2006) A steerable needle technology using curved concentric tubes. IEEE/RSJ International Conference on Intelligent Robots and Systems:2850–2856.

[10] Neubach Z, Shoham M (2010) Ultrasound-guided robot for flexible needle steering. IEEE Transactions on Biomedical Engineering 57(4):799–805.

[11] Gilbert HB, Neimat J, Webster III RJ (2015) Concentric tube robots as steerable needles: achieving follow-the-leader deployment. IEEE Transactions on Robotics 31(2):246–258.

[12] Rossa C, Tavakoli M (2017) Issues in closed-loop needle steering. Control Engineering Practice 62:55–69.

[13] Rossa C, Usmani N, Sloboda R, Tavakoli M (2017) A hand-held assistant for semiautomated percutaneous needle steering. IEEE Transactions on Biomedical Engineering 64(3):637–648.

[14] Majewicz A, Marra SP, van Vledder MG, et al. (2012) Behavior of tip-steerable needles in ex vivo and in vivo tissue. IEEE Transactions on Biomedical Engineering 59(10):2705–2715.

[15] Podder TK, Dicker AP, Hutapea P, Darvish K, Yu Y (2012) A novel curvilinear approach for prostate seed implantation. Medical Physics 39(4):1887–1892.

[16] Murphy DT, Korzan JR, Ouellette HA, Liu DM, Clarkson PW, Munk PL. (2013) Driven around the bend:

novel use of a curved steerable needle. Cardiovascular Interventional Radiology 36(2):531–535.

[17] van de Berg NJ, Sánchez-Margallo JA, Langø T, van den Dobbelsteen JJ (2018) Compliant joint echogenicity in ultrasound images: towards highly visible steerable needles. Medical Imaging: Image-Guided Procedures, Robotic Interventions and Modeling, International Society for Optics and Photonics 10576:105760X

[18] Kallem V, Cowan NJ (2009) Image guidance of flexible tip-steerable needles. IEEE Transactions on Robotics 25(1):191–196.

2

Needle deflection in thermal ablation procedures of liver tumors: a CT image analysis

Tonke L. de Jong, Camiel Klink, Adriaan Moelker,
Jenny Dankelman, John J. van den Dobbelsteen

Published in SPIE proceedings, Medical Imaging (2018)

"According to Chapter 1, the precision of needle placement is proved to be challenging due to, amongst other factors, unwanted needle deflection upon insertion. Bending of the needle inside the patient's body contributes to the total targeting error, and, therefore, decreases the positioning precision. However, the magnitude of deflection in current procedures is unknown. On that account, this chapter quantifies needle deflection in thermal ablation procedures of liver tumors. A large CT dataset, containing the shape of over 350 ablation needles, is used for the analysis."

ABSTRACT – Accurate needle placement is crucial in image-guided needle interventions. A targeting error may be introduced due to undesired needle deflection upon insertion through tissue, caused by e.g. patient breathing, tissue heterogeneity, or asymmetric needle tip geometries. This paper aims to quantify needle deflection in thermal ablation procedures of liver tumors by means of a CT image analysis.

Needle selection was done by using all clinical CT data that were made during thermal ablation procedures of the liver, ranging from 2008-2016, in the Erasmus MC, the Netherlands. The 3D needle shape was reconstructed for all selected insertions using manual segmentation. Subsequently, a straight line was computed between the entry point of the needle into the body and the needle tip. The maximal perpendicular distance between this straight line and the actual needle was used to calculate needle deflection.

In total, 365 needles were included in the analysis ranging from 14G to 17G in diameter. Average needle insertion depth was 95mm (range: 32mm – 182mm). Needle deflection was on average 1.3mm (range: 0.0mm – 6.5mm). 54% of the needles (n=196) had a needle deflection of more than one millimeter, whereas 7% of the needles (n=25) showed a large needle deflection of more than three millimeters.

Needle deflection in interventional radiology occurs in more than half of the needle insertions. Therefore, deflection should be taken into account when performing procedures and when defining design requirements for novel needles. Further, needle insertion models need to be developed that account for needle deflection.

2.1. INTRODUCTION

Liver cancer is the sixth most common cancer worldwide [1]. Radiofrequency (RF) and microwave (MW) ablation of the liver are treatment options for liver tumors when resection cannot be performed [2]. During this radiologic intervention, an electrode needle is placed into the liver to destroy the tumor by means of thermal energy. Accurate placement of the needle is important during these procedures, as inaccurate needle placement can result in decreased treatment efficiency and/or a prolonged procedure time due to an increased number of needle insertions.

Inaccurate placement of the needle tip during medical procedures, also known as needle-targeting error, is defined as the difference between the end-position of the needle and its intended position inside the patient's body. Abolhassani [3] previously summarized, in an extensive review on needle insertions into soft tissue, that such a targeting error may be caused by imaging limitations, image misalignments, human errors, target movement and needle deflection.

The focus of this study is on needle deflection, which is shown in *Figure 2.1*. Needle deflection is the deviation of the needle from its suspected straight insertion path. In other words; it is the bending of the needle inside the patient's body. This can be caused by multiple parameters, such as: patient's breathing, tissue heterogeneity, and asymmetric needle tip geometries. These parameters may cause an unequal force distribution along the shaft and/or tip of the instrument upon, or, in the specific case of breathing motion, also after needle insertion. The magnitude of needle deflection in current clinical radiologic interventions is unknown. Therefore, in the current paper, we aim to quantify needle deflection in thermal ablation procedures of the liver, by means of a CT image analysis.

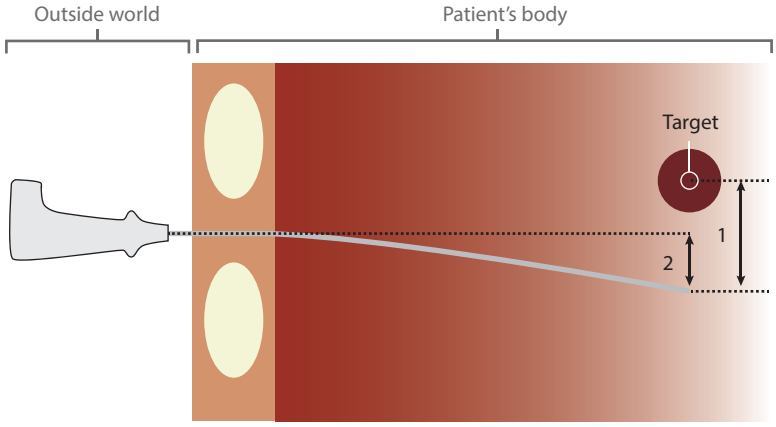

Figure 2.1. *Total needle targeting error and needle deflection. Needle deflection is the bending of the needle inside the patient's body and is one of the parameters that contributes to the total needle targeting error.*

2.2. METHODS

2.2.1 Needle selection

The needles used in the present study were retrieved from CT images made during radiofrequency ablation and microwave ablation procedures of the liver in the Erasmus MC of Rotterdam, the Netherlands, ranging from 2008 to 2016. All potentially relevant patient-IDs were identified from the Picture Archiving and Communication System (PACS) using the queries "RFA", "MW", "ablation", or "microwave" and were reviewed for the presence of CT images visualizing a needle. All CT data were anonymized upon extraction from the PACS system. The medical research ethics committee of the Erasmus University MC approved that the Medical Research Involving Human Subjects Act does not apply to this study and that no informed consent was required according to the local directives for retrospective studies (MEC-2015-414).

Computed tomography is frequently used when ultrasound appears to be insufficient in visualizing the tumor and surrounding structures. Often, multiple CT stacks are made during a thermal ablation procedure, depending on the need during the intervention. For example, CT scans can be made before the ablation starts and after the ablation to verify the needle tip position and ablation zone. One CT set of a procedure could involve multiple treated lesions, and thus multiple CT stacks that contain needles. Therefore, we systematically screened all patient scans for individual needles to be included in the analysis.

2.2.2 Needle shape reconstruction

Needle shape reconstruction was done with the axial plane CT images. The orientation of the needle with respect to these axial CT slices can either be parallel, perpendicular or oblique, as shown in *Figure 2.2*. In case of a parallel needle orientation, the needle is visible on one single axial CT slice. In case of a perpendicular oriented needle, the needle appears as a bright dot on multiple axial CT images.

Needle shape reconstruction was done using MeVisLab 2.7, a modular framework for image processing research and development, by making use of the Contour Segmentation Objects (CSO) library. Manual segmentation was chosen as it is still considered the gold standard in research and clinical practice over (semi)automatic segmentation [4]. The reconstruction method was dependent on the orientation of the needle with respect to the CT slices. In case of the parallel oriented needles, MeVisLab's CSOFreehandprocessor open spline module was used. Several seed points were manually placed following the needle shape. In case of the perpendicular and oblique needles, a point was placed in the middle of the bright shape visualizing that specific part of the needle. This was repeated for all slices that presented a bright shape. We started segmentation at the entry point of the needle inside the patient's body and ended at the needle tip.

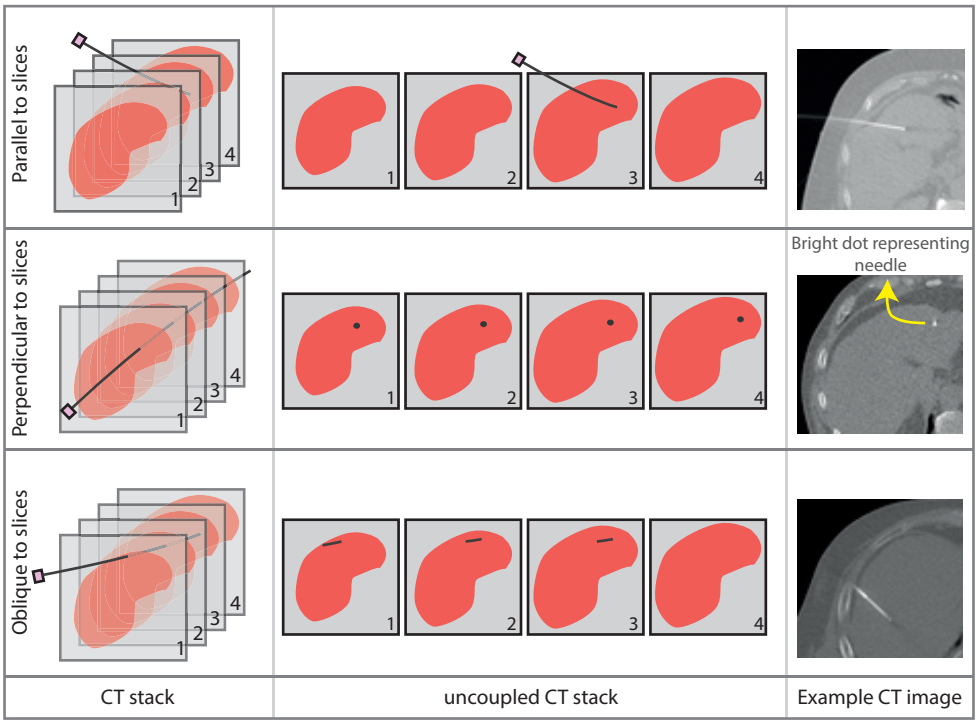

Figure 2.2. *Needle orientations with respect to the axial CT slices. The needle can either be projected parallel, perpendicular, or oblique.*

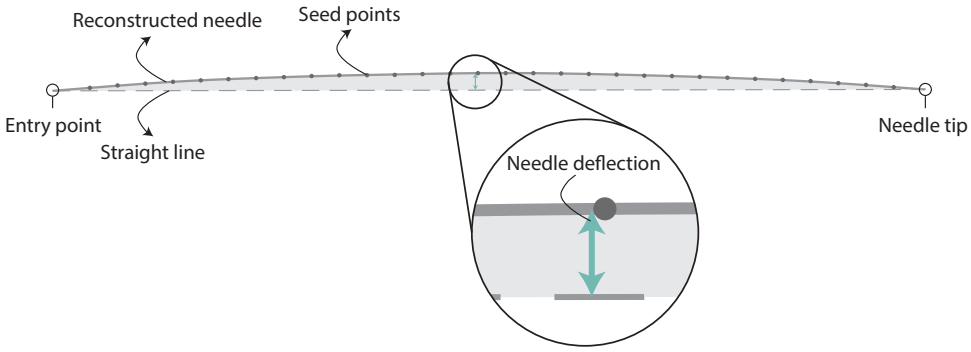

Figure 2.3. *Quantification of needle deflection. Needle deflection was defined as the maximal perpendicular distance between the reconstructed needle and a straight line interpolated between needle entry point and needle tip.*

The XYZ coordinates representing the needle shapes were stored in text files for further analysis, with X and Y being respectively the horizontal and vertical position on the CT slices, and Z being the depth of the CT slice with respect to the whole stack, all in millimeters.

2.2.3 Needle deflection quantification method

Quantification of needle deflection was done using MATLAB 2016b and shown in *Figure 2.3*. All needle coordinates were loaded, after which smoothing and spline interpolation were applied, respectively. Ideally, the contribution of needle deflection to the total needle targeting error would be calculated, as illustrated in *Figure 2.1*. However, extrapolation of a straight part of the needle was not always possible, due to the fact that there was not an existing straight part close to the needle entry point to extrapolate from. Therefore, a straight line was computed between the entry point of the needle into the body and needle tip. The maximal perpendicular distance in millimeters between this straight line and the actual needle was used as a measure to quantify needle deflection.

2.3. RESULTS

Figure 2.4 summarizes the systematic needle selection procedure for analysis in a flow diagram. The initial search in the PACS system resulted in 1749 potential relevant patient IDs, of which 1435 were excluded because no thermal ablation of the liver was

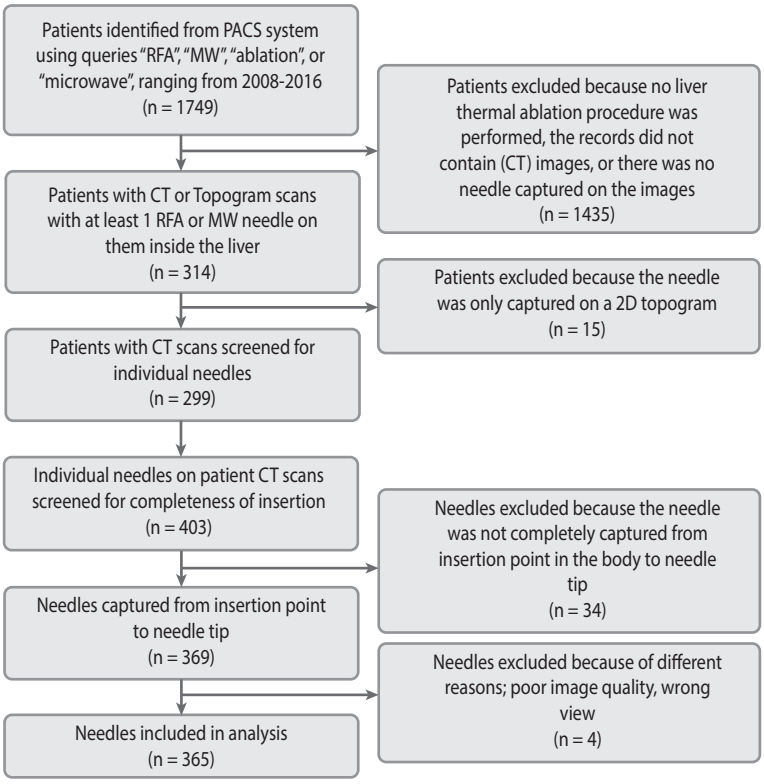

Figure 2.4. *Flow diagram of the systematic needle selection procedure for analysis.*

performed, the records did not contain medical images, or no needles were captured on any of the images. The remaining 314 patient records were screened for the presence of at least one needle on a CT image. Patients (n=15) were excluded as the needle was only captured on a 2D topogram, and not on CT images. Subsequently, the remaining 299 patients were screened for individual needles. The resulting 403 needles were checked for completeness of the needle visualization, i.e. from the entry point of the patient's body up to needle tip, due to which 34 needles were excluded from the analysis. Finally, four extra needles were excluded because of several reasons, such as poor image quality and sagittal capture instead of axial capture. This resulted in 365 individual needles that were included in the needle deflection analysis.

The analyzed needles were either 14G or 17G in diameter. The pixel resolution of the scans varied from 0.4mm to 1mm, whereas the slice thickness ranged from 0.8mm to 6mm. The kernel types that were used to scan ranged from B10f to B31f, i.e. body kernels with smooth images, good contrast detail and low noise level.

A scatterplot of the maximal needle deflection for all insertions with respect to needle insertion depth is shown in *Figure 2.5* (n=365). Overall, needle deflection tends to increase with insertion depth, as indicated by the positive slope of the linear least squares fit on the figure. The variability in needle deflection increases with increased insertion depth (i.e. heteroscedasticity). On average, the insertion depth was 95mm, ranging from 32mm to 182mm. Needle deflection was on average 1.3mm, ranging from 0.0mm to 6.5mm. In total, 54% of the needles (n=196) had a needle deflection of more

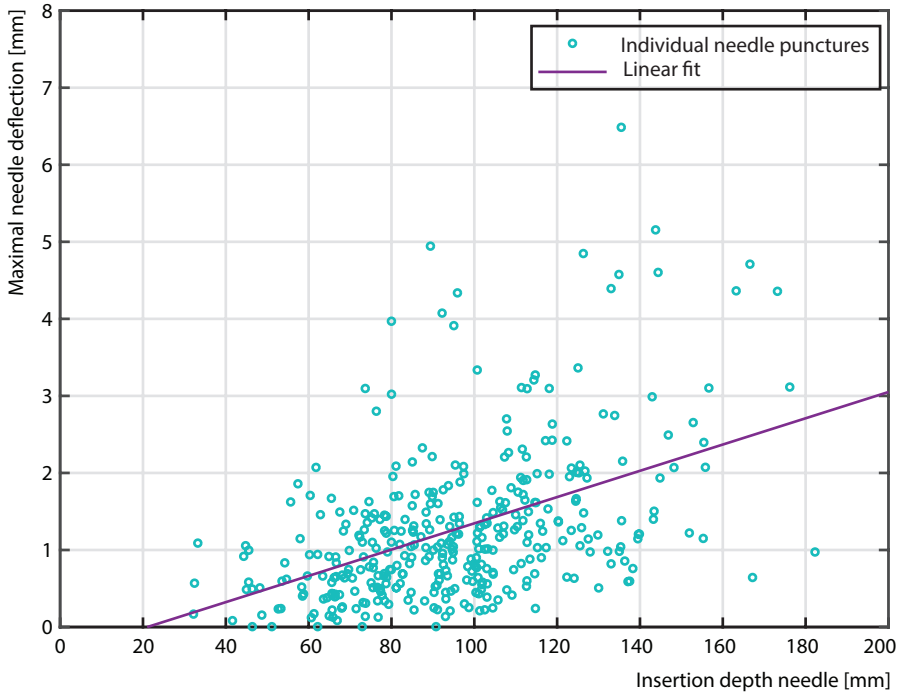

Figure 2.5. *Scatterplot of the maximal needle deflection of 365 needle insertion during thermal ablation procedures of liver tumors.*

than 1mm, whereas 7% of the needles (n=25) showed a needle deflection of more than 3 mm.

2.4. DISCUSSION AND CONCLUSIONS

Despite technological improvements in novel needle design, such as miniaturized steering mechanisms [5] and MRI compatibility [6], a number of clinical questions have remained regarding improved needles for interventional radiology. As a consequence, setting up relevant clinical design requirements for these needles is a challenge. The current work aimed to address one of the clinical questions: is undesired needle deflection an important factor in needle placement in interventional radiology, and what is its magnitude? This is the first time to the authors' knowledge, that needle deflection has been quantified using a large number of needle insertions in a clinical procedure.

Improving needle placement in interventional radiology can be achieved by different means. Examples are: better imaging equipment, improved training, and innovations in needle design. Currently, innovative needle designs focus on the steerability of needles, either manually or robotically inserted, aiming to steer towards a hard-to-reach target and possibly to avoid anatomical obstacles (e.g. [7-9]).

The present study found that needle deflection occurs in over half of the insertions (i.e. needle deflection > 1mm) during thermal ablation procedures of the liver, and is therefore an important parameter that contributes to the total placement error. Whereas a focus exists on actively steering around anatomical obstacles in current needle steering and modeling developments, the findings of the present study suggest that compensating for undesired needle deflection during straight insertion is also of importance. In other words: undesired needle deflection upon insertion should be taken into account, both when designing novel needles, as well as when developing steering algorithms for needle insertion systems and/or path planners, with the ultimate goal to improve needle placement accuracy and precision in interventional radiology.

REFERENCES

[1] Ferlay J, Soerjomataram I, Dikshit R, et al. (2015) Cancer incidence and mortality worldwide: Sources, methods and major patterns", International Journal of Cancer 136:E359-E86.

[2] McDermott S, Gervais DA (2013) Radiofrequency ablation of liver tumors. Seminars in Interventional Radiology 30:49-55.

[3] Abolhassani N, Patel R, Moallem M (2007) Needle insertion into soft tissue: A survey. Medical Engineering & Physics 29:413-31.

[4] Gotra A, Sivakumaran L, Chartrand G, et al. (2017) Liver segmentation: indications, techniques and future directions", Insights into Imaging 8(4):377-392.

[5] Okazawa S, Ebrahimi R, Chuang J, Salcudean SE, Rohling R (2005) Hand-held steerable needle device", IEEE/ASME Transactions on Mechatronics 10:285-96.

[6] Krieger A, Song SE, Cho NB, et al. (2013) Development and evaluation of an actuated MRI-compatible robotic system for MRI-guided prostate intervention. IEEE/ASME Transactions on Mechatronics 18:273-84.

[7] van de Berg NJ, Dankelman J, van den Dobbelsteen JJ (2015) Design of an actively controlled steerable needle with tendon actuation and FBG-based shape sensing. Medical Engineering & Physics 37:617-22.

[8] Alterovitz R, Goldberg K, Okamura AM, (2005) Planning for steerable bevel-tip needle insertion through 2D soft tissue with obstacles. Proceedings of IEEE International Conference on Robotics and Automation:1640-1645.

[9] Abayazid M, Kemp M, Misra S (2013) 3D flexible needle steering in soft-tissue phantoms using Fiber Bragg Grating sensors. Proceedings of IEEE International Conference on Robotics and Automation:5843-5849.

3

CT-based numerical analysis of the reachability of needle targets in the liver

Tonke L. de Jong, Nick J. van de Berg, Adriaan Moelker,
Jenny Dankelman, John J. van den Dobbelsteen

Submitted (2019)

"Chapter 2 quantified needle deflection in thermal ablation procedures of liver tumors and revealed that it occurs in over half of the insertions. This result underlines the need for novel needles that are able to correct for small deviations from the intended straight insertion path. Additionally, another important question remains: are all parts in the liver reachable with a conventional needle? The current chapter studies the reachability of needle targets in the liver based on CT scans of patients, and accounts for state of respiration"

ABSTRACT – Accurate needle placement in the liver is challenging. The purpose of this research was to identify the reachability of liver regions in needle-targeting by numerical analysis and to compare this to expert views.

The liver volumes and surrounding anatomical structures were segmented from CT datasets of four patients that were obtained during both inspiration and expiration. Each liver volume was divided in potential targets, for which reachability was quantified by the number of unobstructed needle paths, divided by the total number of paths, simulated by ray casting from target-to-skin.

The simulation showed that reachability was low (<10%) in the cranial and posterior parts of the liver, and right behind the ribs. This aligned with interventional radiologist views (n=22), who indicated that liver segments I, VII and VIII are hard-to-reach. Mean target reachability was less during expiration (mean: 22%, range: 20%-24%) than during inspiration (mean: 26%, range: 21%-32%), showing that breathing can influence the target reachability.

The results of this study provide general insight into relations between the reachability of liver regions and topology, and the proposed methods can help in optimizing patient-specific planning, in terms of instrument choice and needle targeting approaches in interventional radiology.

3.1. INTRODUCTION

Liver cancer is in the top five of the most common causes of cancer death worldwide [1]. Many liver cancer patients require radiologic interventions in which needles are inserted, for example when taking biopsies, accessing blood vessels or bile ducts, and ablating tumors. Access to hepatic structures is percutaneously acquired via straight needle insertion under image guidance. Accurate needle tip placement in the target is of utmost importance.

Interventional radiologists indicate that certain regions in the liver are difficult to reach with a needle. Multiple attempts are often required to place the needle accurately, which results in prolonged procedure time, an increase in radiation dose for the patient, and a higher risk of complications. Especially lesions in the superior portion of the liver, adjacent to the diaphragm, present challenges, as described in [2]. These lesions require long needle insertion trajectories, and important anatomical structures can obstruct the insertion path, such as the rib cage and lungs. Moreover, breathing causes the liver to move, not only with respect to the outer world, but also relative to its surrounding anatomical structures.

Albeit being recognized and described as challenging, the reachability of liver regions in needle-targeting have never been quantified and studied in detail. An improved understanding of the liver and target topology is essential to estimate procedural complexities and risks, increase needle placement accuracy and lower the number of puncture attempts in interventional radiology.

Therefore, the aim of the current work is to identify reachability of liver regions in needle targeting during inspiration and expiration. We numerically analyze all possible needle paths for the whole liver volume, that was segmented from CT data of patients, and quantify reachability. Results from these simulations were compared with a survey among interventional radiologists on perceived hard-to-reach locations in the liver in needle targeting.

In the current study, reachability is quantified by determining the fraction of rays that adequately reaches the skin from each possible target using ray casting from target-to-skin as a collision detector. Ray casting is a method that has been used in needle trajectory planners (e.g. [3-10]). For instance, Villard et al.[3], Baegert et al. [4,5], and Seitel et al. [6] proposed methods to assist physicians in planning percutaneous radiofrequency ablation of liver tumors. For each face of the skin's surface mesh, a needle trajectory was constructed and considered to be valid if the needle does not cross any organ on its way towards the target [5], i.e. ray casting from skin-to-target. However, these planners aim to optimize the needle insertion point, angle and depth to reach a single target, instead of mapping the reachability for the whole liver volume. Here we use ray casting from target-to-skin to get an estimate of the reachability of targets within different liver regions.

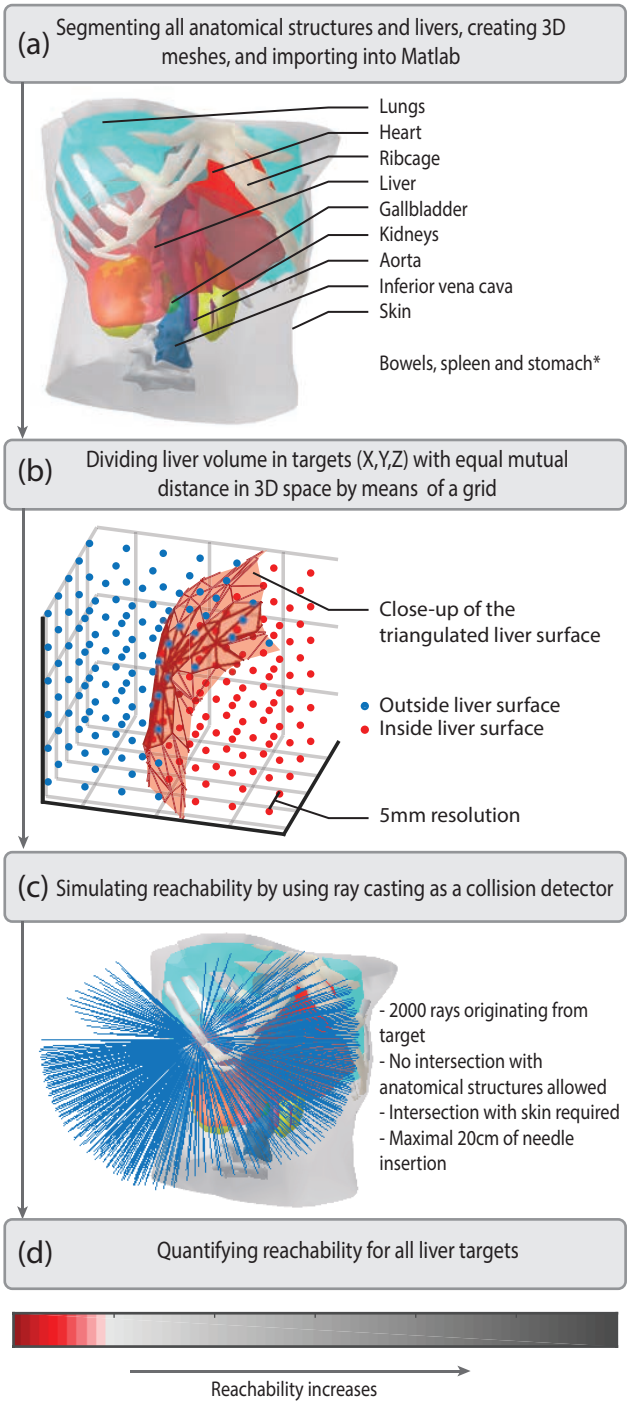

Figure 3.1. *Approach in identifying the reachability of liver regions. (a) Creating computer model by CT image segmentation. (b) Dividing the liver in equally spaced targets. (c) Simulating reachability per target. (d) Quantifying reachability for all targets.*
**Not depicted to ensure a clear visualization.*

3.2. MATERIALS AND METHODS

A number of steps were taken to identify the reachability of liver regions during inspiration and expiration. *Figure 3.1* shows an overview of the adopted approach. First, livers and critical anatomical structures were segmented from a CT dataset of four patients, by applying a region growing method and manual segmentation (*Figure 3.1a*). Second, the liver volume was divided into equally spaced points (*Figure 3.1b*), each representing a possible target location. Rays were constructed with the target as origin and the end points of the rays equally distributed on a sphere. The reachability per target was then simulated by applying ray casting as a collision detector of obstructions, with the rays being the simulated needle trajectories, and the obstructions being the anatomical objects. (*Figure 3.1c*). Finally, the reachability was quantified for all these targets (*Figure 3.1d*), defined as the percentage of rays that reach the patient's skin without piercing critical anatomical structures with respect to the total number of rays. Results were displayed for all targets, with shades of gray representing high reachability (dark gray) and low reachability (white). The targets that could only be reached with 10% or less of the total numbers of rays were displayed with shades of red.

3.2.1 CT Dataset and segmentation

The clinical CT datasets were retrieved from the picture archiving and communications system (PACS) of the Erasmus MC of Rotterdam, the Netherlands. The study population included patients that were suspected of having mesenteric ischemia due to median arcuate ligament syndrome. These patients underwent computed tomographic angiography in both inspiration and expiration for detection of coeliac artery compression by the median arcuate ligament. The datasets were useful for our purposes because they contained both breathing phases. All data were processed and archived anonymously, and patient privacy was ensured. The medical research ethics committee of the Erasmus University MC approved that the Medical Research Involving Human Subjects Act did not apply to this study and that no informed consent was required according to the local directives for retrospective studies (MEC-2016-241). The CT scans were high resolution, with a minimal resolution of 0.72mm/pixel, and a maximal slice thickness of 0.50mm.

The dataset contained four patients (3 male, 1 female). Liver and rib cages during inspiration and expiration were semi-automatically segmented for a study on the design and validation of a PVA liver phantom with respiratory motion for needle-based interventions [11], using 3D slicer 4.8.1 [12] (https://www.slicer.org), and post-processed with Meshlab [13]. The resulting 3D triangulated surface models were stored *Open Access* and can be found online at [14]. In addition to the liver and rib cage, the following critical anatomical structures were segmented for the current study: aorta, bowels, spleen and stomach, gallbladder, heart, inferior vena cava, kidneys, lungs, and skin. The same methods for image segmentation were used, as described in [11], including segment editor modules for the manual (Draw, Paint) and automated (Grow from Seeds) parts of the segmentation. All 3D triangulated surface models have

been made available at [15], and were imported into Matlab 2017b (The Mathworks Inc, Natick, Massachusetts, United States) for further analysis. An example of the segmented structures of one patient during expiration can be seen in *Figure 3.1a*.

The segmented livers varied in shape and size [11]. On average, they measured 198mm in left-right (range: 180mm-223mm), 160mm in posterior-anterior (range: 119mm-200mm), and 161mm in cranial-caudal (range 142mm-178mm) view. A detailed analysis of the movement of the livers during inspiration and expiration is given in [11]. From the state of expiration to inspiration, the livers moved predominantly to the right, anterior and caudal direction.

3.2.2 Dividing the liver volume in targets

From a clinical point-of-view, a lesion can occur in all parts of the liver. Therefore, reachability should be simulated for all these targets. A 3D rectangular grid with equally spaced points (resolution of 5mm) was created around the segmented liver. Each point was checked for being inside, or outside the 3D triangulated surfaces of the segmented liver (*Figure 3.1b*). Points inside the liver were referred to as targets and used for further analysis.

3.2.3 Reachability: Ray casting as a collision detector

Reachability was simulated using ray casting as a collision detector of critical anatomical structures (objects) along needle insertion paths (rays) (*Figure 3.1c*). We applied hard constraints only to determine reachability. No intersection was allowed with anatomical structures, apart from the skin.

First, rays were simulated with the target point as origin (target-to-skin). Ray end points were uniformly distributed over the surface of a sphere, with radius 200mm. This radius represents the modeled needle length. A variety of algorithms has been proposed for the explicit construction of such points, as discussed in [16]. We applied a Fibonacci lattice using the golden ratio and golden angle [17].

Golden ratio (φ) and golden angle (α) are given by:

$$\varphi = \frac{(1 + \sqrt{5})}{2},$$

$$\alpha = 2\pi\left(1 - \frac{1}{\varphi}\right)$$

Using spherical coordinates (θ, ρ), $0 \leq \theta \leq \pi$, and $0 \leq \rho \leq 2\pi$, we set:

$$\theta_i = \arccos\left(1 - \frac{2i}{(N-1)}\right), \qquad 1 \leq i \leq N$$

$$\rho_i = i\alpha,$$

with i being the i^{th} end point of the ray, and N being the total number of rays originating from the liver point. We set N=2.000.

Second, the Möller-Trumbore ray-triangle intersection algorithm [18], implemented by Tuszynski [19], was used to calculate the intersection between the rays and the triangular meshes representing the surfaces of the anatomical objects. Given the inputs rays' origins (O) and normalized directions (D), and triangle vertices (V0, V1, and V2), the function solves:

$$[-D,\ V_1 - V_0\ ,V_2 - V_0\ ]\begin{bmatrix} t \\ u \\ v \end{bmatrix} = O - V_0\ ,$$

with (u,v) being the barycentric coordinates, and t the distance from the ray origin to the intersection point. Rays do intersect with the triangle if u ≥ 0, V ≥ 0 and u+v ≤ 1. This method is geometrically depicted in *Figure 3.2*, translating the triangle to the origin, after which it is transformed to a unit triangle in *y* and *z*, with the ray direction aligned in *x*.

Rays that intersected with anatomical objects were disregarded. The remaining rays were checked for intersection with the skin (*Figure 3.1c*). Subsequently, a reachability percentage was calculated for the targets, by dividing the possible needle paths by the total number of rays. A reachability of 100% implies that the target can be reached with all simulated needle insertions of 200mm, whereas 0% means that the target cannot be reached. Reachability was computed for all targets of the four livers during inspiration and expiration.

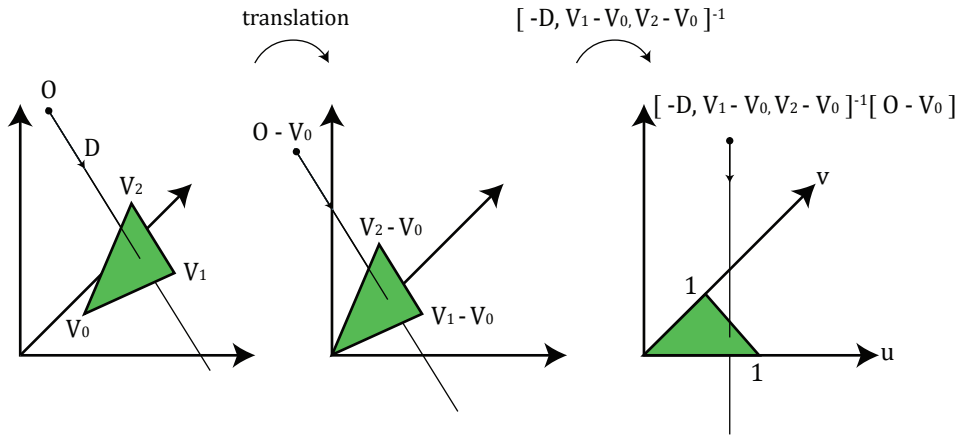

Figure 3.2. *Translation and change of the base of the ray's origin. Adapted from [18].*

3.2.4 Survey – interventional radiologists

A questionnaire was sent to 53 Dutch interventional radiologists via e-mail in 2016. In total, 22 of the experts responded (42% response rate). The interventional radiologists were asked for their opinion on the hard-to-reach liver segments with a needle, according to Couinaud's classification of liver anatomy. More than one segment could be indicated and additional comments could be given. Data were handled confidentially and anonymously. Descriptive statistics were used to analyze the data.

3.3. RESULTS

3.3.1 3D data availability

The computed reachability data for the four livers during inspiration and expiration are three-dimensional. The reader is referred to the supplementary online dataset [20] to review the 3D data, containing: 1) the 3D models of the reachability of the livers as Matlab figures and as U3D files, 2) the workspaces from Matlab that contain all the raw reachability data, and 3) the Matlab script to perform the 3D data visualizations.

3.3.2 Numerical analysis reachability

Figure 3.3 shows illustrative examples of specific targets with high to low reachability. The first target has a reachability of 55%, the second of 24%, and the third of 5%. Certain targets can be reached from both the anterior and posterior part of the body, which is illustrated by *Figure 3.4*.

An overview of the reachability for the livers' surface is given in *Figure 3.5*. Mean reachability for the livers was 22% (range: 20%-24%) during expiration and 26% (range: 21%-32%) during inspiration. Mean percentage of targets with the low reachability with respect to the total number of targets during expiration was 6.0% (range: 1.2%-7.7%) and 4.1% (range: 0.0%-8.2%) during inspiration.

The low reachability targets were mainly found in the cranial and posterior parts of the liver, and right behind the ribs. A blue rectangle outlines the size and position of the livers during expiration. The same outline is shown in the inspiration phase, providing a reference for relative liver motion and deformation during breathing.

Figure 3.6 is an example of a laminated view of one of the livers, which allows for visual inspection of the data inside the liver volume. The volume is divided in five equally spaced slices with a margin of 20mm at the front and back. The targets with lowest reachability were mainly positioned on the outer shell of the liver, whereas the targets inside the liver volume did not have large differences in reachability.

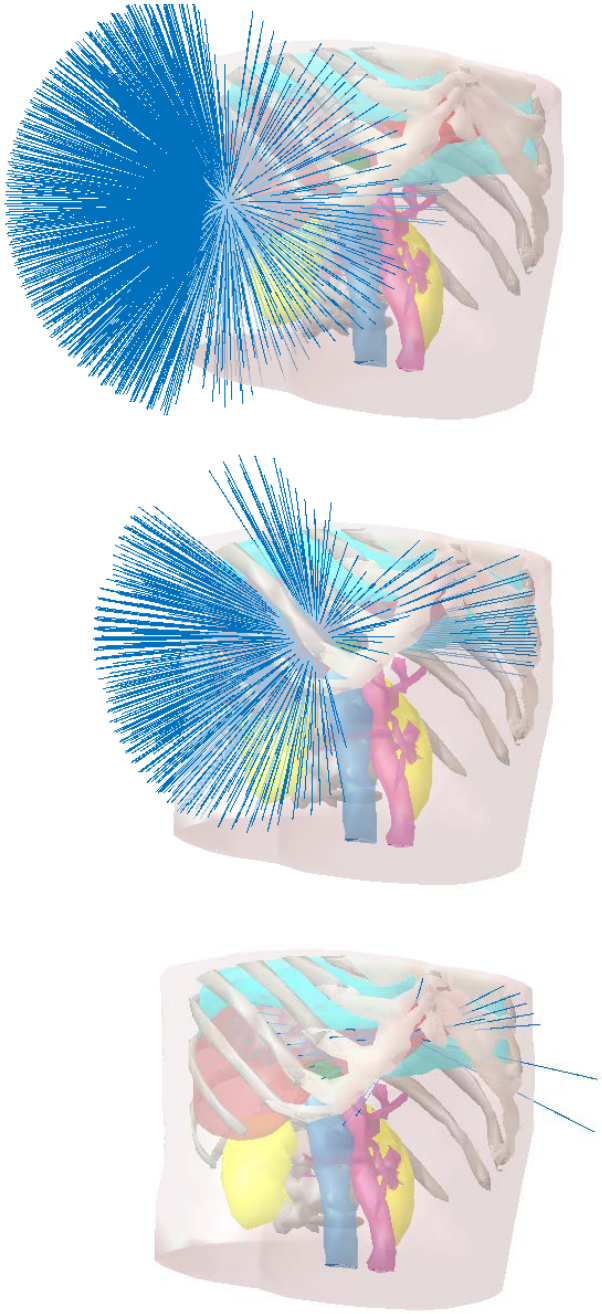

Figure 3.3. *Illustrative examples of targets with a reachability of 55%, 24%, and 5%, from top to bottom respectively.*

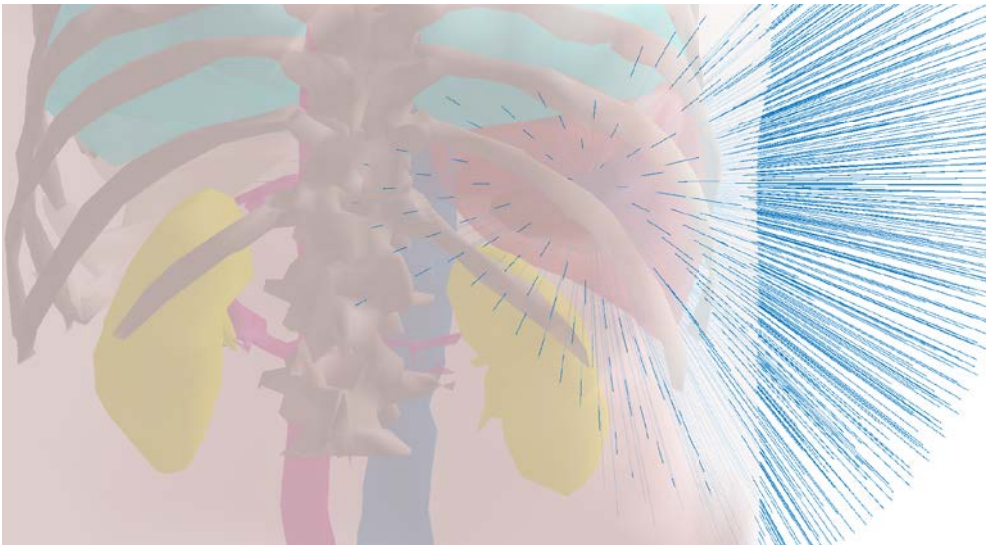

Figure 3.4.*Illustrative example of a target that is theoretically reachable via the back of the patient.*

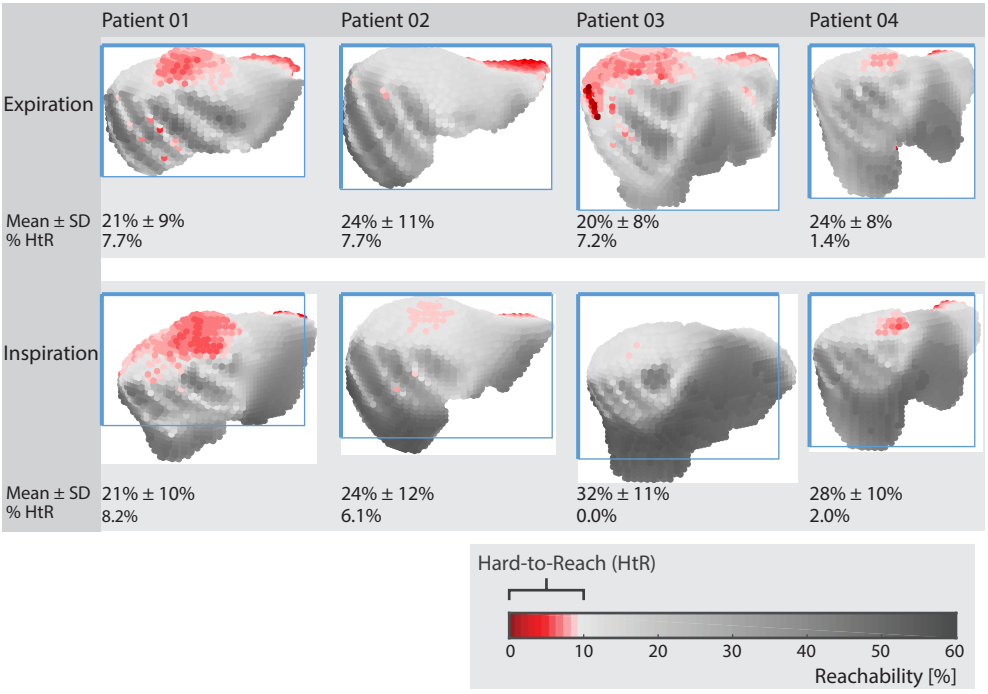

Figure 3.5. *Overview of the reachability for the liver in needle targeting during inspiration and expiration. The blue rectangles outline the position and size of the livers during expiration.*

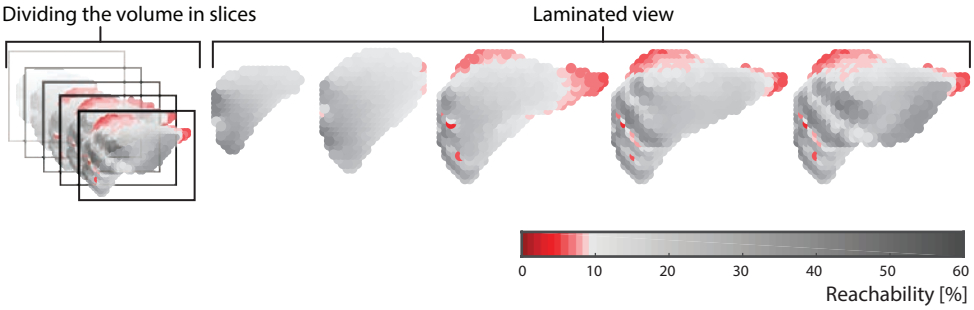

Figure 3.6. *Example of a laminated view of the reachability of one liver in needle targeting. The volume is divided in five equally spaced slices with a margin of 20mm at the front and back.*

3.3.3 Survey reachability

Figure 3.7 shows the response to the question: "What are the hardest-to-reach liver segments with a needle"? Liver segments I, VII and VIII were considered hard-to-reach with a needle, as indicated by respectively 21%, 30% and 28% of the participants. Additional comments were made, such as: "Reachability is also dependent on the location of the lesion within the segment", "There is much variation in reachability", "Needle placement is strongly dependent on the practitioner and expertise, and "a

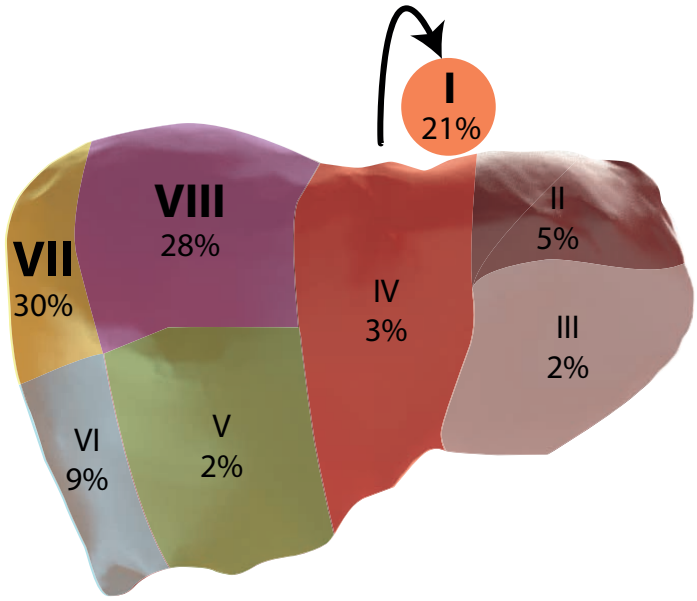

Figure 3.7. *Indication of the hard-to-reach liver segments with a needle, according to 22 interventional radiologists.*

small lesion (~5mm) is harder to target than a big abscess".

3.4. DISCUSSION

The aim of the current work was to identify the reachability of needle targets in the liver during inspiration and expiration. This fundamental problem was addressed by dividing four livers into equally spaced targets and applying a numerical analysis to quantify reachability by means of ray casting from target-to-skin. The data clearly showed that the targets with low reachability in the liver are mainly positioned in the cranial and posterior parts of the liver, and right behind the ribs. Furthermore, it suggests that, on average, reachability of the whole liver volume is increased from the state of expiration to inspiration.

For each patient in this study similar results were found, even though the livers varied in size, shape and liver motion subject to breathing. To further delineate the possible influence of liver size, motion, and deformation on reachability of the different liver regions, a larger dataset is needed.

When comparing the numerical results with the experts' view on perceived hard-to-reach liver regions, we see great agreement. Liver segments I, VII and VIII are hard-to-reach with a needle, according to the interventional radiologists (*Figure 3.7*). These segments are mainly covered with lungs, the heart, and rib cage, and require deep needle insertions to reach the targets. In addition to segments I, VII and VIII, also segment II and the cranial part of segment IV have low reachability, as indicated by the numerical analysis.

In the current study, needle paths were only constrained by colliding with the included anatomical structures and by exceeding the maximal insertion length. Other optimization parameters could e.g. include: restriction of the angle between the needle and tissue, collision with liver vessels, and inclusion of the needle diameter. Moreover, insertion paths via the posterior side of the patient were theoretically an option (*Figure 3.4*), whereas in clinical practice, this is not often done. As a consequence, presumably, the numerical analysis even underestimates the number of targets with low reachability, but at the same time might show insertion opportunities that were not thought of earlier.

Currently, the computing time for N=2.000 rays is within seconds per target, and therefore considered to be fast. The selected value resulted in a difference in reachability for five targets of less than ±0.5% compared with N=20.000. A smaller N would result in higher simulation speeds, at the cost of resolution.

A recent questionnaire has shown that a majority of the interventional radiologists (95%) believe that current needles in interventional radiology need improvement in terms of visibility and manipulability [21]. Recently, an effort has been made to

provide technical solutions to improve needle placement in interventional radiology. Novel solutions include steerable needles (e.g. [22-24]), robotic needle positioning systems with needle trajectory planners (e.g. [25-27], and combinations of these [28-30]. The clinical implementation of these solutions could be advanced with the methods proposed in this study in the future, by enhanced decision-making in patient-specific treatment plans. We foresee two specific features in addition to the general determination of optimal needle insertion paths.

First, we envision that numerical analysis of the reachability of targets can aid in choosing the right instrument for a specific procedure. Steerable needles can be used to avoid anatomical obstructions along the insertion path and to correct for undesired needle deflection. Longer needle insertion paths increase needle deflection [31], and therefore inaccuracy. Shorter, curved needle insertion paths might be possible with steerable needles as opposed to straight insertions. Unfortunately, the clinical rationale for steerable needle development and usage is insufficiently substantiated, and requirements in terms of needle positioning remain unclear. Optimized numerical analysis of a target's reachability could possibly rate the reachability when using a steerable needle over a conventional one, and therefore indicate the right instrument choice.

Second, if the specific intervention and situation allows the patient to hold his/her breath, the methods proposed in this study could assist needle trajectory planners in determining the optimal breathing phase to perform the puncture, before the intervention takes place. Breath holding is a standard technique when taking liver biopsies, during which the patient is asked to hold his/her breath upon puncturing [32]. Although the data indicate an improved or equal mean reachability from the state of expiration to inspiration, thereby favoring to puncture during inspiration, this differs per target (*Figure 3.5*). We found that number of targets with low reachability can even be increased during inspiration.

Medical image segmentation, and optimization should be taken into consideration before this numerical analysis could be used for decision-making in patient-specific treatment plans for needle-based interventions in the future. Currently, medical image segmentation was done semi-automatically to reach a satisfactory segmentation resolution, which is time-consuming. Improvements in the image segmentation field are needed, to be able to automatically segment the liver and critical anatomical structures. In addition, the aforementioned optimization constraints should be included.

3.5. CONCLUSIONS

The results derived from this study clearly show that large portions of the liver volume have low reachability with straight needle insertions, especially right behind the ribs and in the cranial and posterior parts of the liver. Concluding, this study provides

general insight into the reachability of needle targets in the liver during inspiration and expiration, which can be used to find fundamental relations between reachability and anatomical topology. In addition we foresee that the proposed methods can be used in the future to estimate the chances on successfully reaching a target and, as such, can be used for decision-making in patient-specific treatment plans, in terms of instrument choice and needle-targeting approaches in interventional radiology.

REFERENCES

[1] WHO (2015) Cancer - Fact sheet N297. World Health Organization. Available via: www.who.int/mediacentre/factsheets/fs297/en/. Accessed 05 July 2019.

.

[2] Kambadakone A, Baliyan V, Kordbacheh H, Uppot RN, Thabet A, Gervais DA, Arellano RS (2017) Imaging guided percutaneous interventions in hepatic dome lesions: Tips and tricks. World Journal of Hepatology 19:840-849.

[3] Villard C, Baegert C, Schreck P, Soler L, Gangi (2005) Optimal trajectories computation within regions of interest for hepatic RFA planning. In: International Conference on Medical Image Computing and Computer-Assisted Intervention:49-56.

[4] Baegert C, Villard C, Schreck P, Soler L (2007) Multi-criteria trajectory planning for hepatic radiofrequency ablation. International Conference on Medical Image Computing and Computer-Assisted Intervention:676-684.

[5] Baegert C, Villard C, Schreck P, Soler L (2007) Precise determination of regions of interest for hepatic RFA planning. Medical Imaging: Visualization and Image-Guided Procedures, 2007. International Society for Optics and Photonics:650923.

[6] Seitel A, Engel M, Sommer CM, Radeleff BA, Essert-Villard C, Baegert C, Fangerau M, Fritzsche KH, Yung K, Meinzer HP (2011) Computer-assisted trajectory planning for percutaneous needle insertions. Medical Physics 38(6Part1):3246-3259.

[7] Mastmeyer A, Hecht T, Fortmeier D, Handels H (2014) Ray-casting based evaluation framework for haptic force feedback during percutaneous transhepatic catheter drainage punctures. International Journal of Computer Assisted Radiology and Surgery 9(3):421-431.

[8] Liu S, Xia Z, Liu J, Xu J, Ren H, Lu T, Yang X (2016) Automatic multiple-needle surgical planning of robotic-assisted microwave coagulation in large liver tumor therapy. PloS one 11(3):e0149482.

[9] Schumann C, Rieder C, Haase S, Teichert K, Süss P, Isfort P, Bruners P, Preusser T (2015) Interactive multi-criteria planning for radiofrequency ablation. International Journal of Computer Assisted Radiology and Surgery 10(6):879-889.

[10] Ebert LC, Furst M, Ptacek W, Ruder TD, Gascho D, Schweitzer W, Thali MJ, Flach PM (2016) Automatic entry point planning for robotic post-mortem CT-based needle placement. Forensic Science, Medicine and Pathology 12(3):336-342.

[11] de Jong TL, Moelker A, Dankelman J, van den Dobbelsteen JJ (2019) Designing and validating a PVA liver phantom with respiratory motion for needle-based interventions. International Journal of Computer Assisted Radiology and Surgery:1-10.

[12] Kikinis R, Pieper SD, Vosburgh KG (2014) 3D Slicer: a platform for subject-specific image analysis, visualization, and clinical support. Intraoperative imaging and image-guided therapy:277-289.

[13] Cignoni P, Callieri M, Corsini M, Dellepiane M, Ganovelli F, Ranzuglia G (2008) MeshLab: an open-source mesh processing tool. Sixth Eurographics Italian Chapter Conference:129-136.

[14] de Jong TL, Moelker A, Dankelman J, van den Dobbelsteen JJ (2019) 3D models of liver and rib cage of four patients during inspiration and expiration. 4TU Research Data. https://doi.org/10.1007/s11548-019-02029-6.

[15] de Jong TL, Moelker A, Dankelman J, van den Dobbelsteen JJ (2019) 3D models of abdominal and thoracic structures of four patients during inspiration and expiration. 4TU Research Data. doi:uuid:7c82a1c4-0dce-46f9-b263-9350609a7a2f.

[16] Saff EB, Kuijlaars AB (1997) Distributing many points on a sphere. The mathematical intelligencer 19 (1):5-11.

[17] González Á (2010) Measurement of areas on a sphere using Fibonacci and latitude–longitude lattices. Mathematical Geosciences 42(1):49.

[18] Möller T, Trumbore B Fast (2005) Minimum storage ray/triangle intersection. ACM SIGGRAPH Courses:7.

[19] Tuszynski J (2011) Triangle/Ray intersection. Available via: http://www.mathworks com/matlabcentral/fileexchange/33073-triangleray-intersection. Accessed 05 July 2019.

[20] de Jong TL, van de Berg NJ, Moelker A, Dankelman J, van den Dobbelsteen JJ (2019) Dataset underlying the paper entitled: “Numerical analysis of reachability of liver regions in needle targeting”. 4TU Research Data. doi:uuid:f683fe11-9e5d-44ad-9e20-7c8fdb7541a0.

[21] de Jong TL, van de Berg NJ, Tas L, Moelker A, Dankelman J, van den Dobbelsteen JJ (2018) Needle placement errors: do we need steerable needles in interventional radiology? Medical Devices (Auckl) 11:259-265.

[22] van de Berg NJ, Dankelman J, van den Dobbelsteen JJ (2017) Endpoint accuracy in manual control of a steerable needle. Journal of Vascular and Interventional Radiology 28(2):276-283.

[23] Sears P, Dupont P (2006) A Steerable Needle technology using curved concentric tubes. IEEE/RSJ International Conference on Intelligent Robots and Systems:2850-2856.

[24] Scali M, Pusch T, Breedveld P, Dodou D (2017) Ovipositor-inspired steerable needle: design and preliminary experimental evaluation. Bioinspiration & Biomimetics 13(1):016006.

[25] Hiraki T, Kamegawa T, Matsuno T, Sakurai J, Kirita Y, Matsuura R, Yamaguchi T, Sasaki T, Mitsuhashi T, Komaki T (2017) Robotically driven CT-guided needle insertion: preliminary results in phantom and animal experiments. Radiology 285(2):454-461.

[26] Puglisi LJ, Pazmiño RS, Portolés GR, Cena CE, Santonja RA (2017) Experiences on the design of a needle insertion surgery robot: kinematic analysis. Advances in Automation and Robotics Research in Latin America:36-47.

[27] Hungr N, Bricault I, Cinquin P, Fouard C (2016) Design and validation of a CT- and MRI-guided robot for percutaneous needle procedures. IEEE Transactions on Robotics 32 (4):973-987.

[28] Bernardes MC, Adorno BV, Poignet P, Borges GA (2013) Robot-assisted automatic insertion of steerable needles with closed-loop imaging feedback and intraoperative trajectory replanning. Mechatronics 23(6):630-645.

[29] Wartenberg M, Schornak J, Gandomi K, Carvalho P, Nycz C, Patel N, Iordachita I, Tempany C, Hata N, Tokuda J, Fischer GS (2018) Closed-loop active compensation for needle deflection and target shift

during cooperatively controlled robotic needle insertion. Annals of Biomedical Engineering 46(10):1582-1594.

[30] Moreira P, van de Steeg G, Krabben T, Zandman J, Hekman EE, van der Heijden F, Borra R, Misra S (2017) The MIRIAM Robot: a novel robotic system for MR-guided needle insertion in the prostate. Journal of Medical Robotics Research 2(04):1750006.

[31] de Jong TL, Klink C, Moelker A, Dankelman J, van den Dobbelsteen JJ (2018) Needle deflection in thermal ablation procedures of liver tumors: a CT image analysis. Medical Imaging: Image-Guided Procedures, Robotic Interventions, and Modeling. International Society for Optics and Photonics. 10576:105761L.

[32] Sherlock S (1962) Needle biopsy of the liver: a review. Journal of Clinical Pathology 15(4):291.

PART B

LIVER PHANTOM DEVELOPMENT

4

PVA matches human liver in needle-tissue interaction

Tonke L. de Jong, Loes H. Pluymen, Dennis van Gerwen,
Gert-Jan Kleinrensink, Jenny Dankelman, John J. van den Dobbelsteen

Published in Journal of the Mechanical Behaviour of Biomedical Materials
(2017)

"This dissertation aims to improve needle placement in interventional radiology. Part B presents three studies on the developments of liver phantoms for needle-based procedures. Current liver phantoms are not fully tested for the ability of matching the heterogeneous force characteristics of real tissue. For that reason, this chapter presents the suitability of PVA in mimicking the mechanical needle reaction during insertions into ex-vivo human liver. We characterize the force data of needle insertions into real liver and compare them to insertions into PVA specimens of different mass concentrations and freeze-thaw cycles."

ABSTRACT – Medical phantoms can be used to study needle-tissue interaction and to train medical residents. The purpose of this research is to study the suitability of polyvinyl alcohol (PVA) as a liver tissue mimicking material in terms of needle-tissue interaction.

Insertions into ex-vivo human livers were used for reference. Six PVA samples were created by varying the mass percentage of PVA to water (4m% and 7m%) and the number of freeze-thaw cycles (1, 2 and 3 cycles, 16 hours of freezing at -19°C, 8 hours of thawing). The inner needle of an 18Gauge trocar needle with triangular tip was inserted 13 times into each of the samples, using an insertion velocity of 5mm/s. In addition, 39 insertions were performed in two ex-vivo human livers. Axial forces on the needle were captured during insertion and retraction and characterized by friction along the needle shaft, peak forces, and number of peak forces per unit length.

The concentration of PVA and the number of freeze-thaw cycles both influenced the mechanical interaction between needle and specimen. Insertions into 4m% PVA phantoms with 2 freeze-thaw cycles were comparable to human liver in terms of estimated friction along the needle shaft and the number of peak forces.

Therefore, these phantoms are considered to be suitable liver mimicking materials for image-guided needle interventions. The mechanical properties of PVA hydrogels can be influenced in a controlled manner by varying the concentration of PVA and the number of freeze-thaw cycles, to mimic liver tissue characteristics.

4.1. INTRODUCTION

Medical phantoms are often used to investigate needle-tissue interaction and for training of residents in image-guided needle interventions. Studying needle-tissue interaction is important, for example, for the development of navigation models and steerable needles (e.g. [1]), with which can be actively steered towards hard-to-reach lesions deep inside solid organs such as the liver. In addition, insight into needle tissue interaction is necessary for development of training phantoms for image guided interventions, which have been proved to be valuable in residents' training, in terms of improved technique, accuracy and confidence [2].

Phantoms used in needle-tissue interaction studies and medical training simulate human tissue, and reflect different aspects of reality. In general, two phantom types can be used. The first option is the use of biological tissues; cadavers, when freshly frozen, retain most of the textural and imaging properties of human tissue [3]. However, due to practical and ethical issues, the use of biological tissues is not always a feasible option. Alternatively, tissue mimicking materials (TMM) are used. Such phantoms can be customized to the needs of specific research activities or training, are readily available, and in general more durable.

A significant amount of research on tissue mimicking materials has been done. A wide range of materials have been studied on their tissue mimicking properties, such as carrageenan, gellan gum, and oil-in-gelatin dispersions [4-6]. The current study focusses on polyvinyl alcohol (PVA), a synthetic polymer that can be crosslinked both chemically and physically, due to its comparable ultrasound imaging properties to real tissue (e.g. [7,8]).

In addition to the imaging properties, matching mechanical properties of a tissue mimicking material are essential, as organs are typically heterogeneous. For example, a liver consists of several tissue layers, such as collagenous capsule, normal functioning parenchyma and epithelial tissue, which all have their own mechanical characteristics. For this reason, tissue properties vary significantly from one location to another within the same organ [9]. However, few studies have been done on the mechanical properties of PVA. Jiang et al. studied the freeze-thaw cycle number on the hydrogel structure and mechanical properties [10], hereby focusing on the deformation of the PVA phantom, by using two high speed cameras. Additionally, the magnitude of needle insertion forces into PVA were compared with clinical force data of insertions into prostate, gathered in a different study [11]. They concluded that PVA hydrogels may be suitable substitutions for soft tissues in biopsy precision research.

The aforementioned studies indicate the potential of PVA as a tissue mimicking material in terms of imaging and mechanical properties. However, due to a wide variety of materials and methods applied in previous studies, results often do not allow inter-study comparison with data on real tissue. On top of that, more research on the mechanical properties of PVA, especially needle-tissue interaction is needed, so that

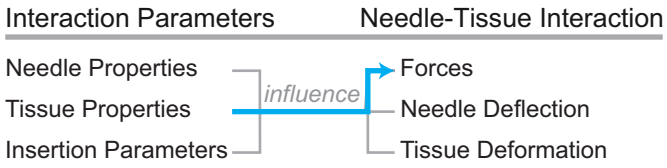

Figure 4.1. *Approach. Schematic depiction of the interaction parameters that influence needle-tissue interaction. In the current study, the tissue (phantom) properties are altered and the needle forces are measured (blue arrow).*

the heterogeneous characteristics of biological tissue can be mimicked. Therefore, the present paper combines these two points: it presents the suitability of PVA specimens in mimicking the mechanical needle reaction during insertion, by comparing it to insertions into human tissue, following the same research protocol.

4.1.1 Approach

The approach adopted for the current study was to insert needles into several PVA samples with variable mass percentages of PVA to water and number of freeze-thaw (FT) cycles, and to characterize the forces. These forces were compared with insertion forces into ex-vivo human liver tissue.

The current study focusses on the influence of tissue (simulant) properties on the needle insertion forces. The other parameters are kept constant (*Figure 4.1*). In addition, the data on PVA phantoms and on ex-vivo human livers are gathered using the same needle insertion parameters. In other words: the data allow for direct comparison between PVA samples and human livers.

In the present study, the axial needle force is used to characterize the mechanical interaction between needle and specimen. Forces acting on the needle can be divided in two main components, described by:

$$F_{Needle}(x) = F_{Friction}(x) + F_{tip}(x)$$

with F_{Needle} being the total forces acting on the needle during insertion into tissue, which are a summation of the forces that are acting on the needle tip during insertion (F_{Tip}) and forces due to friction between the needle and the surrounding tissue ($F_{Friction}$). Axial forces that act on the needle during insertion and retraction have been analyzed previously by several researchers: an extensive review of experimental data on needle-tissue interaction has been written by van Gerwen et al. [12].

4.2. METHODS

4.2.1 Experimental set-up

The experimental set-up consisted of a needle and a linear motion stage holding and moving the needle (*Figure 4.2*). An Aerotech PRO115-400 linear motion stage (Aerotech Inco, Pittsburgh, USA) was used to insert the needle into the specimen at a constant speed by moving the needle vertically with respect to specimen surface. The hub of the needle was connected with a load sensor to measure the axial forces on the needle during insertion and retraction.

The needles used during the experiments were the inner needles of 18Gauge Disposable Two-Part Trocar Needles (Cook Medical, Bloomington, USA), to eliminate the force effects of the cannula and allow for proper comparison between the PVA samples and human livers. These needles are made from stainless steel, 200mm long and have a triangular shaped tip with three facets (*Figure 4.3*). Two-Part Trocar needles are commonly used in radiologic interventions.

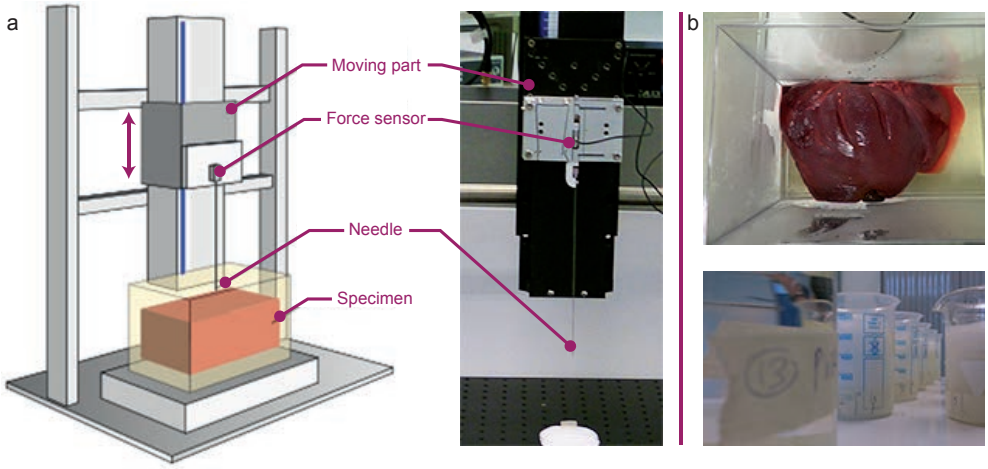

Figure 4.2. *Experimental set-up and specimens. a) An 18 Gauge trocar needle was either inserted into PVA specimens, or ex-vivo human liver specimens embedded in gelatin, while the forces were measured by the load sensor. b) Above: ex-vivo liver specimen placed on a gelatin base layer. Bottom: PVA specimens.*

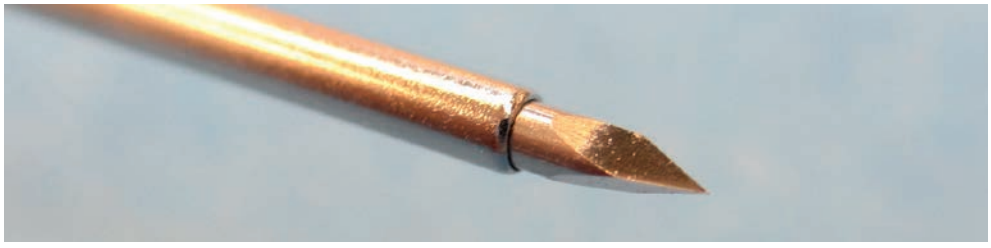

Figure 4.3. *Needle tip of the 18Gauge Two-Part trocar needle.*

4.2.2 Specimen preparation

Human liver

Two human liver specimens were extracted from fresh-frozen cadavers. These livers were obtained from persons without hepatic cirrhosis, as the anatomy did not show any suspicious nodules. The thickness of both livers was approximately 70mm.

The livers were embedded in 10% gelatin (Dr. Oetker, Bielefeld, Germany), to simulate the abdominal environment. Embedding in gelatin took place within one day after extraction. In the meantime, the extracted livers were stored in water in a plastic box in a refrigerator (±4°C). The test specimens were created by placing the livers on a gelatin base layer, to enable puncturing through the whole liver. Subsequently, the liver was submerged by a second gelatin solution, to fixate the liver. This gelatin solution was cooled down to 40°C, to prevent thermal damage of the tissue. Finally, a top gelatin layer was created. The container was stored overnight in the refrigerator to ensure proper stiffening of the gelatin. [Experiments with livers were carried out by T.L.dJ.]

PVA specimens

Physically crosslinked PVA specimens (Selvol PVOH 165, Sekisui Chemical Group NJ, USA) were created by subjecting the samples to freeze-thaw cycles. The degree of hydrolysis is related with the ability of the polymer to form crystalline regions. Therefore, super hydrolyzed PVA was chosen, as optimal crosslinking by FT cycles was desired. For this specific type of super hydrolyzed PVA product, 7m% PVA to water is the maximum recommended soluble concentration.

PVA particles were added to water and magnetically stirred. After submerging of all PVA particles, the solution was heated to 93°C. This temperature was maintained for 30 minutes, after which the solution was poured into a polypropylene beaker and allowed to cool down to room temperature. Then, the specimens underwent freeze-thaw cycles of 16 hours of freezing at -19°C, followed by 8 hours of thawing at room temperature.

Two PVA production variables were varied: the concentration of PVA in water and the number of freeze-thaw cycles. This resulted in six PVA specimens: 4m% and 7m% PVA to water, subjected to 1, 2 and 3 freeze-thaw cycles. No specimen replications were used. [Experiments with PVA were carried out by L.H.P.]

4.2.3 Experimental design

During each run, the needle was inserted by the linear motion stage with a constant insertion and retraction velocity of 5mm/s. The needle insertion depth was 70mm for the PVA phantoms. In case of the livers, the needle was going from the upper gelatin layer through the liver into to the lower gelatin layer, so that the entire liver was punctured (approximate height of 70mm).

The needle insertion locations were predefined to avoid repeated insertion at the same location, and randomized. The livers were each subjected to 20 needle runs, with a mutual distance of at least 10mm. Each PVA specimen was subjected to 13 needle runs, limited by the surface area of the beaker in which the specimen was created (diameter of 60mm). In total, 3 needles were used: one for the PVA experiment and one for each liver.

For every insertion and retraction, the axial forces acting on the needle hub were stored, as well as corresponding time and positions, with a sample frequency of 1KHz. The raw dataset for the liver insertions has been made publicly available [13].

4.2.4 Data analysis – Mechanical characterization

To characterize the mechanical interaction between needle and tissue, we consider three metrics: 1) the *friction* acting on the needle shaft, 2) the *magnitude of the peak forces*, and 3) the *number of peaks* per unit length during insertion. All force data were analyzed using Matlab 2015b and, prior to analysis, filtered with a zero-phase moving average filter with a window of 40 samples, to reduce noise in the signal. Force data were represented in boxplots. In order to find a *"realistic"* PVA specimen, realistic was defined by requiring the median of the PVA results to be within the first (Q1) and third (Q3) quarter of the liver results. This method was chosen as the data were non-normal distributed.

Friction: Figure 4.4 is an example of a force-position diagram of a needle insertion into liver tissue. It is assumed that during needle retraction, no tip forces (F_{Tip}, see Eq. 1) are working on the needle. Previous research has shown that friction along the shaft of the instrument is approximately linearly increasing with the insertion depth [14]. Therefore, friction can be estimated by calculating the slope during retraction of the needle, as previously done by e.g. [15,16].

For all needle retractions in liver and PVA specimens, a linear least squares approximation was performed. The slope of this approximation was used as an estimate for needle friction distribution along the shaft during insertion. A steeper slope, indicates more friction along the shaft of the instrument when inserted.

Peak forces – magnitude: Peaks in the force signal are typical for needle insertions into liver. Such peaks are clearly visible in the force-position diagram in *Figure 4.5*, and may be due to encounters with inner liver structures. The magnitude of these peak forces gives information about the degree of heterogeneity of the liver.

The line simplification algorithm used in [17] was selected as the classification method for the current study. This algorithm, based on the Douglas-Peucker algorithm [18], uses a single parameter, the threshold value "ε", to extract a subset of points from the force-position curve. The threshold value represents a measure of the scale of the smallest

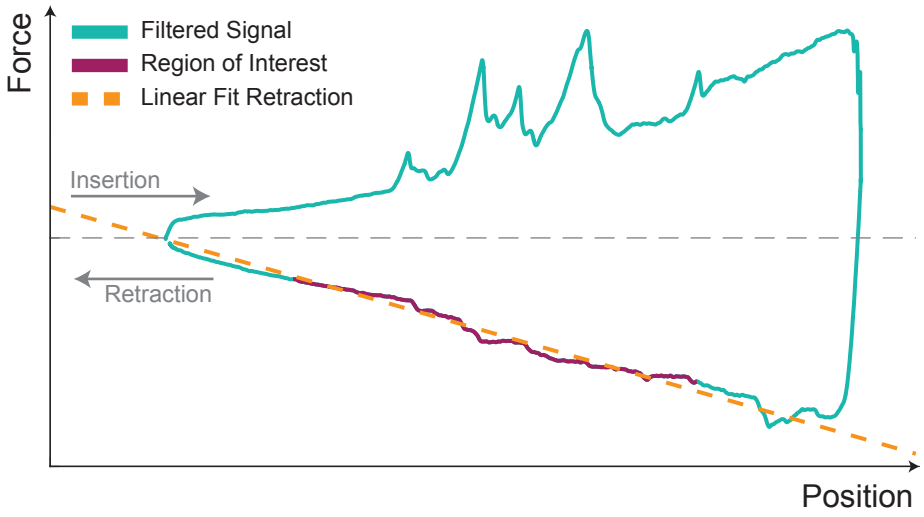

Figure 4.4. *Example of a force-position diagram of a needle insertion into liver tissue. The friction along the needle shaft was estimated by calculating the slope of the force during needle retraction.*

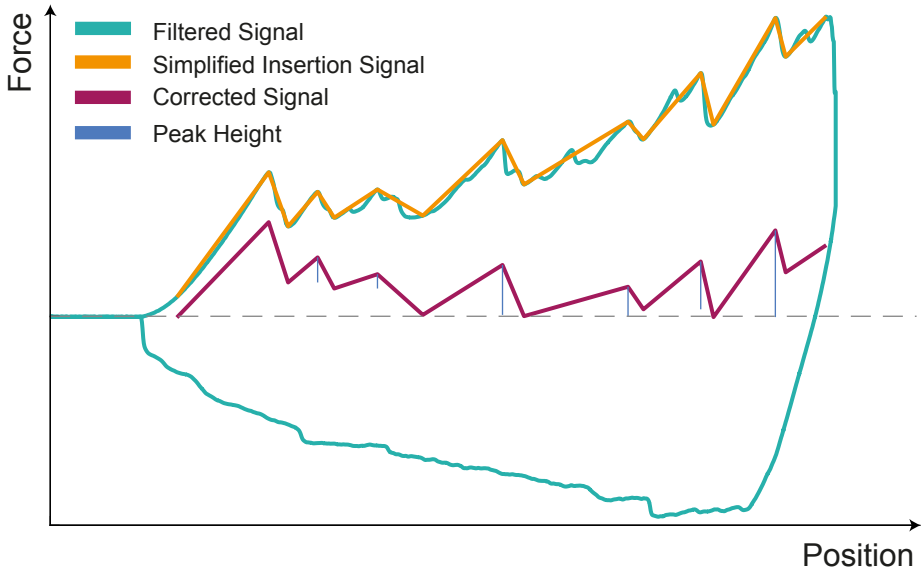

Figure 4.5. *Example of insertion force simplification by Douglas-Peucker algorithm and peak force analysis. First, the signal was simplified. Then, the signal was corrected for friction. For each insertion, peak heights and the number of peaks were calculated.*

peaks to be include, relative to the range of forces and positions measured. For the current study, a threshold value ε = 0.05 was chosen based on visual assessment of the data. This threshold removes relatively small peaks while preserving the characteristics of the signal (*Figure 4.5*, orange line), and thus distinguishes relevant peaks from irrelevant peaks (or noise).

Subsequently, peak height was calculated. In doing so, the signal was first corrected for overestimation, by subtracting the linear least-squares slope of the insertion phase (purple line). Then, the peak height was defined as the vertical distance between the maximum of the corrected peak and its preceding minimum.

Peak forces - number of peaks: A third characteristic of needle insertions into tissue is the number of peaks per unit length for all insertions. This gives information on the degree of heterogeneity of the specimen. The number of peaks per unit insertion length per needle run was calculated for all insertions into PVA and compared with the insertions into liver.

4.3. RESULTS

Note: whereas a total of 40 insertions for the livers were planned, only 39 were taken into the analysis, due to improper saving of the force data of one needle run.

4.3.1 Friction

The estimated friction along the needle shaft [N/mm] can be seen in *Figure 4.6*. The more freeze-thaw cycles, the higher the estimated friction slopes. This holds for insertions into both PVA 4m% and PVA 7m%. In addition, PVA 7m% causes higher estimated friction slopes than PVA 4m%.

The median estimated friction slope for the insertions into liver is 0.011 N/mm with the interquartile range between 0.010 N/mm and 0.013 N/mm. PVA 4m% with 2FT cycles has the same median friction slope as human liver.

The medians of the insertions into the specimens with one freeze-thaw cycle and 4m% and 7m% are respectively 0.001N/mm and 0.003N/mm, and thus below the Q1 of the liver insertions. The median estimated friction slopes of the other specimens, PVA 4m% 3FT, PVA 7m% 2FT, and PVA 7m% 3FT have a steeper friction slope than the insertions into liver.

4.3.2 Peak forces – magnitude

A boxplot of the magnitude of the peak forces for all insertions is shown in *Figure 4.7*. Higher needle peak forces are found when the number of freeze-thaw cycles is increased, both for PVA 4m% and PVA 7m%. In addition, there are no striking differences in peak

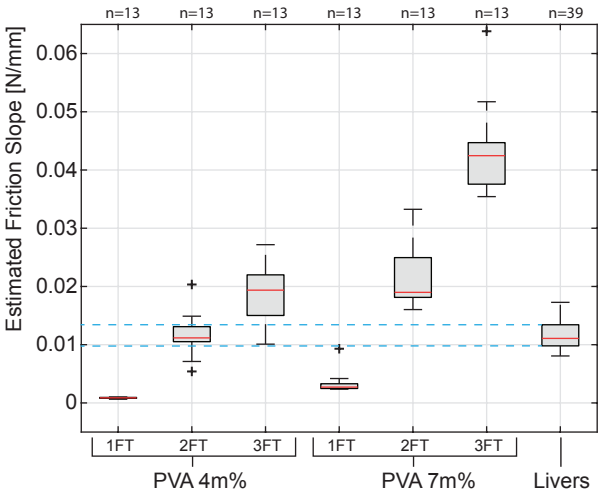

Figure 4.6. *Boxplot of the estimated friction slopes, i.e. the force per unit needle-specimen contact length, for needle insertions into all specimens.*

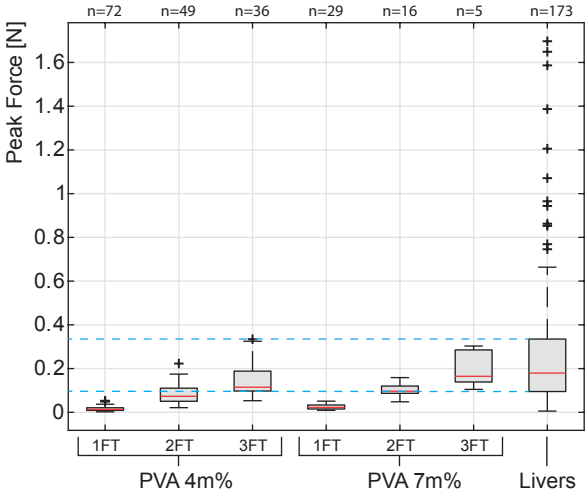

Figure 4.7. *Boxplot of the peak heights, calculated for all peaks found by DPA for all insertions into the specimens (ε=0.05).*

forces between the different specimens with the same number of freeze-thaw cycles.

Median peak forces for insertions into the PVA 4% 3FT, PVA 7m% 2FT, and PVA 7m% 3FT phantoms (respectively: 0.11N, 0.10N, and 0.16N) are all within Q1 and Q3 of the human liver specimens (median peak force = 0.18N, Q1 = 0.10N, Q3 = 0.34N), as is evident from the figure. All other specimens give rise to median needle peak forces below the interquartile range of the insertions into human livers.

4.3.3 Peak forces – number of peaks

Figure 4.8 illustrates the number of peaks per decimeter needle insertion inside the specimen. A large range of variation can be seen for insertions into the PVA specimens and the livers, which means that the encountered number of peaks is dependent on insertion location within the specimen. An increasing number of freeze-thaw cycles causes the number of peaks to go down, which holds for both PVA concentrations. As shown in the figure, the PVA 7m% specimens have fewer peaks per unit insertion length than the PVA 4m% specimens.

The median number of peaks for insertions into liver is 7.5 per dm, with Q1 and Q3 being respectively 5.6 and 9.3 peaks per dm. PVA 4m% 2FT is the only specimen with a median that lies within Q1 and Q3 of the liver insertions (8.3 peaks per dm). The median of the number of peaks for the insertions into PVA 7m% are all below Q1 of the liver insertions.

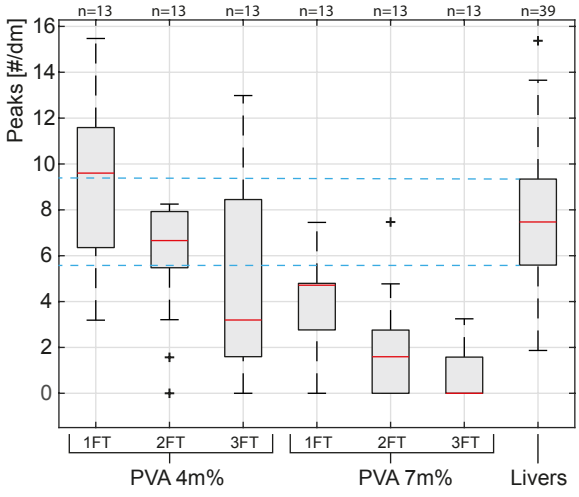

Figure 4.8. *Boxplot of the number of peaks per dm insertion for needle insertions into the specimens (ε=0.05).*

4.4. DISCUSSION

In the current study, the results from needle insertions into PVA specimens were compared to those from ex-vivo human liver, in order to identify the most promising method for the production of liver mimicking phantoms in terms of mechanical reaction on the needle. Needle-tissue interaction exhibits a specific perception to the physician in radiologic needle interventions, as biological tissue is known for being mechanically heterogeneous. Therefore, it is important for a tissue simulant to imitate these heterogenic force characteristics.

PVA was chosen as a study subject, for its good tissue mimicking properties regarding ultrasound. In the present study, three mechanical force metrics were calculated and analyzed: the friction along the needle shaft during needle insertion was estimated, the magnitude of the peak forces were calculated, and the number of peak forces per unit insertion length were determined. For the estimated friction and the number of peaks per insertion length, PVA 4m% with 2FT cycles is the only specimen that is comparable with the insertions into real ex-vivo human livers. However, the magnitude of the peaks forces was most comparable for the PVA specimens that underwent 3FT cycles. In this regard, PVA 4m% with 2FT cycles falls slightly below the Q1 of the insertions into liver.

In addition to these results, the study reveals the following tendencies regarding the effect of altering the mass concentration of PVA to water and the number of freeze-thaw cycles on needle-specimen interaction:

- The friction along the needle shaft increases with an increased number of FT cycles, and with an increased mass fraction of PVA.
- The magnitude of the peaks during needle insertion increases with an increased number of FT cycles.
- The number of peak forces decreases with an increased number of FT cycles, and with an increased mass fraction of PVA.

These trends suggest that mechanical needle-specimen interaction can be influenced in a controlled manner by altering the production variables of PVA. This is the first time, to the authors' knowledge, that these needle-tissue/phantom interactions have been compared using human livers as a reference material, subjected to the same experimental protocol as the PVA phantoms.

In general, when comparing the results of the PVA specimens with the results of the liver specimens, we see more outliers for the magnitude of the peak forces for the needle insertions into liver than for the PVA specimens (*Figure 4.7*). In our study design, we did not plan the insertion location with respect to internal vascular structure of the liver. Therefore, we believe that these outliers might be caused by encounters of the needle with these internal structures.

On the whole, PVA 4m% with 2 freeze-thaw cycles causes the most realistic force reaction on the needle during insertion, when comparing the needle insertion force characteristics with the insertions into liver, according to the criteria defined by the

present study. Median friction along the shaft of the instrument and the median number of peak forces were both within Q1 and Q3 of the insertions into the liver specimens. This indicates that PVA is a suitable liver mimicking material in terms of needle-tissue interaction.

When interpreting the results of this study, some limitations should be taken into account. First, we should note that the properties of PVA cryogels are influenced by many more variables than those that were studied in the current work. Among these are production variables and material properties, such as: the degree of hydrolysis, the degree of polymerization, the amount of ions present in the solvent, the type of solvent, and the duration of freezing and thawing [19]. We believe that making use of these PVA production variables, a specimen could be created that might be even better in mimicking our liver data set, than the PVA 4m% 2FT specimen that has been examined in this study. The published dataset of the insertions into human livers [13] could be used for that purpose. Second, one should note that healthy ex-vivo human livers have been used for reference. The importance of collecting data on diseased tissue should be stressed, in addition to the current data set, as pathologic tissue is known for being stiffer and more heterogeneous [20,21].

The present study focused on three mechanical metrics to compare the needle insertion forces in human liver and PVA phantoms, whereas an ideal liver mimicking phantom should meet requirements in other areas too. Examples include: matching imaging properties, comparable motion of the organ phantom and surrounding tissue, and similar thermal distribution after e.g. ablation procedures. The extent to which these requirements are needed depends on the purpose of the specific medical phantom. Whereas PVA is known for its mimicking imaging properties, more research can be done to see whether the developed PVA specimens mimic other liver characteristics as well.

In short, PVA was found to be a good liver mimicking material in terms of reaction forces on the needle during insertion. A suggestion for future research includes a comparison of PVA specimens with diseased human livers. The present study can be seen as a first step in an iterative process of finding a suitable liver mimicking phantom, that can be used for training in interventional radiology.

4.5. CONCLUSIONS

Needle-tissue force characteristics of PVA phantoms should be studied, in addition to their imaging properties, to make realistic liver mimicking materials. Therefore, the suitability of PVA specimens for mimicking real liver tissue in terms of needle-tissue interaction was assessed. We conclude that PVA has the potential to be a realistic liver mimicking material, according to the criteria that were used in the current study. Its mechanical properties can be altered in a controlled manner by varying the production variables. These findings are relevant for the development of realistic needle insertion

phantoms, which can e.g. be used for clinical training in interventional radiology and in needle-tissue interaction experiments.

REFERENCES

[1] van de Berg NJ, Dankelman J, van den Dobbelsteen JJ (2016) Endpoint accuracy in manual control of a steerable needle. Journal of Vascular and Interventional Radiology 28(2):276-283.

[2] Harvey JA, Moran RE, Hamer MM, DeAngelis GA, Omary RA (1997) Evaluation of a turkey-breast phantom for teaching freehand, US-guided core-needle breast biopsy. Academic Radiology 4(8):565–569.

[3] Hocking G, Hebard S, Mitchell CH (2011) A review of the benefits and pitfalls of phantoms in ultrasound-guided regional anesthesia. Regional Anesthesia & Pain Medicine 36(2):162–170.

[4] Datla NV, Konh B, Koo JJ, Choi DJ, Yu Y, Dicker AP, Podder TK, Darvish K, Hutapea P (2014) Polyacrylamide phantom for self-actuating needle–tissue interaction studies. Medical Engineering & Physics 36(1):140–145.

[5] Kuroda M, Kato H, Hanamoto K, Shimamura K, Uchida T, Wang Y, Akaki S, Asaumi J, Himei K, Takemoto M (2005) Development of a new hybrid gel phantom using carrageenan and gellan gum for visualizing three-dimensional temperature distribution during hyperthermia and radiofrequency ablation. International Journal of Oncology 27(1):175–184.

[6] Lazebnik M, Madsen EL, Frank GR, Hagness SC (2005) Tissue mimicking phantom materials for narrowband and ultrawideband microwave applications. Physics in Medicine & Biology 50(18):4245.

[7] Surry K, Austin H, Fenster A, Peters T (2004) Poly (vinyl alcohol) cryogel phantoms for use in ultrasound and MR imaging. Physics in Medicine & Biology 49(24),:529.

[8] Zell K, Sperl JI, Vogel MW, Niessner R, Haisch C (2007) Acoustical properties of selected tissue phantom materials for ultrasound imaging. Physics in Medicine & Biology 52(2):N475.

[9] Misra S, Reed KB, Douglas AS, Ramesh KT, Okamura AM (2008) Needle-tissue interaction forces for bevel-tip steerable needles. Proceedings of the IEEE RAS & EMBS International Conference on Biomedical Robotics and Biomechatronics:224–231.

[10] Jiang S, Liu S, Feng W (2011) PVA hydrogel properties for biomedical application. Journal of the Mechanical Behaviour of Biomedical Materials 4(7):1228–1233.

[11] Podder TK, Sherman J, Fuller D, Messing EM, Rubens DJ, Strang JG, Brasacchio RA, Yu Y (2006) In-vivo measurement of surgical needle intervention parameters: a pilot study. Proceedings of the Annual International Conference of the IEEE Engineering in Medicine and Biology Society:3652–3655.

[12] van Gerwen DJ, Dankelman J, van den Dobbelsteen JJ (2012) Needle–tissue interaction forces – A survey of experimental data. Medical Engineering & Physocs 34(6):665–680.

[13] de Jong TL, Dankelman J, van den Dobbelsteen JJ (2017) Dataset of force measurements of needle insertions into two ex-vivo human livers. Data in Brief 11:308-310.

[14] Kataoka H, Washio T, Chinzei K, Mizuhara K, Simone C, Okamura AM (2002) Measurement of the tip and friction force acting on a needle during penetration. International Conference on Medical Image Computing and Computer-Assisted Intervention — MICCAI:216–223.

[15] Hing JT, Brooks AD, Desai JP (2006) Reality-based needle insertion simulation for haptic feedback in prostate brachytherapy. Proceedings of the 2006 IEEE International Conference on Robotics and Automation:619–624.

[16] Simone C (2002) Modeling of needle insertion forces for percutaneous therapies Dissertation Department of Mechanical Engineering Johns Hopkins University.

[17] van Gerwen DJ, Dankelman J, van den Dobbelsteen JJ (2014) Measurement and stochastic modeling of kidney puncture forces. Annals of Biomedical Engineering 42(3):685–695.

[18] Douglas DH, Peucker TK (1973) Algorithms for the reduction of the number of points required to represent a digitized line or its caricature. Cartographica.: International Journal for Geographic Information and Geovisualization 10(2):112–122.

[19] Okay O, Lozinsky V (2014) Polymeric Cryogels:Macroporous gels with remarkable properties. Springer International Publishing 263.

[20] Paszek MJ, Zahir N, Johnson KR, Lakins JN, Rozenberg GI, Gefen A, Reinhart-King CA, Margulies SS, Dembo M, Boettiger D, Hammer DA, Weaver VM (2005) Tensional homeostasis and the malignant phenotype. Cancer Cell 8(3):241–254.

[21] Yu H, Mouw JK, Weaver VM (2011) Forcing form and function: biomechanical regulation of tumor evolution. Trends in Cell Biology 21(1):47–56.

5

Designing and validating a PVA liver phantom with respiratory motion for needle-based interventions

Tonke L. de Jong, Adriaan Moelker, Jenny Dankelman,
John J. van den Dobbelsteen

International Journal of Computer Assisted Radiology and Surgery (2019)

"The suitability of PVA as a tissue-mimicking material became clear in the previous chapter; now we can move on to using this material in a novel liver phantom. In addition to finding a proper material, movement of the liver and ribs subject to breathing is, in most phantoms, another absent aspect. These two features are combined in the present chapter: it presents the design and validation of an anthropomorphic PVA liver phantom with respiratory motion, based on patient data."

ABSTRACT – The purpose is to design and validate an anthropomorphic polyvinyl alcohol (PVA) liver phantom with respiratory motion, to simulate needle-based interventions. Such a system can for example be used as a validation tool for novel needles.

Image segmentations of CT scans of four patients during inspiration and expiration were used to measure liver and rib displacement. An anthropomorphic liver mold based on a CT scan was 3D printed and filled with 5% w/w PVA-to-water, undergoing two freeze-thaw cycles, in addition to a 3D printed compliant rib cage. They were both held in place by a PVA abdominal phantom. A sinusoidal motion vector, based on the measured liver displacement, was applied to the liver phantom by means of a motion stage. Liver, rib cage and needle deflection were tracked by placing electromagnetic sensors on the phantom. Liver and rib cage phantom motion was validated by comparison with the CT images of the patients, whereas needle deflection was compared with literature.

CT analysis showed that from the state of expiration to inspiration, the livers moved predominantly towards the right (range: -11mm to 11mm), anterior (mean: 15mm, range: 9mm to 21mm) and caudal (mean: 16mm, range: 6mm to 24mm) direction. The mechatronic design of the liver phantom gives the freedom to set direction and amplitude of the motion, and was able to mimic the direction of liver motion of one patient. Needle deflection inside the phantom increased from 1.6mm to 3.8mm from the initial expiration state to inspiration.

The developed liver phantom allows for applying different motion patterns and shapes/sizes, and thus allows for patient-specific simulation of needle-based interventions. Moreover, it is able to mimic appropriate respiratory motion and needle deflection as observed in patients.

5.1. INTRODUCTION

Research indicated that 90% of interventional radiologists believe that reachability of the lesion is challenged by target movement due to breathing of the patient [1]. Moreover, it is indicated that liver and rib motion due to breathing is one of the factors that contribute to unwanted needle deflection upon insertion. During radiofrequency ablations of liver tumors, needle deflection of several millimeters is encountered [2], thereby increasing the total targeting error. These studies indicate the importance of including proper liver and rib motion in a liver phantom for needle-based interventions.

Current developments in medical robotics and novel instrument design have increased the demand for physical validation set-ups. For example, Van de Berg et al. [3] presented a manually steerable needle to be used in interventional radiology and studied its endpoint accuracy in homogeneous gelatin phantom blocks. Preferably, these prototypes would be tested in-vivo, i.e. in human patients. However, due to safety and ethical reasons, this is not a feasible option. Therefore, realistic alternatives are needed, such as tissue mimicking phantoms that are able to mimic the heterogeneous features of real tissue.

The importance of certain phantom requirements depends on its specific application area, as emphasized by an extensive review on tissue mimicking materials by Li et al. [4]. In the present study, we focus on the development of a liver phantom for needle-based interventions. For this specific case, it requires: 1) a phantom material with matching *needle-tissue interaction forces* and feasibility to be used with *ultrasound,* 2) an *anthropomorphic* phantom shape, and 3) liver and rib *motion* subject to respiration of the patient.

The aforementioned phantom requirements have been studied to a greater or lesser extent. Recent studies indicate the suitability of polyvinyl alcohol (PVA), a polymer that forms molecular crosslinks upon freezing and thawing, in matching the needle-tissue interaction forces of human liver [5,6]. This material resembles the heterogenic structure of real tissue, in contrary to many other homogeneous base materials, such as gelatin [7], PVC [8] and agarose [9]. In addition, PVA has good ultrasound mimicking properties, as shown by several studies, e.g. [10,11].

Other research mimicked the anthropomorphic shape of the liver. For example, Rethy et al. [12] developed a multimodal permanent liver phantom displaying functional vasculature and pathologies, by wax and silicone molding of a donated human liver. In addition, Efthymios et al. [13] presented anatomically realistic ultrasound phantoms based on patient scans, by pouring gel wax in 3D printed molds.

The third requirement, liver and rib motion due to breathing of the patient, is studied to lesser extent. During breathing, the liver moves not only with respect to the static world, but also with respect to ribs and skin. Several attempts have been made to include this motion in a liver phantom. The first one dates back to 1968, and was

described by Stewart et al. [14]. This basic phantom, made from a plastic container and paraffin, simulates breathing by applying longitudinal travel with an amplitude of 3cm. Cleary et al. [15,16] developed a liver respiratory motion simulator, by connecting a human torso and liver model to a linear motion platform at the base of the torso's right abdomen. In addition, a recent paper by Naghibi et al. [17] presented the development of a soft robotic phantom to simulate the dynamic respirator motion of human liver, thereby focusing on MR compatibility. They used pneumatic soft actuators to generate motion patterns resembling those described in literature [18,19]. However, none of these phantoms include a combination of liver and rib motion, and they were not tested for corresponding needle deflection upon insertion.

In short, with the increasing demand for realistic phantoms for needle-based interventions, several studies have been performed. However, there are no phantoms available that fulfil all of the aforementioned requirements in a single set-up. Therefore, the goal of the current study is designing and validating an anthropomorphic PVA liver phantom with respiratory motion, that can be used for needle-based interventions.

5.1.1 Approach

Four steps were defined in the research process, that are illustrated in *Figure 5.1*. First, we semi-automatically segmented the liver and rib cage of four patients using CT images during inspiration and expiration. Second, we quantified the liver and rib motion by calculating motion vectors. In addition, we estimated the error of patient movement during the two respiratory phases. Third, we designed the liver phantom, rib cage and actuation system, divided into structural elements and actuation. Finally, we performed experiments with an electromagnetic tracking system to track the liver phantom's motion and needle bending. Liver phantom's motion was validated with the data from the CT images, whereas needle bending was compared with data that have been described in previous literature [2].

5.2. METHODS

5.2.1 Liver and rib cage segmentation

The study population included patients that underwent computed tomographic (CT) angiography in both inspiration and expiration and were suspected to have mesenteric ischemia because of arcuate ligament syndrome. Patient data were retrospectively acquired from the hospital information system and Picture Archiving Communication System. The total dataset consisted of 40 patients, of which four were included in the analysis, because their scans contained the total liver volume and rib cage during inspiration and expiration. The data were processed and stored anonymously. The medical research ethics committee of the Erasmus University MC approved that the Medical Research Involving Human Subjects Act did not apply to this study and that no informed consent was required according to the local directives for retrospective

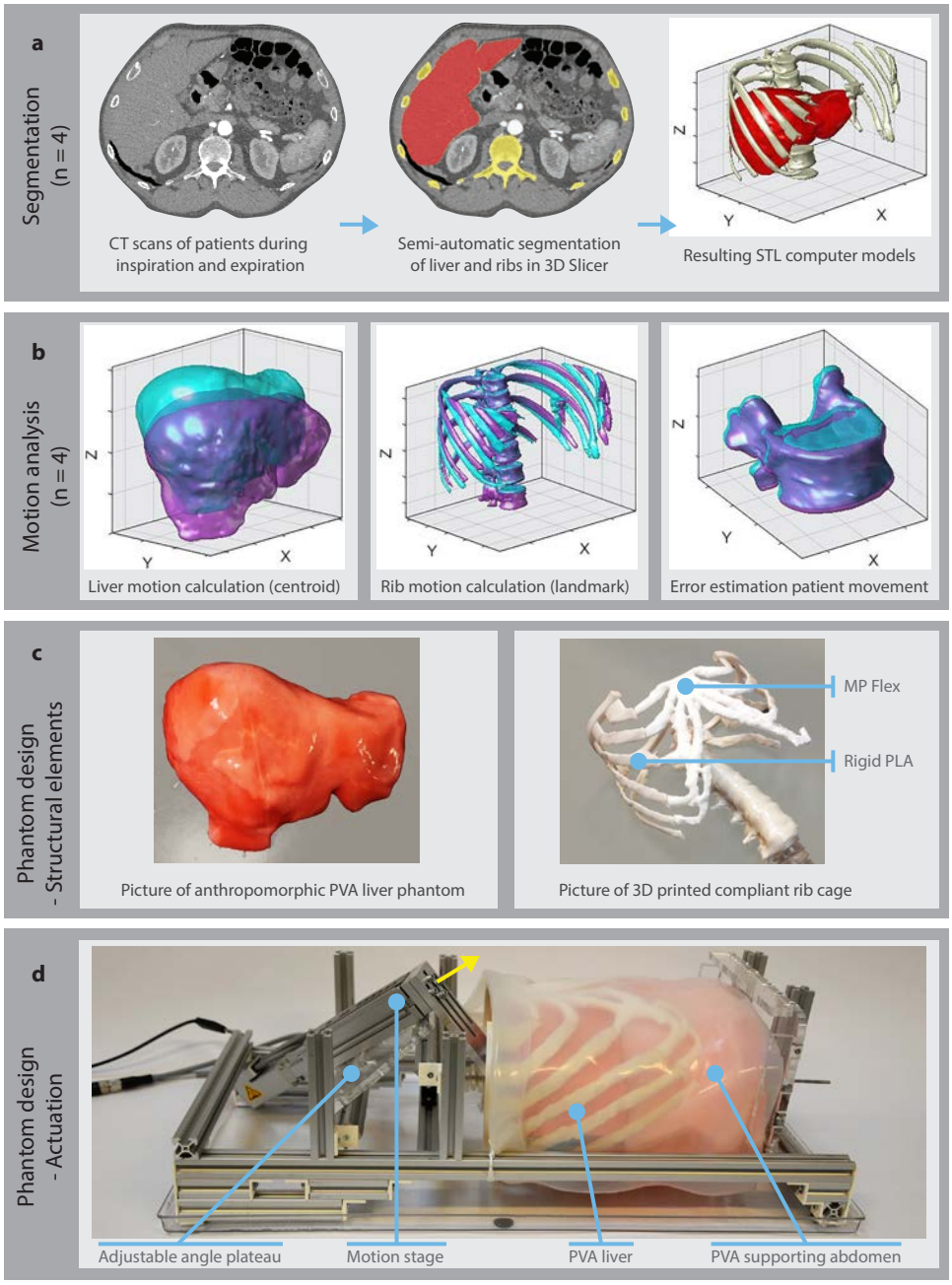

Figure 5.1. *Process of the liver phantom design divided into 4 parts. a) Segmentation of livers and ribs of the CT scans of five patients during inspiration and expiration. Resulting STL models were post-processed in Meshlab. b) Motion analysis of the livers, ribs, and an error estimation of patient movement during image acquisition. Blue = expiration, Purple = inspiration. c) The structural components of the phantom model, consisting of PVA liver phantom, and 3D printed ribs. d) Actuation of the liver phantom using a motion stage.*

studies (MEC-2016-241).

Semi-automatic segmentation of the livers and ribs, illustrated in *Figure 5.1a*, was done with 3D slicer 4.8.1 [20] (http://www.slicer.org), using the following segment editor modules. "Draw", and "paint" were used for the manual part of the segmentation, and "Grow from seeds" was used for the automatic part. The last module applies a fast region growing method, in which final segment boundaries are placed where its master volume changes brightness abruptly, as described in [21]. This method turned out to be suitable for the rib cage, as brightness differences with the surroundings are high. However, in case of the livers, additional smoothing was required.

The resulting models were stored as .stl files and loaded into Meshlab, an open source system for processing and editing 3D triangular meshes [22]. Several simplification, smoothing and re-meshing steps were performed. First, the models were cleaned by removing unreferenced and non-manifold vertices. Second, the Screened Poisson Surface reconstruction was completed, to create a closed surface. Then, the models were simplified to 50000 faces with MeshLab's Quadric Edge Collapse Decimation, resulting in significant smaller file sizes (from ~42mb to 2.5mb) without losing their original shape. Next, Laplacian smoothing was performed, which calculates for each vertex the average position with the nearest vertex. Finally, iso-parameterization was executed for the liver models, as described by Pietroni et al. [23] (*Figure 5.2*), to re-mesh the surfaces to almost regular triangulation with minimal distortion. The resulting files are *Open Access* and can be found online at [24]. The livers measured on average 198mm in left-right (range : 180mm – 223mm), 160mm in posterior-anterior (range: 119mm – 200mm) and 161mm in cranio-caudal (range: 142mm – 178mm) view.

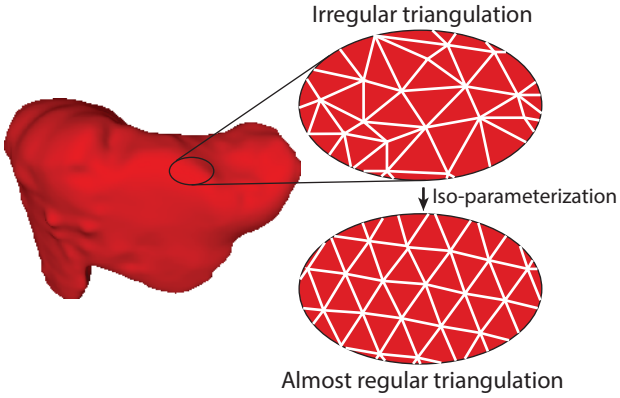

Figure 5.2. *Post-processing of the STL models in MeshLab. The irregular triangulation pattern was iso-parameterized to an almost regular triangulation using [21].*

5.2.2 Liver and rib cage motion analysis

Liver and rib motion

Liver movement was quantified in terms of translational motion, which we defined as the difference between the centers of mass during inspiration and expiration, thereby assuming uniform density of the liver tissue. In addition, rib motion was quantified by calculating the differences between inspiration and expiration at the transition point between bone and cartilage of the 7th rib.

To perform the analysis, the .stl files of the livers and ribs were loaded into Matlab 2017b (The Mathworks, Inc., Natick, Massachusetts, United States). The iso-parameterization, described in the previous segmentation section, allowed for the calculation of the center of mass to quantify liver motion, as the distances between vertices are equally spaced. The following formula was used to compute the center:

$$C_{x,y,z} = \sum_{i=1}^{n} \frac{V_{x_i y_i z_i}}{n}$$

With *C* is the position of the centroid, $V_{x_i y_i z_i}$ is the local position of the vertex, and *n* is the total number of vertices.

Error estimation patient movement

An error estimation of patient movement during the inspiration and expiration phase was performed. This gives an estimate of the error in the quantification of liver and rib motion. We calculated the centroid of the 9th thoracic vertebras and compared the position in 3D space during both respiratory phases. Errors were given as the mean difference between the two states and standard deviation for the four patients.

5.2.3 Liver phantom design

The developed phantom is a real size, anthropomorphic liver phantom made of PVA, and consists of structural components of the liver itself and its actuation. The structural elements of the phantom are shown in *Figure 5.1c*, whereas its actuation is depicted in *Figure 5.1d*. A video of the phantom can be found online as electronic supplementary material.

5.2.4 Structural elements

The structural elements of the liver phantom consisted of a PVA liver, a support PVA abdominal cavity, a rib cage phantom, and a skin phantom made of a 2.5mm layer of silicone (Ecoflex 00-30, Smooth-on Inc., Macungie, Texas, USA). The PVA liver (*Figure 5.1c*, left) was made by pour-molding PVA in a 3D printed liver mold. This mold was

created from the negative imprint of the computer liver model and 3D printed in Polylactid Acid (PLA) with 0.25mm printing resolution. Subsequently, it was filled with 5% w/w PVA-to-water (Selvol PVOH165, Sekisui Chemical Group NJ, USA), undergoing two freeze-thaw cycles for 72 hours each at a temperature of around -18°C. The abdominal cavity phantom was also made of PVA (4% w/w PVA-to-water, two freeze-thaw cycles, 72 hours each), and used to support the PVA liver. It was made by filling a box with PVA and used a 3D printed liver as negative shape, which was removed after curing of the PVA. The concentrations for the PVA liver and abdominal cavity phantom were chosen based on previous research. This study characterized the needle-tissue interaction forces in healthy human liver and PVA phantoms in terms of: magnitude of the needle insertion forces, number of force peaks, and friction along the needle shaft [6]. We chose a higher concentration for the PVA liver (5% w/w) as compared to the abdominal cavity phantom (4% w/w), to simulate the stiffness of diseased liver tissue as compared to its less stiff, healthy abdominal surroundings. All PVA components were colored with food color.

The phantom ribs were 3D printed using two materials. The bony structures of the ribs and rib cage were printed using rigid PLA (MakerPoint, Digital Fabrication Center, The Netherlands), whereas the cartilage was printed with FLEX45, a flexible material (MakerPoint, Digital Fabrication Center, The Netherlands) to allow for compliant motion. These parts were glued together (Figure 5.1C, right). An Ultimaker 3 (Ultimaker B.V., Geldermalsen, the Netherlands) was used for all 3D prints.

5.2.5 Actuation

The phantom liver was actuated by an EGSL-BS-35-50-8P mini motion stage, with a maximal travel distance of 50mm and a minimum and maximum sliding velocity of 0.13mm/s and 350mm/s, respectively (Figure 5.1D). It was powered by a EMMS-ST-28-L-SE stepper motor without brake. The stepper motor was controlled by a CMMS-ST-C8-7-G2 motor controller (all components from Festo BV, Delft, the Netherlands), which, in turn, was directed by a LabJack T7 (Labjack Corporation, Lakewood, USA).

5.2.6 Motion validation of the liver phantom

The liver phantom motion was mimicked using the data of one patient. The generated motion pattern was a sinusoid (frequency: 12Hz, position controlled), based on the measured liver displacement during breathing. A close-up of the linear stage is given in *Figure 5.3*. The direction of breathing motion is adjustable by setting two angles of rotation. By tuning the motion stage around the left-right axis (axis 1) and the forward-backward axis (axis 2), the direction of the motion vector can be set as desired, based on the calculated position of the centers of the liver on the CT scans of a specific patient. The direction and amplitude of the motion vector were based on the results of the liver and rib cage motion analysis of the four patients and is therefore given in the results section. Motion was applied directly to the superior part of the PVA liver.

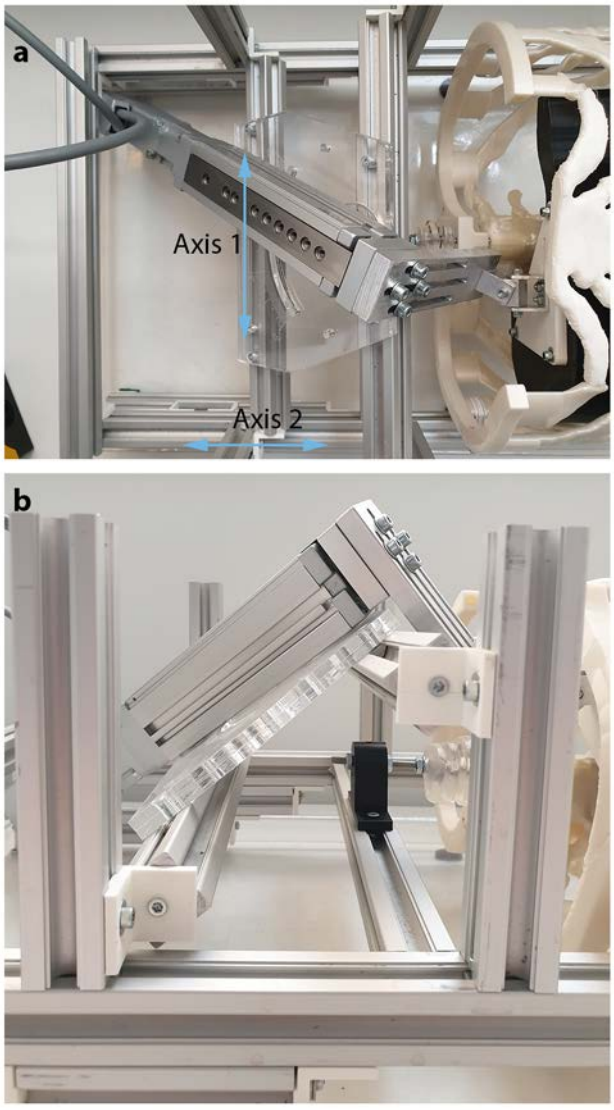

Figure 5.3. *Adjustable direction of the linear stage to simulate breathing motion: a) Top view, indicating the left-right axis (axis 1) and forward-backward axis (axis 2), b) Side view.*

Motion of the liver phantom was validated using NDI Aurora's Tabletop Field Generator (Northern Digital Inc, Ontario, Canada). This system generates an electromagnetic field in which sensors can be tracked real-time in 3D space. Standard 0.8mm Aurora 5DOF sensors were used (part number: NDI 610090). In total, three sensors were placed inside the PVA liver, and one on the rib cage (*Figure 5.4*). One reference sensor was placed on the moving part of the linear stage.

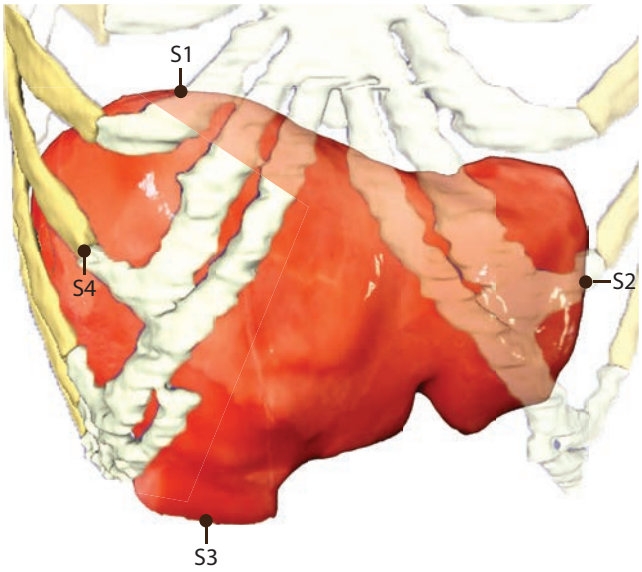

Figure 5.4. *Sensors 1-3 were placed inside the PVA liver. Sensor 4 was placed on the transition between bone and cartilage of the 7th rib. A reference sensor was placed on the moving part of the linear stage.*

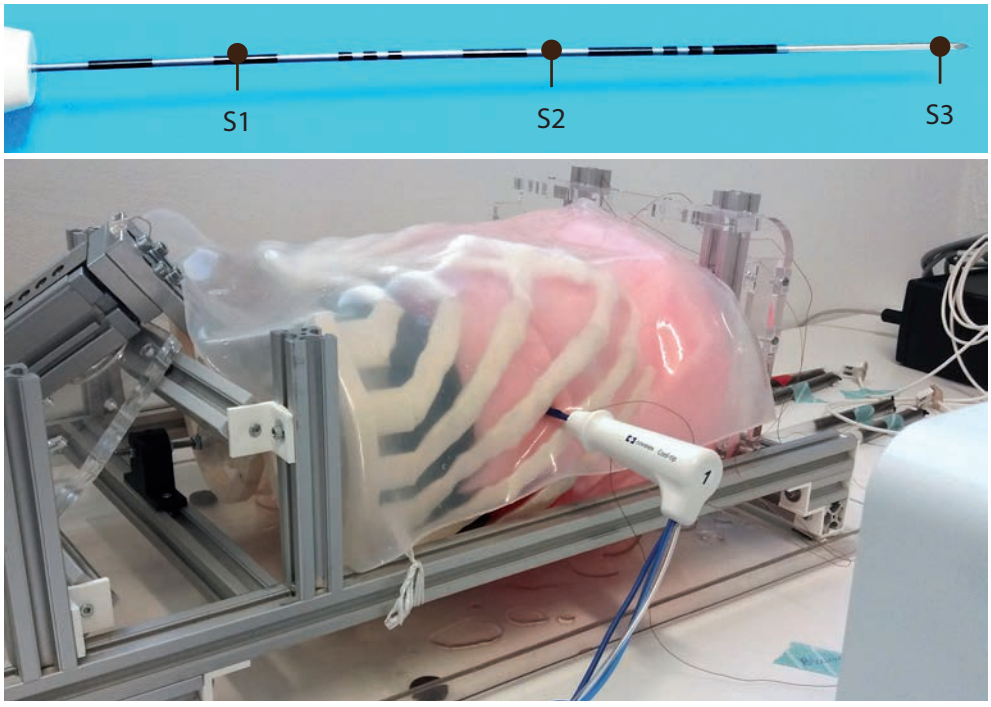

Figure 5.5. *Three sensors were placed on the ablation needle to quantify deflection (upper part). A reference sensor was placed on the moving part of the linear stage. The needle was inserted between the 8th and 9th rib (lower part).*

First, the noise levels were measured for 10s with the motor switched on and off. Second, the phantom liver was actuated by the stage for 60s, while capturing the motion of the different sensors. Then, noise levels were again measured for 10s. This was repeated three times. Noise levels were expressed as a combined standard uncertainty, calculated by taking the root sum of the squares of the standard deviations of the measured positions of the reference sensor in 3D space.

In addition to the validation of system's motion itself, the deflection of a Cool-tip ablation needle (17Gauge Cool-tip RF ablation system E, Medtronic, Minneapolis, USA) was measured for 60s by inserting the needle approximately 10cm into phantom between the 8th and 9th rib. The needle was inserted in expiration phase, i.e. in the initial position of the stage without motion. It had three sensors on it; one at the entry point of the liver phantom, one at the needle tip, and one halfway the insertion (*Figure 5.5*). The sensors were fixed onto the needle with isolation tape. Again, a reference sensor was placed on the moving part of the linear stage. Needle deflection was defined by calculating the point-to-line distance, with the point being the position of sensor 2 and the line being interpolated from the positions of sensor 1 and sensor 3.

5.2.7 Needle visibility – Ultrasound

The liver phantom was checked for needle visibility by inserting the cool-tip ablation needle between the 7th and 8th rib under ultrasound imaging. An iU22 Ultrasound Machine (Philips Medical Systems International B.V., Best, the Netherlands) was used in combination with a C5-1 transducer, which is commonly used in abdominal and interventional procedures. The probe was placed on the right upper quadrant of the abdomen, left of and right under the rib cage. Coupling gel was applied between the skin- and abdominal phantom, and the skin and ultrasound probe. The insertion angle with respect to the ultrasound probe was approximately 30° and 45°. The needle was captured in-plane.

5.3. RESULTS

5.3.1 Liver and rib cage motion analysis

Liver and rib motion

The results of the motion analysis can be seen in *Figure 5.6*. This figure shows the movement of the livers subjected to breathing from expiration towards inspiration in all directions, being: Left-Right (X), Posterior-Anterior (Y), and Cranio- Caudal (Z). From the state of expiration to inspiration, the centroids of the livers moved predominantly towards the right (mean: 2mm, range: -11mm to 11mm), anterior (mean: 15mm, range: 9mm to 21mm), and caudal (mean: 16mm, range: 6mm to 24mm) direction. Note that during inspiration the liver can move to either left or right, depending on the patient. The mean total stroke was 22mm (range: 11mm to 33mm).

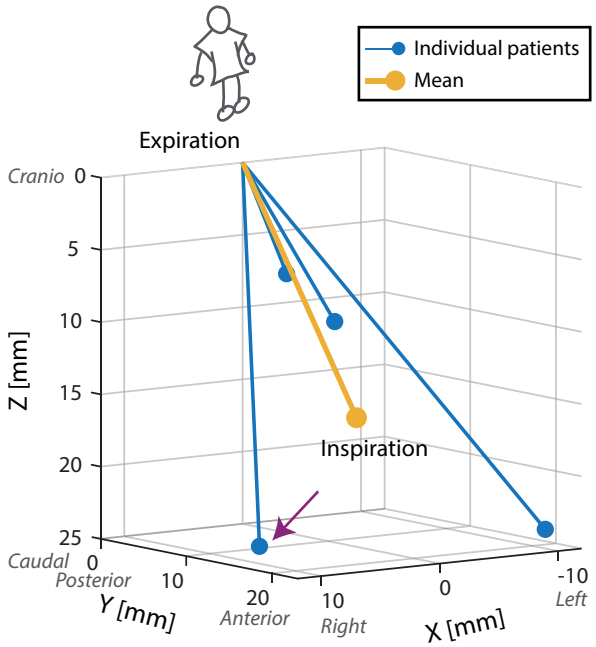

Figure 5.6. *Motion patterns of the liver from expiration to inspiration (n=4). Translational motion is predominantly towards the right (2mm), anterior (15mm) and caudal (16mm) direction.*

The 7th rib of the patients moved also predominantly towards the right (mean: 14mm, range: 7mm to 21mm), anterior (mean: 7mm, range: -3mm to 18mm), and caudal (mean: 1mm, range: -11mm to 10mm) direction. Although the direction of rib motion coincides with liver motion, its magnitude differs. The mean total stroke was 20mm (range: 14mm to 30mm).

Error estimation patient movement

The 9th vertebra of the patients moved predominantly to the right (mean: 0.5mm, range: -0.6mm to 2.1mm), anterior (mean: 1.5mm, range: -0.3mm to 2.8mm) and caudal direction (mean: 0.2mm, range: -0.8mm to 0.1mm) from the state of expiration to inspiration. Total movement of the individual vertebras during breathing was on average 1.6mm, with a minimum of 0.4mm and a maximum of 2.8mm.

5.3.2 Motion validation of the liver phantom

The motion vector and anthropomorphics of the patient indicated with the purple arrow in *Figure 5.6* were chosen as an input for the liver phantom. We chose this patient as it has the largest total stroke towards the right (total stroke: 31mm, right: 11mm, anterior: 17mm, caudal: 24mm). Based on the signal from the reference sensor, the combined standard uncertainty was 0.10mm with the motor of the linear stage turned

on, and 0.07mm with the motor turned off. There is more electromagnetic interference when the linear stage was turned on. We did not subtract these noise levels from the final measurements, as they are negligibly small.

Figure 5.7 shows the results of the motion validation of the liver phantom for the three sensors on the PVA liver, and the reference sensor on top of the stage. The amplitude and direction of the reference sensor is comparable to the imposed motion vector from the CT scans (green dotted line). The direction for all PVA liver sensors (S1 to S3) is comparable to the imposed motion vector, whereas the amplitude decreases for S2 and S3 compared to the real situation. This resulted in larger deformation of the PVA liver than the patient's liver, probably caused by the limited space between the caudal end of the PVA liver end the plastic end plate.

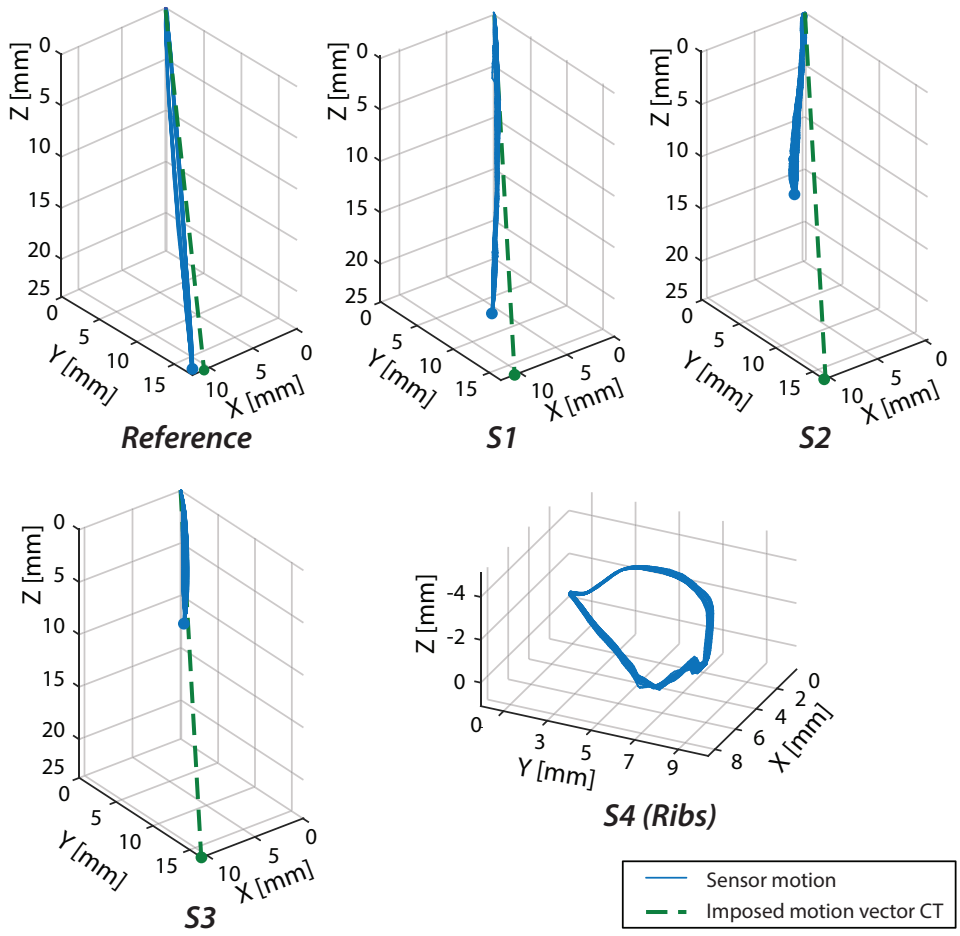

Figure 5.7. *Liver and rib phantom movement during expiration and inspiration.*

Corresponding rib motion in the patient had a total stroke of 30mm (right: 21mm, anterior: 18mm, caudal: 9mm). Compliant rib motion phantom can be seen in *Figure 5.7 - S4* (Ribs). It has a circular pattern, and a total stroke of 13mm (right: 8mm, anterior: 10mm, cranio: 3mm). This means that the movement of the ribs in right-left and anterior-posterior direction correspond with the real situation as opposed to cranio-caudal direction.

Needle deflection from the state of expiration to inspiration is shown in *Figure 5.8*. Upon insertion, i.e. the state of expiration, mean needle deflection (δ) was 1.6mm, whereas the mean deflection increased to 3.8mm during inspiration. The sensors did not change position with respect to the needle itself during the measurements, as there was almost no difference within the expiration and inspiration positions during the 60s trial (standard deviations ranging from 0.1mm to 0.7mm).

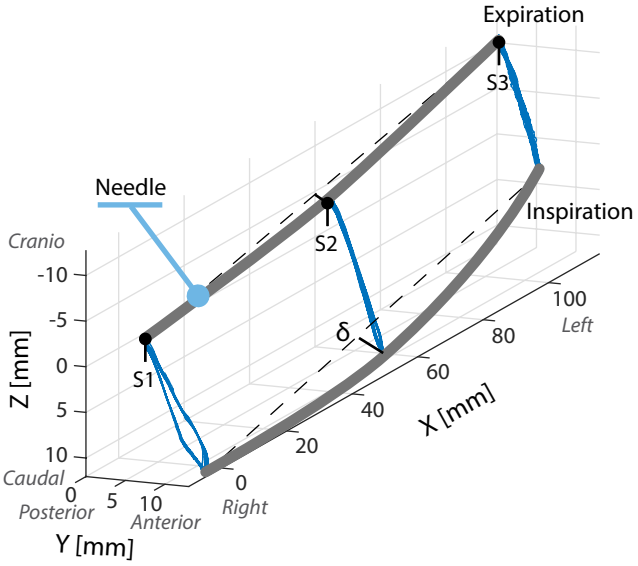

Figure 5.8. *Ablation needle movement during expiration and inspiration state of the liver phantom. δ = needle deflection.*

5.3.3 Needle visibility – Ultrasound

Figure 5.9 shows the result of the needle visibility validation. The needle shaft and the needle tip can be identified on the ultrasound picture (in-plane).

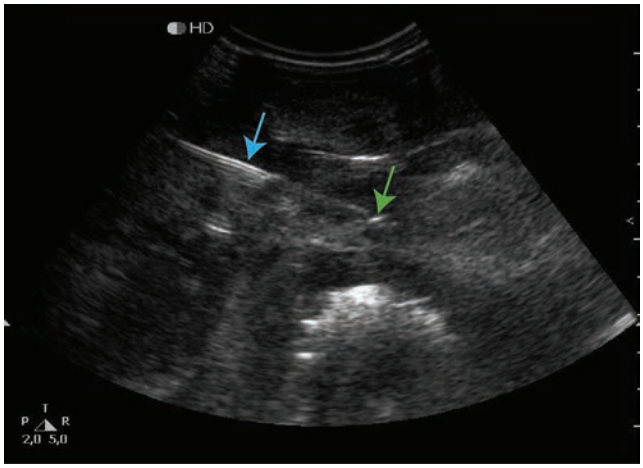

Figure 5.9. Ultrasound picture of the liver phantom and needle. (gain = 49).

5.4. DISCUSSION

This study presents a design and validation of a liver phantom to be used for needle-based interventions. We fabricated a heterogeneous, ultrasound compatible phantom material, PVA, based on CT image segmentations of a real patient, and we simulated breathing motion. We validated the phantom motion of one patient by using an electromagnetic tracking system and compared the results with the CT images. In addition, we compared needle deflection in the phantom with those found in thermal ablation procedures of liver tumors, as previously described in literature [2].

This research studied the motion of the liver and rib cage subjected to respiration as observed in four patients, by comparing the liver centroids during inspiration and expiration. All patients' livers moved to caudal and anterior direction from the state of expiration to inspiration. However, for different patients they moved to either left or right. These results are in agreement with those obtained by Tsai et al. [25]. Presumably, this is caused by a difference in breathing type of the patients; diaphragmatic or chest.

The mean total liver stroke, based on the CT scans of the patients that were included in our study, was found to be 22mm. Previous studies on liver motion show a total stroke ranging from a couple of mm up to a couple of cm (e.g. [25] [26] [27] [28] [29] [30]). Our results are within this range, although being on the higher end of the spectrum. This might be explained by the fact that the patients in our study were specifically asked to perform deep inspiration and maximum expiration, causing larger displacements than during ordinary breathing. As our liver phantom allows for adjustments of its motion vector, in terms of magnitude and direction, we do not foresee any problems in applying different motion patterns.

The motion stage uses one of the aforementioned motion vectors of patients as an input to simulate breathing in our phantom. For the liver, we found comparable motion patterns in terms of magnitude and direction for the superior parts of the liver, whereas the magnitude decreased for the inferior parts of the liver, i.e. the sensors that were placed further away from the applied motion (*Figure* 5.7). This resulted in an observed deformation several mm bigger than in the corresponding patient. However, this is not particularly surprising given the fact that the PVA supporting abdomen is mechanically not exactly the same as compared to the real situation in which the abdomen consists of several different organs and tissue types. If the exact same motion is preferred, more research is needed into the mechanical characteristics of the abdominal organs to correctly mimic the abdomen using PVA-based phantoms. Nevertheless, we believe that the current mimicked motion is sufficient for the purpose of novel instrument validation, as the phantom, in addition to the aforementioned similarities, also shows relative motion between the liver and rib cage, which is one of the factors that contribute to needle deflection. Future liver phantoms could include a layer of phantom muscle tissue, that presumably has an influence on needle insertion forces and deflection too.

The most important clinically relevant finding of this research concerns the comparison between needle deflection in our phantom and the real situation. Unwanted bending of the needle upon insertion is a problem in interventional radiology and complicates precise placement [1]. We compared the needle deflection with the deflection quantified using CT scans of in-vivo procedures of tumor ablations, reported in [2]. Bending was defined in the same manner as in the present study and ranged from 0mm to 7mm, which is in the same order of magnitude as observed in our liver phantom.

Although it is possible to make patient-specific phantoms with the current methods, the PVA phantom production is time-consuming. Several freeze-thaw cycles are needed to reach the desired amount of heterogeneity for it to be comparable to real tissue. Future developments in 3D printing of soft materials might overcome this limitation. For instance, Tan et al. [31], studied super soft 3D printed hydrogels, matching the stiffness of brain and lung tissue.

We emphasize three advantages of a tissue mimicking material such as PVA, over the use of biological tissue. In general, tissue mimicking materials: 1) are durable, 2) are tunable, and 3) can easily be used without violating ethical and regulatory guidelines. Tunability is especially important in case of future additional features of liver phantoms, such as mimicking diseased tissue, and including target lesions. The third advantage is crucial for testing early-prototypes of medical instruments developed by technical research groups, who often do not have easy access to an experimental lab with a permit to handle biological tissue.

Besides its purpose as a validation set-up for novel needles, our liver phantom has the potential to be used as a trainings tool for interventional radiologists. In that specific case, we propose further research by performing user experience tests and extensive

ultrasound compatibility experiments. Although we did not focus on the exact match between ultrasound of real livers and our phantom, we highlighted (*Figure 5.9*) that all important structures are visible, which is sufficient for novel instrument validation. Ultrasound imaging of the phantom could e.g. be improved by applying coupling gel between the PVA liver, PVA abdomen, and the silicone skin phantom, and by the addition of glass beads to induce more realistic acoustic backscattering [32].

As a final note, the gathered motion data of this research cannot only be used for the designing physical liver phantoms, but are applicable for a broader scope, for example for the development of virtual simulators [33]. Therefore, the 3D models of the livers and rib cage during inspiration and expiration have been made publicly available [24].

5.5. CONCLUSION

In conclusion, the experiments showed that the developed anthropomorphic PVA liver phantom is in general able to simulate respiration induced motion of liver tissue that can be found in patients. The magnitude of needle deflection in the liver phantom is comparable to real procedures and increases during breathing. The phantom can be used to validate novel instruments and/or robotic systems for needle-based interventions.

REFERENCES

1. de Jong TL, van de Berg NJ, Tas L, Moelker A, Dankelman J, van den Dobbelsteen JJ (2018) Needle placement errors: do we need steerable needles in interventional radiology? Medical Devices: Evidence and Research (Auckland, NZ) 11:259

2. de Jong TL, Klink C, Moelker A, Dankelman J, van den Dobbelsteen JJ (2018) Needle deflection in thermal ablation procedures of liver tumors: a CT image analysis. In: Medical Imaging 2018: Image-Guided Procedures, Robotic Interventions, and Modeling. International Society for Optics and Photonics 10576:105761L.

3. van de Berg NJ, Dankelman J, van den Dobbelsteen JJ (2017) Endpoint Accuracy in Manual Control of a Steerable Needle. Journal of Vascular and Interventional Radiology 28(2):276-283.e272.

4. Li P, Yang Z, Jiang S (2018) Tissue mimicking materials in image-guided needle-based interventions: A review. Materials Science and Engineering: C 93:1116-1131.

5. Jiang S, Liu S, Feng W (2011) PVA hydrogel properties for biomedical application. Journal of the Mechanical Behaviour of Biomedical Materials 4(7):1228-1233.

6. de Jong TL, Pluymen LH, van Gerwen DJ, Kleinrensink G-J, Dankelman J, van den Dobbelsteen JJ (2017) PVA matches human liver in needle-tissue interaction. Journal of the Mechanical Behaviour of Biomedical Materials 69(Supplement C):223-228.

7. Nicholson R, Crofton M (1997) Training phantom for ultrasound guided biopsy. The British Journal of Radiology 70(830):192-194.

8. Li W, Belmont B, Shih A (2015) Design and manufacture of Polyvinyl Chloride (PVC) tissue mimicking

material for needle insertion. Procedia Manufacturing 1:866-878.

9. Hungr N, Long JA, Beix V, Troccaz J (2012) A realistic deformable prostate phantom for multimodal imaging and needle-insertion procedures. Medical Physics 39(4):2031-2041.

10. Zell K, Sperl J, Vogel M, Niessner R, Haisch C (2007) Acoustical properties of selected tissue phantom materials for ultrasound imaging. Physics in Medicine & Biology 52(20):N475.

11. Cournane S, Cannon L, Browne JE, Fagan AJ (2010) Assessment of the accuracy of an ultrasound elastography liver scanning system using a PVA-cryogel phantom with optimal acoustic and mechanical properties. Physics in Medicine & Biology 55(19):5965.

12. Rethy A, Sæternes JO, Halgunset J, Mårvik R, Hofstad EF, Sánchez-Margallo JA, Langø T (2018) Anthropomorphic liver phantom with flow for multimodal image-guided liver therapy research and training. International Journal of Computer Assisted Radiology and Surgery 13(1):61-72.

13. Maneas E, Xia W, Nikitichev DI, Daher B, Manimaran M, Wong RY, Chang CW, Rahmani B, Capelli C, Schievano S, Burriesci G (2018) Anatomically realistic ultrasound phantoms using gel wax with 3D printed moulds. Physics in Medicine Biology 63(1):015033.

14. Stewart HR, Bes EB (1968) Practical inferences from studies with a “breathing” liver phantom. American Journal of Roentgenology 104(3):686-691.

15. Banovac F, Glossop N, Lindisch D, Tanaka D, Levy E, Cleary K (2002) Liver Tumor Biopsy in a Respiring Phantom with the Assistance of a Novel Electromagnetic Navigation Device. Medical Image Computing and Computer-Assisted Intervention — MICCAI:200-207.

16. Banovac F, Cleary K, Levy E, Lindisch D, Onda S, Tanaka D (2001) Design and construction of a liver phantom for CT imaging and interventions that simulates liver motion seen during respiration. Radiologic Society of North America.

17. Naghibi H, Costa PA, Abayazid M (2018) A Soft Robotic Phantom to Simulate the Dynamic Respiratory Motion of Human Liver. 7th IEEE International Conference on Biomedical Robotics and Biomechatronics (Biorob):577-582.

18. Hu Y, Zhou Y-K, Chen Y-X, Zeng Z-C (2017) Magnitude and influencing factors of respiration-induced liver motion during abdominal compression in patients with intrahepatic tumors. Radiation Oncology 12(1):9.

19. Rohlfing T, Maurer Jr CR, O’dell WG, Zhong J (2004) Modeling liver motion and deformation during the respiratory cycle using intensity-based nonrigid registration of gated MR images. Medical Physics 31(3):427-432.

20. Kikinis R, Pieper SD, Vosburgh KG (2014) 3D Slicer: a platform for subject-specific image analysis, visualization, and clinical support. Intraoperative imaging and image-guided therapy:277-289.

21. Zhu L, Kolesov I, Gao Y, Kikinis R, Tannenbaum A (2014) An effective interactive medical image segmentation method using fast growcut. MICCAI workshop on interactive medical image computing.

22. Cignoni P, Callieri M, Corsini M, Dellepiane M, Ganovelli F, Ranzuglia G (2008) MeshLab: an Open-Source Mesh Processing Tool. Sixth Eurographics Italian Chapter Conference:129-136.

23. Pietroni N, Tarini M, Cignoni P (2010) Almost isometric mesh parameterization through abstract domains. IEEE Transactions on Visualization and Computer Graphics 16(4):621-635.

24. de Jong TL, Moelker A, Dankelman J, van den Dobbelsteen JJ (2019), 3D models of liver and rib

cage of four patients during inspiration and expiration. 4TU centre for Research Data, Dataset, DOI: uuid:1a6ebda2-dbba-4814-bdad-ba723632ea95

25. Tsai Y-L, Wu C-J, Shaw S, Yu P-C, Nien H-H, Lui LT (2018) Quantitative analysis of respiration-induced motion of each liver segment with helical computed tomography and 4-dimensional computed tomography. Radiation Oncology 13(1):59.

26. Hallman JL, Mori S, Sharp GC, Lu H-M, Hong TS, Chen GT (2012) A four-dimensional computed tomography analysis of multiorgan abdominal motion. International Journal of Radiation Oncology Biology Physics 83(1):435-441.

27. Wysocka B, Kassam Z, Lockwood G, Brierley J, Dawson LA, Buckley CA, Jaffray D, Cummings B, Kim J, Wong R (2010) Interfraction and respiratory organ motion during conformal radiotherapy in gastric cancer. International Journal of Radiation Oncology Biology Physics 77(1):53-59.

28. Bussels B, Goethals L, Feron M, Bielen D, Dymarkowski S, Suetens P, Haustermans K (2003) Respiration-induced movement of the upper abdominal organs: a pitfall for the three-dimensional conformal radiation treatment of pancreatic cancer. Radiotherapy and Oncology 68(1):69-74.

29. Balter JM, Brock KK, Litzenberg DW, McShan DL, Lawrence TS, Ten Haken R, McGinn CJ, Lam KL, Dawson LA (2002) Daily targeting of intrahepatic tumors for radiotherapy. International Journal of Radiation Oncology Biology Physics 52(1):266-271.

30. Brandner ED, Wu A, Chen H, Heron D, Kalnicki S, Komanduri K, Gerszten K, Burton S, Ahmed I, Shou Z (2006) Abdominal organ motion measured using 4D CT. International Journal of Radiation Oncology Biology Physics 65(2):554-560.

31. Tan Z, Parisi C, Di Silvio L, Dini D, Forte AE (2017) Cryogenic 3D Printing of Super Soft Hydrogels. Scientific Reports 7(1):16293.

32. Culjat MO, Goldenberg D, Tewari P, Singh RS (2010) A review of tissue substitutes for ultrasound imaging. Ultrasound in Medicine & Biology 36(6):861-873.

33. Villard PF, Jacob M, Gould D, Bello F (2009) Haptic simulation of the liver with respiratory motion. Studies in Health Technology and Informatics.142:401-406.

6

Mimicking needle-hepatic vessel interaction forces to develop liver phantoms

Tonke L. de Jong, Sander van der Velden, Jenny Dankelman,
John J. van den Dobbelsteen

Submitted (2019)

"The previous chapter demonstrated a liver phantom that accounts for two specific aspects: respiratory motion and heterogeneous tissue mimicking characteristics. Apart from these features, including a vascular system would also add functionality to such a system. However, we first need data on needle forces that arise during puncturing of blood vessels in the liver. Consequently, this chapter studies the importance of including walls in the hepatic vascular structure, and explores an option to incorporate them in a PVA phantom."

ABSTRACT – Data on needle-tissue interaction are needed to develop state-of-the-art liver phantoms. However, the forces involved upon puncturing vessels in the human liver are unknown. Therefore, this study gives insight into the needle tip forces upon insertion through hepatic vessel walls, which is used to provide a phantom material that mimics these forces.

Liver tissue and vessels, i.e. arteries, portal and hepatic veins, were extracted from three fresh-frozen human cadavers. An 18Gauge trocar needle was inserted through the specimens under a constant velocity, capturing the forces.

Puncturing hepatic veins (median: 2.2N, IQ range: 1.5N–3.7N, n = 173) resulted in the highest forces, followed by hepatic arteries (median: 1.3N, IQ range: 1.2N–1.8N, n = 11), and surrounding liver tissue (median: 0.4N, IQ range: 0.3N–0.5N, n = 47).

Based on these data, we conclude that it is important to mimic vessel walls in liver phantoms. In addition, we were able to mimic these forces in silicone specimens with mesh fabric attached. These can be added to liver phantoms, for example to test novel needle designs, to validate robotic systems, and to train medical residents.

6.1. INTRODUCTION

Precise needle placement is crucial in needle-based interventions, but also difficult. These difficulties consist of, but are not limited to: unwanted needle deflection upon insertion, limited medical imaging, undesired movement of the target and anatomical obstructions [1]. To improve needle placement in interventional radiology, there is a need for high fidelity phantoms, which can for example be used as a training model for medical residents, to validate robotic needle placement systems and to test novel needles. However, more data are needed on needle-tissue interaction forces to develop these phantoms.

The Transjugular Intrahepatic Portosystemic Shunt procedure (TIPS) is considered to be one of the most technically challenging needle-based interventions in radiology[2]. In the TIPS procedure, a stent is placed between the hepatic and the portal vein, thereby restoring the blood flow in the cirrhotic liver (*Figure 6.1*). In doing so, the needle punctures the walls of the hepatic vein and the portal vein. Therefore, a liver phantom, for a procedure such as TIPS, should be made of a tissue mimicking material that includes hepatic vasculature, and should be ultrasound compatible.

Recently, several organ phantoms have been made from a heterogeneous tissue

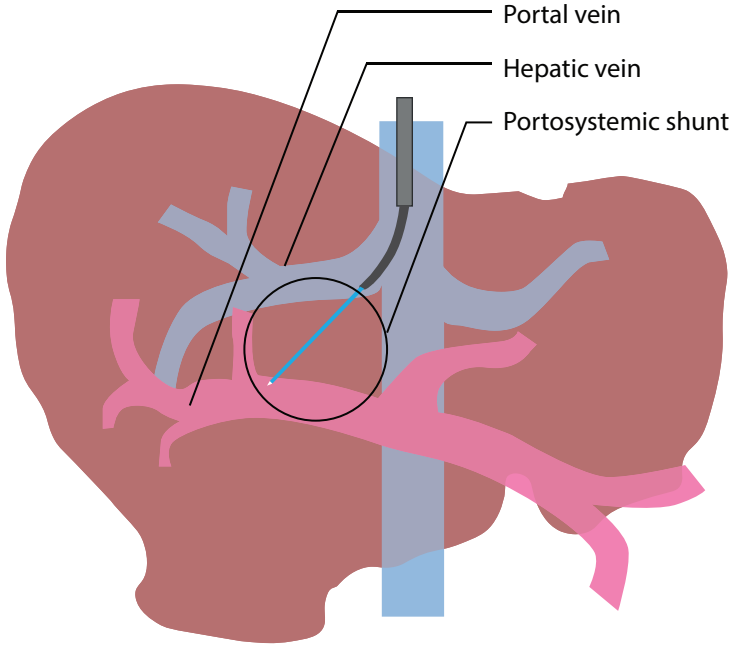

Figure 6.1. *During the Transjugular Intrahepatic Portosystemic Shunt (TIPS) procedure, a tract is created between the hepatic vein and the portal vein to restore the bloodflow.*

mimicking material called polyvinyl alcohol[3, 4], due to its good medical imaging mimicking [5, 6], mechanically mimicking[7, 8] and matching needle-tissue interaction properties[9]. However, none of these phantoms include the hepatic vasculature with matching needle-tissue interaction forces. To be able to include such a system in a liver phantom, more insight is needed into these forces. Little research has been done on needle-blood vessel interaction forces by experiments, and as a result, experimental data are scarce.

For example, Elgezua et al. studied needle blood vessel interaction using porcine liver [10-12]. It took around 1N to puncture a porcine liver vein with an 18Gauge needle and different insertion velocities[10]. Puncturing a vein or artery resulted in a higher peak force than puncturing surrounding porcine liver tissue, with puncture forces ranging from 0.4N to 1.3N[11]-[12]. In addition, Jiang et al. [13] conducted experiments to examine the effect of different needle geometries, insertion methods and tissue characteristics on the needle force. A needle puncture force of 0.6N was reported, for insertion into ex-vivo porcine liver vessels. However, neither needle diameter, nor sample size were provided.

In addition, needle insertion experiments in vessel walls outside the liver have been performed, resulting in four studies with human tissue[14-17] and six with animal tissue [18-23]. For example, for the development of an automatic blood sampling system, Okuno et al. [15] studied the maximal puncturing force of the vena mediana cubiti, located in the forearm on human volunteers, by manually inserting the needle. This resulted in a mean maximum puncture force of 0.6N and 0.2N, for needles of 0.8mm and 0.4mm in diameter, respectively. Additionally, Healey et al. [16] examined the forces involved in interventional radiology using fingertip-mounted force sensor pads. Needle insertions were done manually on in-vivo human femoral artery with an unknown needle diameter. Forces required to puncture the arterial wall varied between 0.1 and 9N. Zhai et al. [14] presented a force sensor that can be used to measure axial needle insertion forces during needle puncture procedures in patients. Measurements were done on in-vivo human femoral arteries using an 19G needle. A peak force of around 2N was reported. Finally, Peply et al. [17] measured needle forces when puncturing the jugular vein of a fresh-frozen human body, by using a customized syringe. The maximal peak forces were in the range of 1N to 2N for 18Gauge needles.

In short, literature gives an indication of the needle forces that can be encountered during puncturing of vessel walls. Puncture forces vary from less than 1N up to around 10N. However, no data are available on the forces needed to penetrate the vessel walls in the human liver. Moreover, data are difficult to compare, as most studies use different methods and often not all crucial experimental design specifications are described, such as sample size, insertion velocity, and needle type/diameter.

Therefore, the present study gives insight into the axial needle forces during puncturing of blood vessels in the human liver, and provides a phantom material that mimics these forces. The approach adopted for this study is as follows. First, we carried out needle

insertion experiments with three livers from fresh-frozen human cadavers, thereby measuring the needle penetration forces in the hepatic vein, portal vein, hepatic artery and liver tissue. Second, we compared these data with insertions into silicone specimens with or without a polyamide-lycra mesh fabric attached. This mesh allows for the attachment of silicone with PVA. Finally, we checked for matching force profiles with combined silicone-mesh-PVA specimens.

6.2. METHODS

6.2.1 Experimental set-up

The experimental set-up (*Figure 6.2*) consisted of a linear mini slide that was mounted vertically with respect to the table. The slide was equipped with a force sensor. The base of the needle was connected to this force sensor. The needle tip was aligned with the specimen holder, consisting of a manual motion stage and metal plates with five holes (diameter of 7mm) to clamp the test specimens. The clamps of the specimen holder were custom made. The mutual distance between the holes was 10mm from center to center. The manual motion stage was moved in horizontal direction to align the needle with the holes in the specimen clamps. This way, a total of five insertions could be done for a single test specimen.

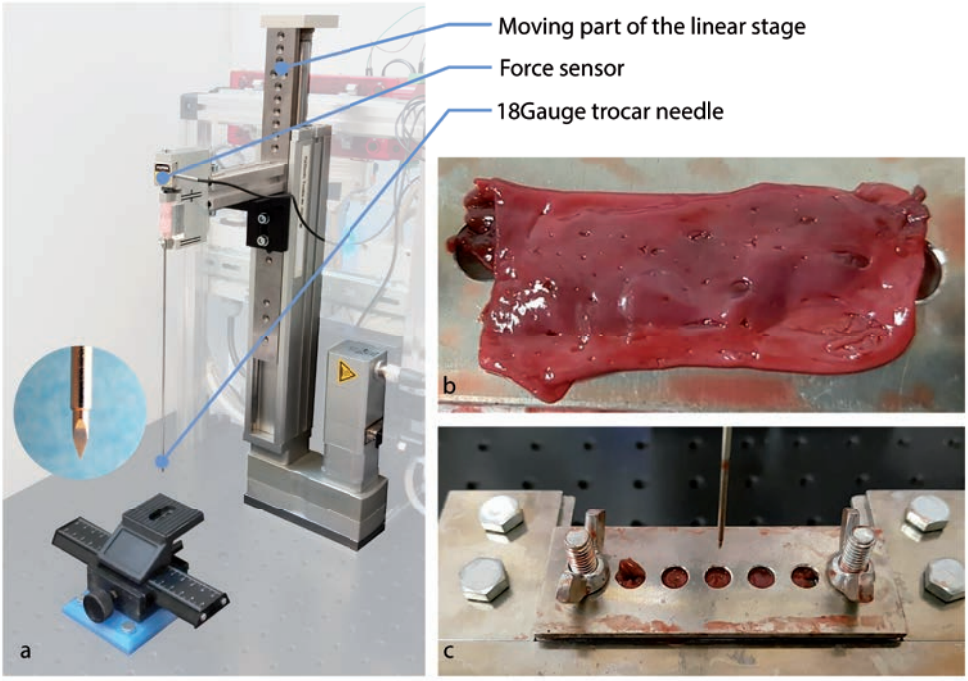

Figure 6.2. *Experimental set-up. a) The experimental set-up consisted of a linear stage, a force sensor connected to the hub of the needle and a manually movable slider to move the tissue specimens. b) Example of a hepatic vessel wall that was cut open, with an approximate length of 45mm and width of 20mm. c) Tissue clamp that was connected to the manually movable slider.*

The EGSL-BS-45-2003P linear mini slide had a maximal travel distance of 200mm and a minimum and maximum sliding velocity of 1mm/s and 30mm/s, respectively. It was powered by an EMMS-ST-42-S-SEB-G2 stepper motor with brake. The stepper motor was controlled by a CMMS-ST-C8-7-G2 motor controller (all components from Festo BV, Delft, the Netherlands).

An LSB200-FSH00104 miniature S-beam load cell with a measurement range of 10lb (45.5N) and an IAA100 amplifier measured the forces that were acting on the base of the needle during puncturing, i.e. insertion and retraction (components from FUTEK Advanced Sensor Technology, Southern California, USA). In combination with a 16bit A/D converter, over a range of +/-10V, on a LabJack T7 (LabJack Corporation, Lakewood USA), the theoretical resolution of this system resulted in 0.31mV, whereas the effective resolution was found to be 2mV, corresponding with 0.018N, probably caused by interfering surroundings.

6.2.2 Specimen preparation

Thin liver specimens

Three fresh-frozen livers were obtained at the department of Neuroscience at the Erasmus MC in Rotterdam. The anatomy of these livers did not show any suspicious nodules by visual inspection, and therefore hepatic cirrhosis was not assumed. Before preparation of the liver specimens, liver hardness was estimated using a Shore OO durometer (HT-6510-OO, Landtek, Guangzhou, China), by manually measuring at 20 random locations on the surface of the liver.

Four different liver specimens were included in this study: the hepatic artery, the hepatic vein, the portal vein and liver tissue specimens without vessel structures (control). An example of a liver specimen is shown in the upper right corner of *Figure 6.2*. The different blood vessels were carved out of the livers using medical scalpels and cut open. Preliminary experiments showed the necessity of including a layer between 2mm to 5mm of liver tissue on the outside of the blood vessel wall, to prevent damaging the vessel wall. The control specimens were pieces of liver tissue with a thickness of 5mm without visible vessel structures. Phosphate Buffer Saline solution was used for all specimens to prevent drying. Experiments were immediately conducted after specimen preparation.

Thin silicone specimens

Preliminary test showed that Dragon Skin 20 specimens (Shore A of 20, Smooth-On Inc., Macungie, PA, USA), PVA (Selvol PVOH 165, Sekisui Chemical Group, NJ, USA) 7m% specimens with up to eight freeze-thaw cycles, and PMC-780 Dry PU rubber specimens (Smooth-On Inc., Macungie, PA, USA) did either not result in sufficient peak forces, or did not match the force profiles during puncturing of the liver veins.

Therefore, hepatic vessel wall phantoms were created from a specific type of silicone, being Smooth-Sil 950 (Smooth-On Inc., Macungie, PA, USA) (*Figure 6.3- top left*). This silicone has a shore A hardness of 50. Thi-Vex was added during the production of the silicon. It increases the viscosity of the silicone, so that it can be more easily applied to non-horizontal surfaces. The addition of Thi-Vex did not influence the needle forces.

The thickness of the final specimens ranged from 0.6mm–1.2mm. To further increase the peak forces, a 92% Polyamide and 8% Lycra mesh fabric (80 gram/m^2, Rijs Textiles B.V., Tilburg, The Netherlands) was connected to the silicone (*Figure 6.3 – bottom left*). In addition to increasing the force, the mesh fabric also enabled proper bonding between silicone and PVA. The mesh fabric was either applied during the hardening process of the silicone, or afterwards, using Sil-Poxy glue (Smooth-On Inc., Macungie, PA, USA), which did not have any effect on the needle forces.

Thick Hepatic vessel wall-tissue and silicone-mesh-PVA specimens

Besides the smaller specimens, also thicker test specimens were created to compare force profiles of needle insertions (*Figure 6.3 - right*). In doing so, hepatic vein and portal vein blood vessel test specimens with about 15mm of liver tissue still attached were created. Also silicone specimens with mesh fabric and a 15mm layer of PVA attached (4m%, two freeze-thaw cycles, 8 hours each) were made. For the silicone layer, a thickness of 0.6mm and 1.1mm was used. All experiments were done with the (PVA) tissue on top of the (phantom) blood vessel wall.

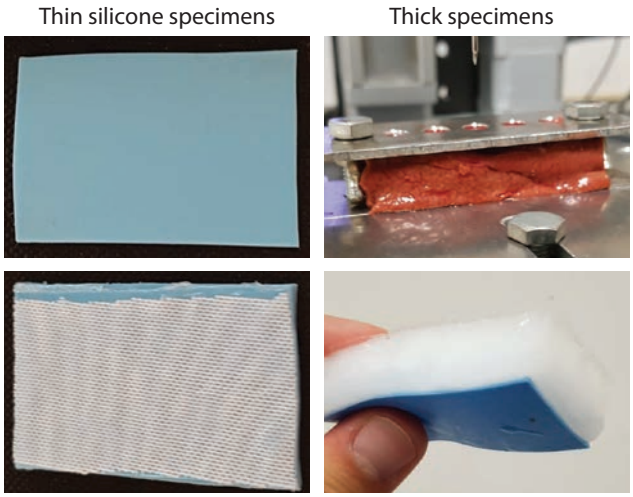

Figure 6.3. *Test specimens. Left are the thin silicone specimens without and with mesh. Right are the thick specimens, consisting of a hepatic vessel wall with a layer of tissue attached and silicone-mesh specimen with a layer of PVA attached.*

6.2.3 Experimental design

Peak forces of the thin specimens

The thin liver and silicone specimens were used for the peak force comparison. An 18Gauge two-part trocar needle (Cook Medical, Bloomington, IN, USA) was inserted, as it is commonly used during radiologic interventions, and has a symmetric three facets needle tip (*Figure 6.2a*). The needle was inserted with a constant speed of 5mm/s. The peak forces of the blood vessel mimicking specimens were compared to those of the tissue specimens. Desired specimen peak forces were defined as those that fell within the interquartile range (IQR) of the peak forces of the tissue specimens. Data were analyzed with Matlab 2018b (The Mathworks Inc., Natick, MA, USA) and results were presented as box plots. Force data were made publicly available at [28].

Force profiles of the thick specimens

The thick specimens were used to compare the force profiles. The same insertion settings were applied as aforementioned. Force profiles were visualized with force-time diagrams using the mean encountered needle force per specimen and minimal-to-maximal force range.

6.3. RESULTS

6.3.1 Peak forces of the thin liver and silicone specimens

A total of 231 measurements in liver specimens were done. All force data of the three livers were combined, because there were no clear differences. The livers' Shore OO hardness (mean ± standard deviation) were: 28±6, 27±6 and 31±7, respectively. *Figure 6.4* shows a boxplot with the peak forces per specimen group. Puncture forces in surrounding liver tissue are lowest (median: 0.4N, IQR: 0.3N-0.5 N), followed by the arteries (median: 1.3N, IQR: 1.2N-1.8N). The biggest peak forces and variability are found for the needle punctures in the portal vein (median: 1.98N, IQR: 1.5N-3.0N) and hepatic vein (median: 2.5N, IQR: 1.5N-4.4N). Combining the portal vein and the hepatic vein gives a median of 2.2N with an interquartile range of 1.5N–3.7N for insertions into liver veins.

In *Figure 6.5* the peak forces of the insertions through the silicone specimens with and without mesh are presented. They were grouped according to layer thickness. The range of the desired peak forces for the blood vessel phantoms, i.e. the combined interquartile range of the hepatic and portal vein, is shown by the blue dotted lines. In general, the groups with the mesh attached show higher variability in peak forces than the ones without. The peak forces of the insertions into silicone specimens ranging from 0.6mm-0.8mm in thickness are too low (median: 0.9N), whereas the thicker specimens of 0.9mm-1.1mm fall within the desired range (median: 1.7N). Median peak forces of the silicone specimens with mesh are within the specified range (1.6N and

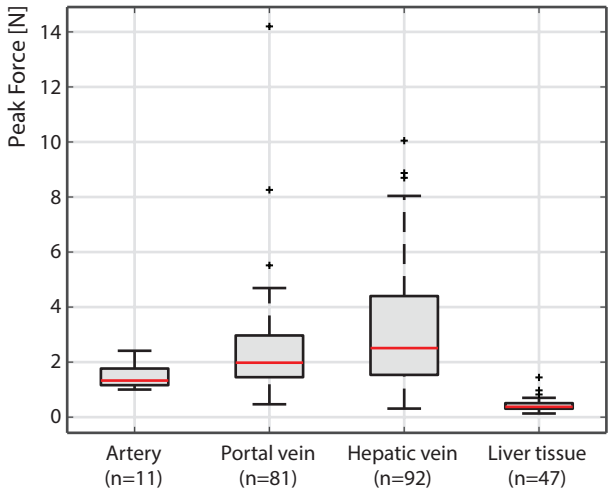

Figure 6.4. *Boxplot of the peak forces when puncturing arteries, portal veins, hepatic vein and liver tissue of three ex-vivo human livers.*

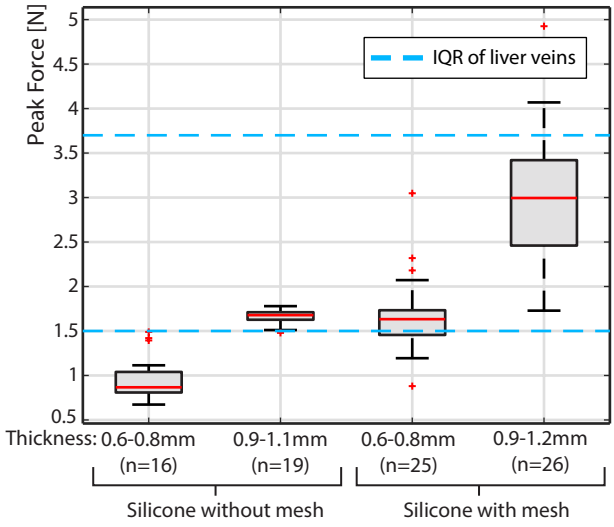

Figure 6.5. *Boxplot of the peak forces in the silicone specimens grouped according to thickness, with and without mesh attached, compared to the interquartile range of the insertions into liver veins.*

3.0N for a thickness of 0.6mm-0.8mm and 0.9mm-1.2mm,respectively).

6.3.2 Force profile comparison of the thick hepatic vessel wall-tissue and silicone-mesh-PVA specimens

Based on the aforementioned results, silicone specimens of 0.6mm and 1.1mm thickness with a mesh and a PVA layer attached were made. The needle insertion force profiles were compared to insertions into liver specimens consisting of a single vein wall and a directly attached tissue layer of 15mm. Examples of these specimens and the results are shown in *Figure 6.6*. Force profiles are comparable among the different specimens. Overall, the forces are lower for the insertions in the specimens with the thinner silicone layer, whereas they are almost the same for the insertion in the specimens with the thicker silicone layer. In general, during puncturing of the silicone and mesh fabric, a double peak is shown.

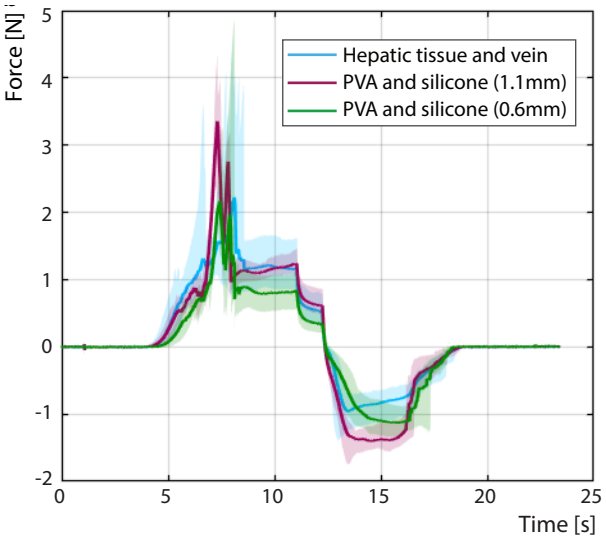

Figure 6.6. *Force-time diagrams (5mm/s) showing the mean and maximal and minimal force encountered during puncturing of the hepatic tissue (n=20), PVA and 1.1mm silicone (n=10), and PVA and 0.6mm silicone (n=10).*

6.4. DISCUSSION, OUTLOOK & CONCLUSION

6.4.1 Interpretation

This research studied the peak forces of needle insertions through hepatic vessel walls of three ex-vivo human livers. The results show that puncturing the vessel walls causes higher needle peak forces than puncturing surrounding liver tissue. Therefore, we conclude that it is important to mimic vessel walls in future liver phantoms for needle-

based interventions. Smooth-Sil 950 silicone was chosen as a blood vessel mimicking material. The addition of a polyamide-lycra mesh fabric and a silicone thickness between 0.6mm and 1.2mm results in the desired range of peak forces.

As for the needle insertions into human liver tissue and veins, large variability was encountered (*Figure 6.4*). Partially, this might be due to the fact that blood vessels contain many side branches. When puncturing such a branch, which inevitably leads to local thickening of the blood vessel wall, higher needle forces could be encountered as a result. Remarkably, we observed higher peak forces for the insertions through the hepatic and portal vein than the hepatic artery. This is presumably caused by their differences in layer composition. Arteries contain relatively more smooth muscle tissue, whereas veins contain more collagenous tissue [24]. Also, the diameters of the arteries were smaller than the veins.

This study was done with human livers. However, when interpreting these results, it must be considered that in-vivo blood vessels may have different mechanical properties than ex-vivo blood vessels, for example due to blood irrigation. Puncturing in-vivo blood vessels could therefore result in different needle forces, compared to ex-vivo [25, 26]. The same applies to blood vessels from diseased livers. Due to scarcity and logistic challenges, collecting needle-tissue interaction data on fresh diseased livers remains a challenge.

Finally, different needle insertion parameters, such as needle diameter, insertion velocity and insertion angle, can influence the needle force as well. However, as we used exactly the same insertion parameters for the tissue and phantom measurements, we believe that our results can properly be compared.

6.4.2 Outlook

To show the full potential of the proposed methods, we tested the feasibility of including the silicone specimens into PVA phantoms, in terms of connection, ultrasound compatibility and shape. Thin-walled tubes with mesh fabric were fabricated using the silicone (*Figure 6.7a*) and implemented in a PVA phantom. The connection between the silicone and PVA was ensured via the mesh. Several needle punctures did not affect bonding between the layers. In addition, the phantom was tested for ultrasound compatibility. This resulted in a clear visible distinction between the PVA and silicone vessel wall phantom.

However, real hepatic vasculature is more complex than the aforementioned structures. Therefore, we made a computer model of the liver veins using 3D Slicer 4.8.1 [27] (www.slicer.org) (*Figure 6.7b*), by semi-automatic segmentation of the hepatic vein and the portal vein captured on CT scans of one patient. Subsequently, a part of the portal vein (indicated by the white arrow on *Figure 6.7b*) was simplified and 3D printed with water-soluble PVA. Then, silicone was brushed onto this surface, and, after hardening of the silicone, the structure was placed into water. The water-soluble PVA dissolved,

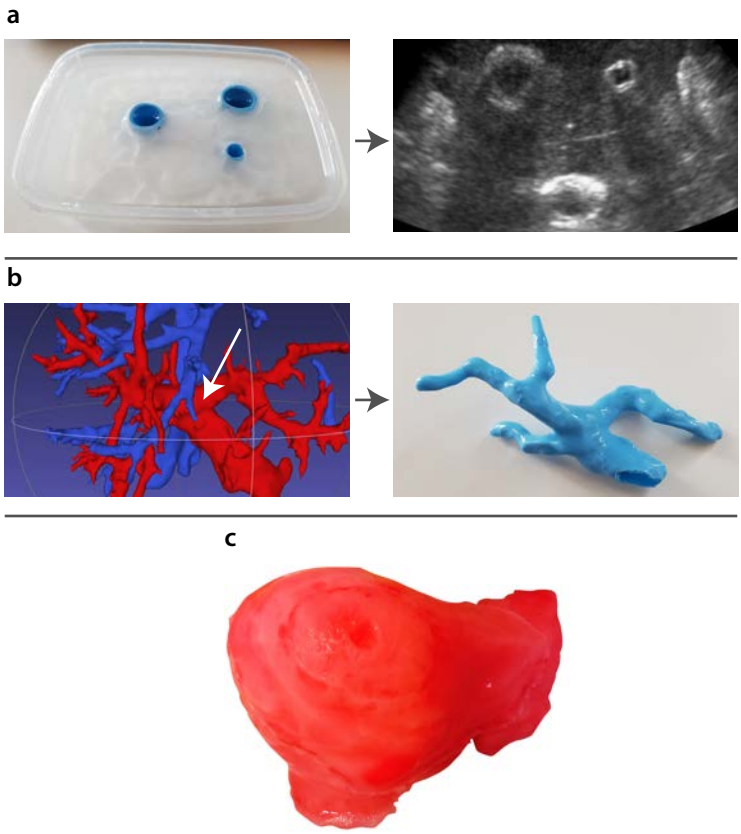

Figure 6.7. *Outlook showing the potential of the developed silicone phantoms. a) Ultrasound compatibility; a phantom with circularly shaped silicone vessel phantom walls and mesh surrounded by PVA (left), and the ultrasound image of the phantom (gain = 59) (right). b) Picture of the silicone blood vessel (right) created with a simplified, 3D printed, portal vein model (left, indicated with the white arrow) based on a CT scan of a patient. c) Example of an anthropomorphic PVA liver phantom to which the portal vein model can be added.*

and a thin-walled 3D silicone structure of the portal vein remained. The developed portal vein wall phantom can be added to a PVA phantom (*Figure 7.5c*), by means of the connecting mesh between silicone and PVA.

6.4.3 Conclusion

In conclusion, we gathered data on needle forces during puncturing of blood vessels from ex-vivo human livers. These data are publicly available and cannot only be used for the current study, but also, for example, to further develop needle path planners and to design novel needles. One of the main observations from this research is that puncturing the hepatic vein and the portal vein with a needle results in higher peak forces than liver tissue. Therefore, it is important to include vessel walls in liver phantoms for

needle-based interventions. By making that statement, this study developed a silicone vessel wall phantom with a mesh layer attached, that is able to mimic the needle-tissue interaction forces. The phantom can be made in the desired vessel structure, can be attached to PVA, and allows for ultrasound guidance. Therefore, it is suitable to implement in future PVA liver phantoms.

REFERENCES

[1] de Jong TL et al. (2018) Needle placement errors: do we need steerable needles in interventional radiology? Medical Devices (Auckl, NZ) 11:259.

[2] Rössle M, Siegerstetter V, Huber M, Ochs A (1998) The first decade of the transjugular intrahepatic portosystemic shunt (TIPS): state of the art. Liver 18:73-89.

[3] Li P, Jiang S, Yu Y, Yang J, Yang Z (2015) Biomaterial characteristics and application of silicone rubber and PVA hydrogels mimicked in organ groups for prostate brachytherapy. Journal of the Mechanical Behavior of Biomedical Materials 49:220-234.

[4] de Jong TL, Adrichem DR, Dankelman J, van den Dobbelsteen JJ (2018) Design of a PVA liver phantom with respiratory motion for simulation of needle interventions. Computer Assisted Radiology and Surgery:S66-S67.

[5] Chen SJS, et al. (2012) An anthropomorphic polyvinyl alcohol brain phantom based on Colin27 for use in multimodal imaging. Medical Physics 39(1):554-561.

[6] Zell K, Sperl JI, Vogel MW, Niessner R, Haisch C (2007) Acoustical properties of selected tissue phantom materials for ultrasound imaging. Physics in Medicine and Biology 52(20):N475.

[7] Jiang S, Liu S, Feng W (2011) PVA hydrogel properties for biomedical application. Journal of the Mechanical Behavior of Biomedical Materials 4(7):1228-1233.

[8] Tan Z, Dini D, Baena FR, Forte AE (2018) Composite hydrogel: A high fidelity soft tissue mimic for surgery. Materials & Design 160:886-894.

[9] de Jong TL et al. (2017) PVA matches human liver in needle-tissue interaction. Journal of the Mechanical Behavior of Biomedical Materials 69:223-228.

[10] Elgezua I, Kobayashi Y, Fujie MG (2013) Survey on current state-of-the-art in needle insertion robots: Open challenges for application in real surgery. Procedia CIrP 5:94-99.

[11] Elgezua, I., Song, S., Kobayashi, Y. & Fujie, M. G. Event classification in percutaneous treatments based on needle insertion force pattern analysis. Control, Automation and Systems (ICCAS), 13th International Conference on. 288-293 (IEEE) (2013).

[12] Elgezua I, Song S, Kobayashi Y, Fujie MG (2013) Online event classification for liver needle insertion based on force patterns. Intelligent Autonomous Systems 13:1145-1157.

[13] Jiang S, Li P, Yu Y, Liu J, Yang Z (2014) Experimental study of needle–tissue interaction forces: effect of needle geometries, insertion methods and tissue characteristics. Journal of Biomechanics 47(13):3344-3353.

[14] Zhai J et al. (2013) A sensor for needle puncture force measurement during interventional radiological procedures. Medical Engineering & Physics 35(3):350-356.

[15] Okuno D, Togawa T, Saito H, Tsuchiya K (1998) Development of an automtic blood sampling system: control of the puncturing needle by measuring forces. Engineering in Medicine and Biology Society, Proceedings of the 20th annual international conference of the IEEE:1811-1812.

[16] Healy AE et al. (2005) In vivo force during arterial interventional radiology needle puncture procedures. Medicine Meets Virtual Reality: The Magical Next Becomes The Medical Now 111:178-184.

[17] Pepley D et al. (2017) Measurement of syringe needle forces for a haptic robotic training device. Design of Medical Devices Conference, American society of mechanical engineers. V001T008A017-V001T008A017.

[18] Kobayashi Y et al. (2012) Development of a needle insertion manipulator for central venous catheterization. The international Journal of Medical Robotics and Computer Assisted Surgery 8:34-44.

[19] Kobayashi Y et al. (2014) Preliminary in vivo evaluation of a needle insertion manipulator for central venous catheterization. ROBOMECH Journal 1(1):18.

[20] Kobayashi Y et al. (2013) Use of puncture force measurement to investigate the conditions of blood vessel needle insertion. Medical Engineering & Physics 35(5):684-689.

[21] Saito H, Togawa T (2005) Detection of needle puncture to blood vessel using puncture force measurement. Medical and Biological Engineering and Computing 43(2):240-244.

[22] Saito H, Mitsubayashi K, Togawa T (2006) Detection of needle puncture to blood vessel by using electric conductivity of blood for automatic blood sampling. Sensors and Actuators A: Physical 125(2):446-450.

[23] Clement RS, Unger EL, Ocón-Grove OM, Cronin TL & Mulvihill ML (2016) Effects of axial vibration on needle insertion into the tail veins of rats and subsequent serial blood corticosterone levels. Journal of the American Association for Laboratory Animal Science 55(2):204-212.

[24] de Jong TL, van der Velden S, Dankelman J, van den Dobbelsteen JJ Data on needle-hepatic interaction forces to develop liver phantoms. 4TU ResearchData. http://doi.org/10.4121/uuid:774f1b78-4b11-4f0a-b049-0d5cf05191ab

[25] Mahrieb NM, Hoehn K (2015) Chapter 19 - The cardiovascular system: blood vessels – Table 19.1 in Human Anatomy & Physiology, 721 (Pearson Education Limited, 2015).

[26] Barbé L, Bayle B, de Mathelin M, Gangi A (2007) In vivo model estimation and haptic characterization of needle insertions. The International Journal of Robotics Research 26:1283-1301.

[27] Majewicz A et al. (2012) Behavior of tip-steerable needles in ex vivo and in vivo tissue. IEEE Transactions on Biomedical Engineering 59(10):2705-2715.

[28] Kikinis R, Pieper SD, Vosburgh KG (2014) 3D Slicer: a platform for subject-specific image analysis, visualization, and clinical support. Intraoperative Imaging and Image-Guided Therapy:277-289 (Springer).

DISCUSSION AND CONCLUSION

CONNECTING THE DOTS

This thesis focused on: 1) defining design considerations for novel needles, and 2) developing and validating a high fidelity liver phantom. These two points have the general aim to improve needle placement in radiology.

Despite the ongoing technological developments in steerable needles and liver phantom designs, we still face several shortcomings. First, the exact clinical need regarding the needles remains unknown, thereby hampering the possibility to define relevant design considerations, which are needed to advance these prototypes into clinical practice. Second, the current liver phantoms for needle-based interventions lack in high fidelity regarding mechanical properties combined with breathing motion.

This thesis adopted a mixed-method approach to address these issues from several directions. The current chapter discusses the accomplishments of the work, proposes design considerations for novel needles in interventional radiology, and provides recommendations for future research in the development of realistic liver phantoms.

For more specific discussions on the limitations and recommendations, please refer to the chapter discussions.

Part A: DESIGN CONSIDERATIONS FOR NOVEL NEEDLES

Accomplishments

In the present years, several needle steering prototypes have been developed. Most steerable needle prototypes are general-purpose. Conceptually, these are developed to: 1) correct for unwanted needle deflection upon insertion, 2) steer actively around anatomical obstacles, such as vessels and ribs.

More data to gain insight into needle insertion in interventional radiology was needed to define the specific clinical needs and design considerations for such novel needles. The first three chapters concentrated on collecting these data, by using a multi-method approach. We accomplished this by distributing a questionnaire to interventional radiologists, by quantifying needle deflection in clinical practice, and by carrying out a numerical analysis of the reachability of liver regions in needle targeting.

First, the questionnaire on needle placement studied the clinical need for steerable needles (*Chapter 1*). It reveals patient-specific and technical factors that challenge needle placement. In addition, it clearly shows that interventional radiologist believe that needles need improvement in visibility and manipulability, and that they see the

added value for steerable needles in current interventions.

Second, we carried out a CT image analysis on needle deflection in thermal ablation procedures (*Chapter 2*). Deflection (>1mm) occurs in more than half of the needle insertions, and is increased with longer insertions. Therefore, there is a need for novel needles that are able to correct for needle deflection.

Third, a numerical analysis was performed to quantify the reachability of the liver during inspiration and expiration with a needle (*Chapter 3*). This fundamental research showed that cranial and posterior targets, and targets positioned directly behind the ribs, have lowest reachability. On average, reachability increases from the state of expiration to inspiration.

Design considerations for novel needles and recommendations for future work

Based on the findings in *Chapter 1-3* we identified the clinical need for novel needles. We propose design considerations for novel needles in interventional radiology and we provide recommendations for future work.

In general, novel needles should be developed with their specific purpose, target organ and intervention in mind. Interventional radiologists see added value for steerable needles in clinical practice, especially for targeted lesions in the liver and for taking biopsies. Novel needles should be manually placed, until more support is created for robotic needle placement among interventional radiologists.

Current developments in steerable needles focus more on steering around anatomical objects, than on correcting for needle deflection. Currently, the minimally required accuracy for needle placement is not sufficiently reached in clinical practice, and needle deflection is observed. Therefore, needle deflection deserves more attention in the field. Interventional radiologists should be able to correct needle trajectories during insertion.

We foresee that in specific situations, steerable needles have the potential to lower the number of puncture attempts, to increase accuracy and precision of the placement. This may lead to a decrease in radiation dose for the patient, increased safety and an improved treatment. We found that the magnitude of needle deflection is related with insertion depth. Therefore, when possible, shorter, curved insertion paths should be favored over long conventional insertion paths.

We would like to emphasize that steerability is not a requirement itself, but one of the means to eventually reach a target accurately and precisely, with the least number of puncture attempts. Therefore, the advantages of using such an instrument over a conventional needle, should be justified. We foresee that the proposed numerical analysis of target reachability with ray casting from target-to-skin can be used for decision-making in patient-specific treatment plans in the future, determining the

best insertion parameters, choosing the right instrument and optimizing the breathing phase.

Although instrument development is a crucial factor in improving needle placement in interventional radiology, care should be taken that this is not the only means by which the patient can be optimally treated. As stated by the medical doctors that participated in the questionnaire of *Chapter 1*, improvements can also be found in the field of medical imaging, and, when looking with a broader view, in radiotherapy.

Part B: LIVER PHANTOM DEVELOPMENT

Accomplishments

The last three chapters of this thesis center around the development of a liver phantom for needle-based simulations. For this specific purpose, one of the requirements was that the phantom had to be made of a tissue mimicking material in terms of needle-tissue force characteristics.

We started therefore with the search for a material that could mimic the heterogenic properties of real liver tissue (*Chapter 4*). Polyvinyl alcohol specimens with different mass percentages and freeze-thaw cycles were fabricated. Needles were inserted into these specimens and compared to insertions into ex-vivo human livers, in terms of friction forces along the needle shaft, the magnitude of the peak forces, and the number of peak forces per unit length. The findings suggest that PVA specimens with 4m% and two freeze-thaw cycles are most suitable in mimicking healthy liver tissue.

Then, we used this material to make a liver phantom in an anthropomorphic shape, based on CT scans of patients (*Chapter 5*). Another requirement for the phantom was that it could mimic respiratory movement. To this end, we analyzed the liver and rib cage motion during inspiration and expiration of human patients, and incorporated this into our phantom by means of a linear stage. The whole set-up can be adjusted for applying different motion patterns and liver shapes/sizes.

In addition, we measured deflection of an ablation needle in our phantom and compared it with the clinical results from *Chapter 2*. Needle deflection in our phantom is in the same order of magnitude as found in real procedures. Moreover, these results quantitatively suggest that breathing contributes to needle deflection, and therefore also to the total needle targeting error.

Lastly, we developed a silicone vessel wall phantom, which can be seen as a first step to simulate the liver vasculature in terms of needle-tissue interaction and shape (*Chapter 6*). We were able to attach the silicone phantoms to PVA with a polyamide-lycra mesh fabric. The most important experimental finding from this study is that puncturing the hepatic vein and portal vein with a needle results in higher peak forces than liver tissue,

indicating the need for including vessel walls in a phantom.

Apart from these accomplishments, we believe that the experimental force data that were gathered in the aforementioned studies can be useful for other researchers as well. Therefore, all data were made publicly available, and care was taken to specifically describe all important experimental design parameters, such as sample size, needle type and insertion velocity.

General limitations and recommendations for future work

The general limitations of the last three chapters of this thesis relate to the use of the biological test specimens, and the choice for PVA as a phantom material. They are discussed in this section. Furthermore, recommendations are given for future research.

The biological specimens that were used for the experiments in thesis have certain limitations that are important to consider. We used fresh-frozen ex-vivo human livers, which are different from in-vivo ones. To what extent these livers are comparable to the real situation cannot easily be stated, as discussed in greater detail in *Chapter 4* and *Chapter 6*. Future research should study the effect of freezing on needle-tissue interaction in detail.

Data on needle-tissue interaction are scarce, but essential for the field. Current developments in novel needle design are often hampered from clinical implementation by limited experimental validation. The research and data gathered on human livers presented in this thesis can be seen as a start. Next steps include experiments with cirrhotic livers, preferably directly obtained after extraction from patients undergoing transplantation surgery. This will bring with it a great logistic challenge, that needs to be dealt with by the researchers upfront.

We worked with PVA as a liver phantom material. All phantom materials have their own pros and cons. For the validation of novel instruments, mimicking the heterogenic properties tissue is crucial; a feature that PVA has. Nevertheless, we did not study in-depth other imaging and mechanical properties of PVA in this thesis, such as ultrasound-mimicking qualities and material stiffness. Future work should study to what extent these phantom properties could be optimized to mimic real tissue.

Another limitation concerns the production process of PVA. Although we monitored the production variables carefully, they could affect the final properties of the phantom. Examples of these variables are the freeze-thaw time and temperature, and the temperature during dissolving of PVA in water. On top of that, we used one specific type of PVA for the experiments. The results derived from the studies cannot be generalized to PVA from other suppliers, as differences in degree of hydrolysis and molecular weight might influence the material properties.

The purpose of the developed liver phantom is twofold: it can be used to validate

novel instruments and/or robotic systems for needle-based interventions, and to train interventional radiologists. Future work should make use of the possibilities to tune the mechanical properties of PVA, thereby mimicking diseased tissue, including target lesions. Moreover, extensive user experience tests should be performed to optimize it as a trainings tool.

CONCLUSION

- In this thesis we identified the clinical need for novel needles in interventional radiology and defined design considerations, that have been studied via a multi-method approach. A clinical need for steerable needles in interventional radiology was indicated, both in terms of correcting for needle deflection, and actively steering towards a target. We recommend that novel needles should be developed with a specific purpose in mind. Furthermore, steerability is a means, not a goal in itself, and should therefore be justified. We foresee that numerical analysis of the reachability of targets cannot only find fundamental relations between reachability and anatomical topology, but also aid in decision-making in patient-specific treatments, for example in choosing the right instrument and selecting the optimal breathing phase.

- Moreover, we developed an anthropomorphic liver phantom that can be used for the simulation of needle-based interventions. The design features respiratory motion and mimics the forces upon needle insertion. Liver phantoms based on PVA do mimic human livers in needle-tissue characteristics. Therefore, we recommend to use PVA-based phantoms for pre-clinical testing of novel needles, instead of homogeneous phantoms. The phantom was technically evaluated by comparing the motion with CT scans of patients, and showed needle deflection in the same order of magnitude as observed in clinical practice. A first step towards the implementation of vasculature inside the phantom was performed by developing vessel wall phantoms with matching needle-tissue interaction as was found by experiments using ex-vivo human liver specimens.

In conclusion, this thesis covered two aspects that can be seen as a means to improve needle placement in interventional radiology in the future, making needle-based interventions safer and quicker. The results presented in this thesis are useful for future studies in needle steering, validation of steerable needle prototypes, needle-tissue interaction experiments, and enhanced decision-making in patient-specific needle trajectory planners.

DANKWOORD

Op dit moment zit ik in het vliegtuig naar Houston voor een congres. Te midden van de blauwe stoeltjes en veelal slapende mensen, vraag ik me af hoeveel PhD kandidaten hun dankwoord in het vliegtuig hebben geschreven. Zonder afleiding door internet vliegen de woorden op het scherm, en denk ik terug aan de afgelopen tijd.

Heel vroeger, ik was nog een klein blond meisje met een Twents accent op de Franciscusschool in Oldenzaal, wilde ik graag schrijfster worden. Met een moeder als bibliothecaresse, en daarmee de vele uitstapjes naar de plaatselijke bibliotheek, is het niet verwonderlijk dat ik ontspanning kan vinden in lezen en schrijven. Ik was gek op spannende boeken waarin de vampiers, weerwolven en zombies elkaar afwisselden. Inmiddels ben ik mijn accent en de fascinatie voor spookverhalen kwijtgeraakt, maar is het boek er gekomen! Alhoewel het onderwerp zeker anders is dan dat ik toen voor ogen had, ben ik er niet minder trots op. Ik wil graag deze pagina's benutten om de mensen te bedanken die hieraan hebben meegewerkt en die belangrijk zijn geweest voor mij in de afgelopen vier jaar.

Allereerst mijn promotoren: **John van den Dobbelsteen** en **Jenny Dankelman**, beiden bedankt voor de begeleiding en het vertrouwen in mij. **John**, ik ben blij met de vrijheid en zelfstandigheid die je me hebt gegeven tijdens dit traject, waardoor ik de onderzoeksvragen kon beantwoorden waar ik het nut van in zag. Bedankt daarvoor. **Jenny**, ik vind het nog steeds bizar hoe snel jij een tekst kan lezen en er de belangrijkste punten eruit kan halen. Ook bedankt voor de goede gesprekken over vrouwen in de technische en/of academische wereld tijdens de congressen en de borrels. Ik kan deze gesprekken zeer waarderen.

Ik wil graag **de promotiecommissie** bedanken voor het nemen van de tijd om mijn proefschrift te lezen en voor het deelnemen aan mijn verdediging.

De nauwe samenwerking met het Erasmus MC was voor mij van groot belang. **Adriaan Moelker** en **Camiel Klink**, wat fijn om jullie om input te kunnen vragen wat betreft de klinische zaken. Bedankt voor jullie open houding, enthousiasme en fijne samenwerking. **Gert-Jan Kleinrensink** en **team**, bedankt dat ik mijn experimenten kon doen bij de anatomieafdeling. Tot slot, **Theo van Walsum**, bedankt voor het delen van je inhoudelijke kennis met betrekking tot medische beeldvorming.

MISIT collega's: **Annetje, Arjan, Arjo, Daniël, Dennis, Jan, Julie, Hoda, Linda, Lisette, Marit, Nick, Roos, Tim, Tomas,** en **Sara**, bedankt voor de vele goede gesprekken, de gedeelde congressen, de gezelligheid en de vele borrels. Bedankt **Arjan**, voor al je technische ondersteuning. **Nick**, wat fijn dat jij dezelfde bijzondere voorliefde voor naalden hebt, en dat ik altijd met je kon discussiëren over inhoudelijke zaken. **Lieve Julie, Hoda, Linda, Lisette en Roos**; ik krijg vaak de vraag of een promotieonderzoek

eenzaam is, of dat ik alleen met mannen “opgescheept” zit. Op zo’n moment moet ik altijd hardop lachen en denk ik aan jullie. Ik vond het heel fijn om jullie om me heen te hebben!

Ook veel andere **PhD collega’s** van de afdeling hebben mijn tijd aan de TU onvergetelijk gemaakt. Bedankt voor alle goede koffiepauzes, lunches en feestjes.

Dames van het secretariaat, ik bedank jullie ook graag voor jullie ondersteuning. **Heren van de werkplaats**, bedankt voor jullie hulp en voor het feit dat ik nu kan frezen!

Dit boek zou niet mogelijk zijn geweest zonder de hulp van studenten. **Loes**, jij begon precies met afstuderen toen ik begon met promoveren. Bedankt voor het samen schrijven van de paper, en je gezelligheid. **Ahmed, Don, Ivardi, Kauzi, Omar, Safien, Sander,** en **Thom**: Bedankt dat ik jullie mocht begeleiden tijdens jullie Bachelor/Master scriptie, dat jullie me scherp hielden, en voor de interessante onderzoeksresultaten. Ik heb veel van jullie geleerd. **Jang** en **Jan**, bedankt voor jullie enthousiasme om mij te helpen met het opzetten van de logistiek rondom het verzamelen van onderzoeksdata over zieke levers. Ik hoop dat jullie in de toekomst als medisch specialist blijven samenwerken met ingenieurs.

Ook wil ik graag de **subsidieverstrekker TTW** bedanken voor het mede mogelijk maken van dit onderzoek. Daarnaast waren de halfjaarlijkse voortgangsmeetings met nuttige feedback en de discussies met **Davide Ianuzzi** en **Steven Beekmans** waardevol. Bedankt daarvoor!

Tijdens mijn promotietraject heb ik een half jaar gewerkt bij DANS; een onderzoeksinstituut voor datamanagement. Bedankt **DANS collega’s**, ik heb een fijne tijd bij jullie gehad en veel geleerd. **Ingrid**, bedankt voor het feit dat je me zonder aarzelen aannam voor deze periode. Ik waardeer je pragmatische houding, en de fijne communicatie vanuit jou en de beleidsgroep. **Maaike** en **Cees**, ik wil jullie graag bedanken voor de prettige begeleiding. **Ricarda**, bedankt voor de gezelligheid en de wandelingen in de volkstuintjes.

PLEK collega’s in Apeldoorn, bedankt dat jullie me met open armen hebben ontvangen tijdens deze laatste fase van mijn promotietraject. Wat een fijne, warme werkomgeving hebben jullie gecreëerd. Jullie zijn zeker nog niet van me af!

Lieve paranimfen **Roos** en **Michèlle**, wat fijn dat jullie op deze belangrijke promotiedag naast mij staan! **Roos**, het was een feest dat we TU Delft collega’s werden na onze studietijd in Groningen. Ik kan alles bij je kwijt. Ik wil je ook graag bedanken voor je motivatie, want zonder jou had ik mijn proefschrift niet op dit moment al af gehad. **Mi**, ik vond het zo fijn dat jij net als ik in Den Haag ging wonen. Jij bent er altijd voor me als er iets is, ook al wonen we nu weer verder bij elkaar vandaan. Wie weet wat de toekomst brengt!

Lieve **Pracht**, ik ben zó blij met jullie! Lieve **Anniek, Chris, Mi, Laurien, Lin** en **Tannes**, bedankt dat jullie mijn vriendinnen zijn. Op nog heel veel meer lekkere kooksessies, wijnproeverijen, festivals, boottochtjes, en buitenlandtripjes samen. **Linda**, mijn mede-Promotie-Prachtvriendin: samen in hetzelfde schuitje. Nog even en dan ben ik ook bij jouw verdediging.

Ook mijn andere **vrienden en vriendinnen** wil ik graag bedanken. Niet in de laatste plaats **Awaz**, ik mis onze koffies op de TU nog steeds. Gelukkig hebben we nu ook veel gezelligheid en fijne tijden met onze mannen erbij. **Marlou**, het is fijn dat we elkaar al zo lang kennen en dat we altijd eerlijk tegen elkaar kunnen zijn. **Roos**, van voorzitters van de kookcommissie naar beiden een promotieonderzoek. Laten we daar inderdaad heel snel samen op proosten. **Saskia**, samen lekkere wijntjes drinken en heel de avond kletsen. Je bent goed gezelschap in stressvolle tijden! Ook bedankt **meiden van de volleybal** voor alle gezelligheid tijdens, voor en na het sporten. Además, muchísimas gracias a **las Zumberas** por bailar conmigo con tanta alegría.

Lieve **mama**, **Janne**, **Aljan**, en **schoonfamilie**, bedankt! **Mam**, jij denkt altijd dat ik alles kan. Dat is zeker niet waar, maar het helpt me op de onzekere momenten dat er iemand is die grenzeloos vertrouwen in me heeft. Bedankt daarvoor en voor het feit dat ik altijd even met je kan kletsen. Lieve, grote zus, **Janne**, jaren geleden heb je wel eens gezegd dat je je af en toe mijn kleine zusje voelde. Ook dat is zeker niet waar. Ik bewonder jou juist om hoe sterk je bent en hoe je je overal doorheen slaat. Dat doe je nu weer. Op naar hele fijne vakanties en meer genieten voor jullie. Met zijn drieën kunnen we alles aan!

Lieve **Mink**, grappig om te bedenken dat je in het begin nog niet eens wist waar de lever in het lichaam gepositioneerd was, en je nu bijna een expert bent op mijn promotieonderwerp. Ik ben gelukkig met jou en vind het fantastisch dat we dezelfde kijk op het leven hebben en dat we dat leven samen vieren en waarmaken. Dankjewel voor al je geduld, je vertrouwen, je grapjes en je liefde.

ABOUT THE AUTHOR

Tonke Leonie de Jong
01 April 1990

WORK EXPERIENCE

Apr 2015 | Nov 2019	PhD Candidate, Delft University of Technology, the Netherlands
May 2017 | Nov 2017	Junior Policy Maker, Data Archiving and Networked Services (DANS), the Netherlands
Feb 2014 | May 2014	Visiting researcher (internship), Universidad Politécnica de Madrid, Spain

TRAVELING

Sep 2011 | Apr 2012	Spanish learning in and cycling through South-America

EDUCATION

2012 | 2015	MSc. Biomedical Engineering, Delft University of Technology *Cum Laude*
2012 | 2013	Extra-curricular courses in Mechanical Engineering, Delft University of Technology
2008 | 2011	BSc. Life Science & Technology, University of Groningen
2002 | 2008	Pre-University Education, Twents Carmel College Oldenzaal

SCIENTIFIC OUTPUT

CT-based numerical analysis of reachability of liver regions in needle targeting
T.L. de Jong, N.J. van de Berg, A. Moelker, J. Dankelman, J.J. van den Dobbelsteen
Submitted for publication 2019.

Mimicking needle-hepatic vessel interaction forces to develop liver phantoms
T.L. de Jong, S. van der Velden, J. Dankelman, J.J. van den Dobbelsteen
Submitted for publication 2019.

Designing and validating a PVA liver phantom with respiratory motion for needle-based interventions
T.L. de Jong, A. Moelker, J. Dankelman, J.J. van den Dobbelsteen
International Journal of Computer Assisted Radiology and Surgery 2019: p. 1-10

Needle deflection in thermal ablation procedures of liver tumors: a CT image analysis
T.L. de Jong, S.J.C. Klink, A. Moelker, J. Dankelman, J.J. van den Dobbelsteen
Proc. SPIE Medical Imaging 2018. 10576L

Needle placement errors: do we need steerable needles in interventional radiology?
T.L. de Jong, N.J. van de Berg, L. Tas, J. Dankelman, J.J. van den Dobbelsteen
Medical Devices: Evidence and Research 2018. 11: p. 259-265

PVA matches human liver in needle-tissue interaction
T.L. de Jong, L.H. Pluymen, D.J. van Gerwen, G. Kleinrensink, J. Dankelman, J.J. van den Dobbelsteen
Journal of the Mechanical Behavior of Biomedical Materials 2017. 69: p. 223-228

The influence of tip shape on bending force during needle insertion
N.J. van de Berg, **T.L. de Jong**, D.J. van Gerwen, J. Dankelman, J.J. van den Dobbelsteen
Scientific Reports, 2017, 7:40477: p. 1-8

Feasibility of tracking laparoscopic instruments in a box trainer using a Leap Motion Controller
I. Oropesa, **T.L. de Jong**, P. Sánchez-González, J. Dankelman, E.J. Gómez
Measurement 2016. 80: p. 115-124

Refereed contributions to >10 (inter)national conferences and four Open Access datasets published